UNIVERSITY OF KWAZULU-NATAL
COLLEGE OF AGRICULTURE ENGINEERING AND SCIENCE

AN ALTERNATIVE APPROACH TO IMPULSIVE NOISE CHARACTERISATION AND STATISTICAL MODELLING FOR BROADBAND POWERLINE COMMUNICATION NETWORKS

by:

Florence Chelangat
217080965

Supervisor:
Prof. Thomas Joachim Odhiambo Afullo

in fulfilment of the academic requirements for the degree of Doctor of Philosophy in Electronic Engineering, School of Engineering, University of KwaZulu-Natal

January, 2024

As the candidate's supervisor, I have approved this thesis for submission.

Signed [redacted] Date 9th August 2024

Name: Prof. Thomas J. O. Afullo

Declaration 1 - Plagiarism

I, **Florence Chelangat**, declare that

1. The research reported in this thesis, except where otherwise indicated, is my original research.
2. This thesis has not been submitted for any degree or examination at any other university.
3. This thesis does not contain other persons' data, pictures, graphs or other information, unless specifically acknowledged as being sourced from other persons.
4. This thesis does not contain other persons' writing, unless specifically acknowledged as being sourced from other researchers. Where other written sources have been quoted, then:
   (a) Their words have been re-written but the general information attributed to them has been referenced
   (b) Where their exact words have been used, then their writing has been placed in italics and inside quotation marks, and referenced.
5. This thesis does not contain text, graphics or tables copied and pasted from the Internet, unless specifically acknowledged, and the source being detailed in the thesis and in the References sections.

Signed  Date _____

Declaration 2 - Publications

DETAILS OF CONTRIBUTION TO PUBLICATIONS (includes publications submitted and published) that form part and/or include research presented in this thesis

Journal Publications

1. Chelangat and F., Afullo, T., "Low-Voltage PLC Noise Modelling," (2022) *International Journal on Communications Antenna and Propagation (IRECAP)*, 12 (4), pp. 237-250. doi:https://doi.org/10.15866/irecap.v12i4.22089. (Overlapping Chapter 4)

2. Florence Chelangat and Thomas Joachim Odhiambo Afullo, "Variational Bayesian Learning for the Modelling of Indoor Broadband Powerline Communication Impulsive Noise," *Progress In Electromagnetics Research B*, Vol. 100, 109-131, 2023. doi:10.2528/PIERB23020808. (Overlapping Chapter 5)

3. Chelangat and T. Afullo, "Time Series Modelling of Powerline Communication Impulsive Noise: Queuing Theory Approach," *SAIEE Africa Research Journal* - under review. (Overlapping Chapter 6)

Conference Proceedings

1. F. Chelangat and T. J. O. Afullo, "Modelling of the Powerline Communication Bursty Impulsive Noise," 2023 *Photonics & Electromagnetics Research Symposium (PIERS)*, Prague, Czech Republic, 2023, pp. 1450-1455, doi: 10.1109/PIERS59004.2023.10221275.

2. F. Chelangat and T. Afullo, "Analysis of the Steady-State Distribution of PLC Impulsive Noise Characteristics," 2023 *Southern Africa Telecommunication Networks and Applications Conference (SATNAC)*, KwaZulu-Natal, South Africa, 2023, pp. 27-29.

3. F. Chelangat and T. Afullo, "K-Means Initialisation for the Modelling of PLC Noise in Indoor Environment," 2023 *IEEE AFRICON*, Nairobi, Kenya, 2023, pp. 1-6, doi: 10.1109/AFRICON55910.2023.1029355. (Overlapping Chapter 4)

Signed [redacted] Date _____

Acknowledgements

I wish to express my heartfelt gratitude to God for granting me good health and grace and seeing me through this research. Great is Thy faithfulness.

I would like to express my sincere gratitude to my supervisor, Prof. Thomas Joachim Odhiambo Afullo, for his invaluable insights on my research area, excellent mentorship, patience, and unwavering support throughout my period of study. I believe the knowledge and wisdom gained through his mentorship will have a great impact on society. The opportunity to explore and develop this work has been truly rewarding. I am confident that the outcome of this research will be instrumental in shaping the field of powerline communications.

I would like to express my deepest appreciation to my parents, Mr. Joseph Biwott Chemirmir and Mrs. Priscila Biwott, as well as my sisters, Chepng'eno, Chepkoech, and Cheptoo, and my brothers, Victor and Brian, for the boundless love, nurturing, and encouragement they have given me throughout my life. Their support has been invaluable. I would also like to express my sincere gratitude to the entire Chemirmir family; they have been my biggest supporters and have motivated me to reach this far, with a special mention to my grandma, Mrs. Elizabeth Chemirmir, for her steadfast support and prayers. My deepest gratitude goes out to Stephen Lewis Opot, my spouse, for his patience and support throughout my research period.

To the individuals who provided unwavering support and enabled the smooth completion of this research, I would like to acknowledge Miss SZ. Ntombela (Administration Officer-CRART), Mr. J. Mpisi, Mr. D. Maharaj, Mr. G. Thula, Mr. R. Yuraj, Ms. T. Mpisi (the Lab Technicians), and Mr. N. Hlambisa (ICT Officer). I also want to express my gratitude to Teacher Olivia Pillay (Lilliput Pre-primary) for taking good care of my daughter during this research journey.

Once again, I express my gratitude to everyone who supported me throughout this journey.

Dedication

To my dearest daughter, Charlotte Amani Opot, my Cherono.

Abstract

Research into the modelling of powerline communication impulsive noise – which exhibits unpredictable behaviour in its time domain characteristics of amplitude, inter-arrival time, and service time - is still in progress. As a result, in order to propose an appropriate mitigation strategy to address the interference generated by powerline communication impulsive noise, an appropriate characterization of its time domain parameters is crucial. Given the complex structure of the powerline communication network that includes a heavy wiring system, the models proposed for the various noise characteristics are stochastic in nature. In this work, extensive noise measurements were carried out over various indoor networks in the School of Engineering, University of KwaZulu-Natal, Durban, South Africa. The measurements were conducted at the following sites: the Computer Laboratory, the Machines Laboratory, the Electronic Laboratory, the Second-year Laboratory, the Post-graduate office, as well as at an adjacent apartment. This campaign was undertaken to adequately capture the behaviour of powerline communication noise, which varies randomly depending on location, time, and the devices linked to the electrical network.

To begin with, the amplitude distribution of the powerline communication impulsive noise was examined. The Gaussian mixture model was used to analyse the amplitude distribution of powerline communication noise, which is essential in estimating the level of noise reaching the receiver. Gaussian mixture models are commonly employed in modelling the powerline communication impulsive noise amplitude distribution. However, the weights of the Gaussian mixture components are derived using statistical distributions, with the most common models employing the Bernoulli and Poisson distributions. These models, however, have been found to be insufficient in describing powerline communication noise. This thesis contributes to the modelling of the amplitude distribution of powerline communication impulsive noise by using unsupervised learning to determine the parameters of the Gaussian mixture. Regression analysis is also proposed to solve the issue of singularity in the likelihood function of this model as well as to determine the optimum number of Gaussian components. Further analysis of the amplitude distribution is performed using a fully Bayesian treatment referred to as the Variational Bayesian model, where the parameters of the Gaussian mixture model are assumed to be random variables, such that prior distributions over the parameters are introduced. Moreover, the optimal number of components is determined from the measurement data through the Variational Bayesian criterion. This ensures that improved accuracy due to the increased number of components in modelling the powerline communication impulsive noise amplitude distribution is eliminated thus reducing the model complexity while adequately describing the data. The variational-expectation algorithm, analogous to the expectation-maximisation algorithm employed in the Gaussian mixture model, is used to

determine the model parameters.

Measurements have shown that the powerline communication impulsive noise can be modelled as a superposition of several exponential distributions. Consequently, most of the research models proposed for modelling the inter-arrival and service time distribution are based on the Markov chain. There is still no defined method of evaluating the number of states, with existing models employing various curve-fitting techniques to find the optimum model for the measurement data. This work provides an alternative approach based on the queueing theory technique, where the impulsive noise occurrence in the powerline communication channel is modelled as an Erlangian queue. A straightforward method for obtaining the optimum number of exponential phases by employing the mean and the variance of the Erlang-k distribution is presented. The proposed model assumes that the impulsive noise passes through k arrival stages before entering the powerline communication network and another k service stages before leaving the powerline communication network. In all of the measurement data under consideration, impulsive noise events are observed to achieve steady-state in the inter-arrival and service time distributions.

In this work, the measurements indicate that the powerline communication noise can occur as a single-impulse noise or a burst-impulse noise. The burst-impulse noise is caused by the overlap of three or more high-amplitude single-impulse noise events that occur successively in an impulse train. The amplitude of the noise, as well as the inter-arrival and service time distribution, vary depending on the location and time. As a result, the impulsive noise is categorised as low, medium, or highly impulsive, depending on the noise levels. The probability density function of the noise amplitude exhibits heavy tails comparable to the Gaussian mixtures. The performance of the maximum likelihood estimate and the Variational Bayesian model in finding the parameters of the Gaussian mixture are validated through measurements, where the maximum likelihood estimate yields better accuracy. However, cases of singularity are encountered in addition to an increase in performance as the number of impulsive noise components is increased. Therefore, the implementation of the Variational Bayesian approach in modelling the parameters of the Gaussian mixture enables the determination of the appropriate number of Gaussian mixture components and no singularity case is found. Although the Variational Bayesian model provides a good generalization to the measured data, the maximum likelihood technique gives better accuracy since the Variational Bayesian model provides an approximate solution, as it is based on maximising the lower bound. Both models are observed to have a high level of significance as well as a good correlation to the measured data and thus either can be used in modelling the amplitude distribution of the powerline communication noise. In modelling the inter-arrival and service time distributions, the Erlang-k distribution is observed to be more appropriate for modelling the burst-impulse noise events with a high level of significance to the measured data. The exponential distribution, which is a special case of the Erlang-k distribution, is determined to be appropriate in estimating the inter-arrival time of the single-impulse noise events, indicating high variance in the measurement data. The models proposed in this thesis

can be used as simulation tools to assist the development of physical layers of powerline communication systems.

Table of Content

List of Figures

List of Tables

Chapter 1

INTRODUCTION TO POWER LINE COMMUNICATION

1.1 Introduction

Powerline communication (PLC) is a technology that transmits data through the electrical network. It has several advantages over other communication technologies such as wireless, Ethernet, and optical fibre, including inexpensive implementation costs due to pre-existing electrical network infrastructure. PLC also allows communication despite obstacles that usually impair wireless signals, and it provides high data speeds of up to 2 Gbps with good service quality, which is comparable to domestic Ethernet and wireless fidelity (WiFi), making it an appealing solution for in-home video applications [1, 2]. In addition, it has a ubiquitous infrastructure which provides wide coverage as compared to other data transmission media while being adequately reliable in most situations [3]. Furthermore, there is a global increase in demand for communication services, as evidenced by the tremendous demand for PLC devices for in-home and smart grid applications, as reported by chip manufacturers indicating that PLC is a formidable rival and a suitable complement to existing networking technologies [2].

PLC technology has been employed in unique applications such as robotics [4], wireless power transfer [5], mining security systems [6], as well as in major fields such as transportation systems, smart grids, and smart cities, to name a few. In transportation systems, PLC technology has been researched for use in areas such as aircraft systems, in-vehicle communication, marine, and trains [7–10]. Smart cities also offer services such as automated urban lighting, traffic light control, and irrigation, all of which are linked to the electrical network, rendering PLC an appealing communication option [11, 12]. Smart grid applications are a significant area of research interest in PLC technology [2, 13–16].

The essential components of the smart grid include advanced metering infrastructure (AMI), electric vehicles, and grid telecontrol among others, all of which can use PLC technology. In the AMI, for example, PLC technology enables two-way communication between service providers (utilities) and consumers. Accordingly, the AMI system collects and manages real-time data from the consumers/prosumers and sends them to utilities, which then use the data to provide improved services to consumers while complying with the defined minimum regulatory requirements for service quality [11]. PLC is also employed in the management of consumption, generation, and distribution in grid telecontrol, allowing for more efficient use of electrical energy [17], as well as improving

fault detection and self-correction of electrical networks through automation schemes, reducing the need for human operators [11]. One of the objectives of smart grids is to use environmentally friendly solutions, which has prompted the use of electric vehicles (EVCs) that produce less carbon emission in comparison to the fossil-fuelled vehicles. In order to operate, these EVCs require charging, which can be either alternating current (AC) or direct current (DC) depending on the type of plug and connection used in the EV charging post and the electric vehicle [11]. In the EVC DC charging technique, PLC is used to control communication between the EVC and the charging post. Additionally, the standard used for the integrated charging system specification, which includes user identification, load balancing capabilities, and charging safety, is based on PLC technology [11]. PLC is thus an attractive and feasible option across a wide range of applications, making it a particularly active research area.

Despite the low-deployment cost, ubiquitous infrastructure PLC technology has to offer, it was initially designed for the transmission of low-frequency, high voltage mains supply. This also means that the heterogeneous wiring configurations present in the PLC network are not ideal for data transmission. In contrast to the low-frequency high-voltage mains supply transmission it was initially designed for, data transmission across the PLC channel requires high frequency and low voltage. As a result, the electrical network employed in PLC presents a particularly hostile environment for data transmission, including impulsive noise, cable joints, and impedance mismatch, which produce multiple reflections resulting in multipath signal propagation. Consequently, the PLC network suffers from high frequency selectivity and attenuation [18, 19]. Numerous studies have been conducted, including modelling and the design of matching circuits to improve impedance matching at access points [18, 20–23]. PLC impulsive noise on the other hand, has been the subject of sustained research through the years, yet still, a standard unified model that describes its characteristics has not been established. This is due to the adverse effect of this erratic noise on the transmitted signal that may even lead to burst errors resulting in a complete signal loss. As a result, significant efforts are still in progress to fully explain PLC impulsive noise characteristics so as to design mitigation strategies that will improve the electrical network's reliability and efficiency.

1.2 Problem Statement

The impulsive noise in the PLC network emanates from two main sources; interference by other communication signals transmitted through amplitude modulation that cause the electrical wires to behave like antennas due to rhe lack of electromagnetic shield in power cables, and the unpredictable loads that are haphazardly plugged in and out of the power outlets. A significant contribution to the use of this cost-effective and vast infrastructure is the development of statistical models that fully describe the impulsive noise characteristics of the PLC network. Due to the intricate nature of the electrical network, most of the PLC noise models proposed are stochastic, where measurements are

first performed, and then statistical models are developed to fit the data. As a result, extensive measurements have been carried out [24–28], and still need to be carried out in order to acquire statistically sufficient data for designing good models. The PLC impulsive noise model can be broadly categorized into frequency domain models, which capture the average noise spectrum, and time domain models, which capture the impulse amplitude, inter-arrival time, and duration, depending on the measurement method employed. All of the proposed models are based on the time domain, which can be further classified as those that focus on the amplitude distribution of the PLC impulsive noise and those that model the temporal correlation of the impulsive noise. The amplitude of the PLC impulsive noise as well as the duration and the inter-arrival time greatly determine the extent to which the transmitted signal is affected. As a result, developing models that can fully and adequately describe these time domain characteristics is crucial.

Among the predominantly used models for describing the amplitude distribution are the symmetric alpha stable model and those based on Gaussian mixtures such as the Bernoulli-Gaussian and the Middleton Class A models [29–32] which exhibit the heavy tails similar to those exhibited by the PLC impulsive noise. The symmetric alpha stable model, however, has no closed form and is described only by its characteristic equation, whereas the Bernoulli-Gaussian model is limited to the impulsive and impulse-free states, with the likelihood of either occurring following a Bernoulli distribution. The Middleton Class A model improves on the Bernoulli-Gaussian model by assuming a finite number of states that occur according to the Poisson distribution. However, it was determined that the Middleton Class A model does not accurately describe PLC impulsive noise because it was designed for man-made impulse interference [25]. In this work, the amplitude of the PLC impulsive noise is assumed to be a superposition of various Gaussian mixture components, and the mixture weights are directly derived from the data through unsupervised learning. Consequently, the occurrence of the impulse states is not defined by a particular distribution, but rather, obtained from the data itself in form of mixture weights of the Gaussian mixture model.

Several contributions about the PLC impulsive noise service time and inter-arrival time explore the implementation of the exponential distribution due to the random behaviour exhibited by this noise [24, 33–37]. However, it has also been observed to be insufficient in approximating the inter-arrival and service time characteristics of PLC impulsive noise in different raw data [24]. Moreover, duration and inter-arrival time distribution of the PLC impulsive noise has been established to result a superposition of a number of exponential distributions from the measurement carried out in [24]. The Markov chain approach has been employed in modelling the PLC time series characteristics, where the appropriate number of exponential distributions needed for a specific measurement data under consideration is obtained through curve fitting methods. Therefore, this work proposes the Erlang-k model, which offers greater modelling flexibility for the data under consideration, while taking advantage of the exponential distribution properties. The standard deviation for an Erlang-k model ranges between 0 and $1/ku$ (where k and μ denote the shape and rate parameter respectively), such that when the value

of k is 1, it reduces to the exponential distribution, and when k is ∞, it becomes a degenerate distribution. Data with a high variation will thus have a lower number of stages (exponential distributions) as compared to data with a less variation, and as $k \to 1$ represents a high fluctuation and as $k \to \infty$ the change in the service time or the inter-arrival time is constant.

1.3 Research Objectives

The main objectives of this work are as follows:

1. To carry out measurements in order to examine and characterise the PLC impulsive noise behaviour in the time domain and propose the most suitable models.
2. To characterise and model the amplitude distribution of PLC impulsive noise in various indoor environments and determine the appropriate number of of Gaussian mixture components needed to describe the heavy tail characteristic of the PLC impulsive noise through unsupervised learning.
3. To determine the appropriate queueing model and the optimum number of exponential distributions for describing the inter-arrival and service time distribution of the PLC impulsive noise.

1.4 Contribution to Knowledge

The main contributions to the modelling of PLC impulsive noise are discussed in detail in chapters 4, 5 and 6, and are as follows:

- The PLC impulsive noise amplitude distribution, which presents different behavioural characteristics depending on the time, location and loads connected to the electrical network, is characterised and modelled using unsupervised learning, where the maximum likelihood technique is used to determine the appropriate Gaussian mixture model parameters. Consequently, the parameters are tuned to suit each of the measurement data. Since this method suffers from singularity cases where the expectation maximisation algorithm does not converge, regression analysis is proposed to determine the iteration that best suits the measured data.
- The use of the maximum likelihood technique in estimating the PLC impulsive noise amplitude distribution in low-voltage indoor electrical networks provides a suitable fit. However, it has a few drawbacks such as the tendency to over-fit data and a high preference for complex models, such that better accuracy in fitting the data is obtained as the number of Gaussian components increases, in addition to the singularity problem earlier mentioned. As a result, in order to solve these problems,

the variational Bayesian learning approach is proposed for determining the Gaussian mixture model estimates.

- A statistical impulsive noise model is developed to describe the PLC impulsive noise as a queueing system that provides a simple method of determining the steady-state probability of the inter-arrival and service time distribution. In addition, it provides a straightforward method of determining the appropriate number of exponential distributions for a specific data set under consideration, as opposed to the curve fitting methods previously employed since the inter-arrival and service time distributions have been determined to be appropriately modelled as a superposition of various exponential distributions.

1.5 Publication in Journals and Conference Proceedings

The following publications include materials that have appeared in peer-reviewed and accredited journals, as well as conference proceedings, and are part of this thesis:

1. Chelangat, F. and Afullo, T., "Low-Voltage PLC Noise Modelling," (2022) *International Journal on Communications Antenna and Propagation (IRECAP)*, 12 (4), pp. 237-250. doi:https://doi.org/10.15866/irecap.v12i4.22089.

2. Florence Chelangat and Thomas Joachim Odhiambo Afullo, "Variational Bayesian Learning for the Modelling of Indoor Broadband Powerline Communication Impulsive Noise," *Progress In Electromagnetics Research B*, Vol. 100, 109-131, 2023. doi:10.2528/PIERB23020808.

3. Chelangat and T. Afullo, "Time Series Modelling of Powerline Communication Impulsive Noise: Queuing Theory Approach," *SAIEE Africa Research Journal* - under review.

4. F. Chelangat and T. J. O. Afullo, "Modelling of the Powerline Communication Bursty Impulsive Noise," 2023 *Photonics & Electromagnetics Research Symposium (PIERS)*, Prague, Czech Republic, 2023, pp. 1450-1455, doi: 10.1109/PIERS59004.2023.10221275.

5. F. Chelangat and T. Afullo, "Analysis of the Steady-State Distribution of PLC Impulsive Noise Characteristics," 2023 *Southern Africa Telecommunication Networks and Applications Conference (SATNAC)*, KwaZulu-Natal, South Africa, 2023, pp. 27-29.

6. F. Chelangat and T. Afullo, "K-Means Initialisation for the Modelling of PLC Noise in Indoor Environment," 2023 *IEEE AFRICON*, Nairobi, Kenya, 2023, pp. 1-6, doi: 10.1109/AFRICON55910.2023.1029355.

1.6 Thesis Structure

This thesis is organised as follows:

Chapter 1 gives a general overview of PLC, its advantages, applications, the main challenges in PLC deployment, the objectives of this study as well as contribution to knowledge in the PLC field.

In Chapter 2, previous works regarding the modelling and characterisation of the PLC impulsive noise are discussed. The popular models used to describe the amplitude distribution of the PLC impulsive noise classified into either as memory or memoryless models are discussed.

Chapter 3 presents a detailed discussion of the measurement equipment, the locations in which the measurement was carried out including the loads present in these locations. The results obtained from the measurement campaigns will serve as the basis for the development of statistical models as well as the validation of the models in the preceding chapters.

The formulation of the maximum likelihood technique in modelling the PLC noise amplitude distribution using the Gaussian mixture model is discussed in Chapter 4. Due to the highly sensitive nature of the expectation maximisation algorithm to initial parameters, various initialisation techniques are discussed, and the two most appropriate initialisation models - the K-means and the random initialisation methods- are employed and their performance compared.

In Chapter 5, the variational Bayesian learning approach, which is also an unsupervised learning approach is also utilised in modelling the amplitude distribution of the PLC impulsive noise. This approach is an improvement on the ML approach employed in Chapter 4 as it solves the singularity problem in addition to providing a method of determining the optimum number of components present in the Gaussian mixture. The performance of the Gaussian mixture model in modelling the PLC impulsive noise amplitude distribution in different indoor environments based on the maximum likelihood technique and the variational Bayesian learning is compared.

After conducting a comprehensive analysis of the amplitude distribution of the impulsive noise in PLC, the queueing theory approach is employed in modelling the inter-arrival and service time distribution. The PLC impulsive noise is characterised into single impulse and burst impulse noise events in Chapter 6. The Erlang-k distribution is employed in modelling the inter-arrival and service time distribution giving rise to different queue models for different impulsive noise events in the various data sets. The steady-state equilibrium of the impulse noise events inter-arrival and service time distribution is also examined.

This thesis then concludes in Chapter 7 where a summary of the results of each of the chapters is presented and the future direction of PLC noise is discussed.

Chapter 2

LITERATURE REVIEW

2.1 Introduction

Even though the PLC technology already has an extensive electrical network infrastructure, which makes it an appealing means of data transmission. However, it also presents a significant challenge since the topology of the PLC network was initially designed for power transmission, presenting an extremely hostile environment for communication signal transfer. The numerous loads that are haphazardly plugged in and out of the electrical network in addition to the multiple branching points present in the electrical network result in impedance mismatches, signal attenuation, and noise from both within and outside the PLC network. Furthermore, electrical wiring practices differ from country to country, and even from one location within a country to another. Therefore, to improve the reliability and efficiency of the PLC technology in data transmission, accurate models PLC impulsive noise must be developed that describe the electric power system's behaviour.

The two primary approaches for modelling PLC characteristics are the top-down and the bottom-up [38]. In order to create models that explain PLC transfer and noise characteristics, the bottom-up approach requires a thorough understanding of all components of the electrical network. This method has the benefit of generating random electrical network topologies, which leads to the creation of statistically representative channels [39]. Furthermore, the primary cause of the observed system behaviour can be identified and addressed because the model parameters are well-defined. This approach, however, has higher computing demands in model development due to the large number of parameters. Moreover, it would be complex to precisely determine the parameters associated with each of the network's components. In the top-down approach, the PLC model is developed using the parameters derived from the measurement data after the measurement has been carried out. This approach has the advantage of requiring less computation in comparison to the bottom-up approach. It is particularly beneficial for modelling the characteristics of PLC noise, which are difficult to examine using pure analytical derivation.

This chapter presents an overview of the PLC network topology, PLC technology, and the standards that govern PLC deployment. The challenges impacting the performance of the PLC network are also discussed with a particular emphasis on PLC noise, which is a very active area of study and the primary subject of this work; thus, a review of the noise classification and models extensively used PLC are presented.

2.2 Electrical Network Structure

PLC technology employs the electric power grid to transmit communication signals. The electrical network was originally developed for AC power transmission and distribution at low frequencies of 50/60 Hz, depending on the country, from generating stations to consumers. The electrical network is classified as high-voltage (HV), medium-voltage (MV), and low-voltage (LV), with voltage levels of $110 - 330\ kV$, $10 - 30\ kV$, and $0.4\ kV$, respectively.

2.2.1 High-voltage Electrical Network

This section of the electrical network spans from the generating stations traversing over long distances of up to several hundreds of kilometres to the substations. In order to minimise losses during these long distances, the electrical energy is transmitted at high voltage via overhead three-phase conductors. The HV electrical network, however, suffers from a few challenges including heat loss, corona losses in power transmission, as well as periodic short-duration impulsive interference and permanent broadband interference in data transmission [40–42].

The heat loss results from resistance of the powerline material and leakage losses while corona losses are due to high electric field strengths at high voltages that cause discharge activities in the vicinity of the conductors. To mitigate heat loss in the HV lines to acceptable levels, the nominal voltage may be increased, in addition to the use of proper dimensions and correct selection of the wire material of the transmission line. It is worth noting that increasing the nominal voltage might result in increased leakage losses [40]. In regards to corona loss, a suitable geometric arrangement of the high voltage wires can be employed, as corona loss increases when thinner conductors are used for HV transmission. Corona losses also affect data transmission because they can generate significant high-frequency impulses that interfere with radios operating in the medium and low voltage frequency bands [40]. Periodic short-duration impulsive interference caused by atmospheric discharges and switching events, produces harmful peaks at the receiving end. Broadband interference, on the other hand, has a relatively high power spectral density that is heavily reliant on weather conditions. Despite these setbacks, PLC is employed in the HV line to determine the average change in height of the horizontal high-voltage overhead wires as well as remote fault detection [43], and provides a much better communication medium than MV and LV lines.

2.2.2 Medium-voltage Electrical Network

Medium-voltage lines transmit power from substations to individual manufacturing plants, urban centres, and rural areas, serving as a link between the HV and LV electrical networks. For MV lines, both overhead and underground cables are utilised, and the preference is determined by criteria such as location, with underground cables preferred in

densely populated areas. MV lines transfer electrical energy over shorter distances than HV lines, allowing for smaller poles and wire cross-sections. PLC has been employed in the MV network for fault surveys, power quality measures, temperature measurements for oil transformers, and voltage measurements on the secondary winding of HV/MV transformers [44].

2.2.3 Low-voltage Electrical Network

The low-voltage PLC network distributes 100 V−400 V electric energy from the MV/LV transformer to users via LV lines that span 500 m [40]. Identical to MV lines, both overhead and underground lines are employed. LV and MV lines are composed of aluminium or copper and insulated with polyvinyl chloride or vulcanised polythene. PLC applications in the LV PLC network section include management of indoor energy, automatic meter reading and vehicle-to-grid communication among other applications [45].

2.3 Classification of PLC Systems

PLC systems can be divided into three main categories based on the bandwidth namely, ultra-narrowband (U-NB), narrowband (NB) and broadband (BB) PLC technology. The U-NB PLC technology refers to the transmission of data in frequencies below 3 kHz. The PLC systems operating in this very narrow bandwidth (30Hz−300 Hz) transmit data at frequencies close to the mains frequency when the electrical signal around zero [11, 45]. The transmitted signal can reach long distances and even go beyond transformers without the incorporation of repeaters due to the low frequency employed by U-NB PLC systems which is less affected by transmission losses. As such, the U-NB PLC technologies can be employed both in the LV and MV sections of the PLC network. The U-NB PLC technology is; however; limited to very low data transmission rates of up to a few hundred bps, which is a main drawback in its implementation in more advanced and complex applications. The various technologies that employ the U-NB PLC technology include Aclara Two-way Automatic Communication System [46, 47] deployed for automatic meter infrastructure and X10 technology [48], employed in in-home automation.

As regards the NB PLC technology, it utilises the 3kHz−500 kHz frequency band for the transmission of data and can be further categorised into the low data rate (LDR) and high data rate (HDR) technologies. The LDR technology can achieve data transmission rates of up to a few kbps and is based on single carrier modulation while the HDR technology can achieve data rates ranging from hundreds of kbps up to 1 Mbps in the frequency band of up to 500 kHz. The Open Smart Grid Protocol (OPSG) and Metres and More (MM), which are deployed in AMI, employ LDR technology [11]. The Powerline Intelligent Metering Evolution (PRIME) and G3 Alliance, on the other hand, employ the HDR NB frequency and are the preferred solutions for the last mile smart-metering applications [11, 49].

BB PLC technology operates at frequencies ranging between 1 MHz−250 MHz and can

achieve high data rates of up to 1 Gbps within home networks. Its applications include home network multimedia applications in the LV PLC network and distribution telecontrol/automation and AMI in the MV PLC network. For energy-efficient transmission, the HomePlug has specified HomePlug Green PHY standards in the 1.8 MHz−30 MHz band [50]. Measurements and analysis for BB PLC in the 1 MHz−30 MHz band have been carried out in this study.

2.4 PLC Standards

PLC systems are subject to regulations that limit the strength of signals coupled into power lines. The PLC signal should preferably be completely contained within the proximity of the power line in most cases. However, electromagnetic radiation occurs because the power grid has not been designed to conduct relatively high-frequency signals. This mainly affects BB PLC systems, whose signals often have shorter wavelengths compared to the length of the power lines. As a result, the regulatory constraints that apply to NB and BB PLC systems differ [2]. The PLC standards specify the frequency ranges, emission constraints, background noise, measuring standards, coupling, and maximum modem output levels [51]. PLC standards also make it possible to enact large-scale economic policies, leading different countries forming alliances comparable to the European Union. The PLC standardisation organisations can be divided into those that propose and develop standards and those that develop and deploy standards and technologies. The International Electrotechnical Commission (IEC), International Telecommunication Union (ITU), European Committee for Electrotechnical Standardization (CENELEC) and the Institute of Electrical and Electronic Engineers (IEEE) are among those that propose and develop standards, whereas, PRIME, G3-PLC and HomePlug are among those in the latter group [52].

PLC standards have been developed for the NB and the BB PLC technologies. In regards to the NB PLC, the IEC protocol for example, is used to standardise the PHY and MAC layers of the Open Smart Grid Protocol (OPSG) which has the highest penetration rates in Russia and the Nordic Countries [53], and the Meters and More technologies that have been deployed in 100% of the smart meters in Italy, that provide low data rates [11]. The ITU-T G.9903 and ITU-T G.9904 standards, on the other hand, provide specifications for the physical, data link, and convergence layers for the G3-PLC and PRIME technologies that provide high data rates in NB PLC [11, 54]. The G3-PLC technology targets the American and Asia Pacific regions since it can be employed in frequencies of up to 500 kHz while the PRIME technology is widely deployed in some European countries [11]. One objective of the standardisation is to facilitate the implementation of integrated solutions. The IEEE 1901.2 standard provides mechanisms for the coexistence of both the PRIME and the G3-PLC technologies by dynamically changing the frequencies used as data subcarriers. The IEEE P1901.2 though based on OFDM in the $10 - 490$ KHz frequency band, allows the transceiver to be configured with different parameters that correspond to the

frequency band under consideration such as CENELEC or U.S. Federal Communications Commission (FCC) [11]. As regards the BB PLC technology, The main standards employed include ITU-T G.hn, IEEE 1901, and the HomePlug Alliance [55]. The ITU-T G.hn specification enables equipment interoperability, while IEEE 1901 specifies standards for broadband communication over MV and LV lines [56]. The HomePlug Alliance, on the other hand, provides specifications for home automation and control, as well as electric vehicle charging and home energy management systems. It is worth mentioning that the IEEE 1901-compliant products are fully interoperable with the HomePlug AV-compliant products.

The electrical network is well known to produce radiated electromagnetic fields which cause interference to radio communication services operating within the same frequency band [57, 58]. This radiation emission can be the upstream signals at either the consumer or adjacent consumer premises, and downstream signals at the substations. As such, the CENELEC/European Telecommunication Standards Institute has been set up to develop a single general EMC emission standard for all types of telecommunication networks to ensure fair treatment of the different technologies as regards emission limits and measurement methods [59].

2.5 PLC Channel Characteristics

PLC media characteristics include impedance mismatch, attenuation, and noise, which vary depending on the time, frequency, and location of the transmitter and receiver in the specific PLC infrastructure [59]. The impedance mismatch in the PLC network varies significantly with frequency, ranging from a few Ω to a few kΩ [60]. This is because residential low-voltage electrical networks are heavily branched, with each branch having a varying signal attenuation level owing to the number of socket outlets present in each location. Each branch node reflects the propagation signal multiple times, resulting in fluctuations in power line impedance [61]. In addition, various loads are randomly unplugged and plugged in at each outlet leading to impedance fluctuation, and thus, only a fraction of the transmitted signal reaches the receiver [62]. Previous studies conducted on the indoor access impedance established that the impedance exhibits peaks at frequencies, and thus can be modelled as a parallel resonant circuit [60]. The number of peaks corresponds to the length of the branches of the PLC networks. Thus, the network topology and the loads connected to the electrical network influence the access impedance characteristics [59, 60]. Consequently, extensive research has been carried out in regards to impedance matching between the transmitter and receiver to the PLC impedance [23, 63–67].

The transmitted signal is attenuated due to leakage and corona losses in transmission lines, in addition to electrical loads on intra-building powerlines. The attenuation changes significantly over time, reaching up to 20 dB at any given frequency [62]. Longer transmission paths result in higher attenuation values, exceeding 20 dB. Furthermore,

signal attenuation increases with frequency due to the skin effect, which reduces the conductor's effective area at high frequencies [68]. Extensive research has been performed in relation to the PLC channel modelling, where several models have been proposed for modelling the PLC channel transfer function [18, 20–22, 69].

2.6 PLC Noise

PLC noise in indoor electrical networks is a non-Gaussian random process, and thus, modulation and decoding schemes optimised for Gaussian channels may not be suitable for PLC channels, as it cannot be modelled as the typical additive white Gaussian noise. As a result, research on PLC noise characterisation and modelling has been conducted and is still in progress, where the PLC noise has been broadly classified into two categories background noise and impulsive noise [24]. The background noise comprises the coloured background noise and the narrowband interference, while the impulsive noise comprises periodic noise synchronous with the mains supply, periodic noise asynchronous with the mains supply and asynchronous impulsive noise. A summary of the noise condition as the transmitted signal traverses through the PLC channel is shown in Fig. 2.1 where each of the noise types is briefly described as follows:

- Coloured background noise emanates from a combination of several low-power noise sources and is characterised by a comparatively low power spectral density (PSD) that fluctuates with frequency. It occurs for long periods, from minutes to even hours.
- Narrowband interference, on the other hand, is present across virtually the entire frequency spectrum and is caused by broadcast transmitters in the short and medium-wave frequency bands. This noise is characterised by sinusoidal signals with modulated amplitudes [27, 28, 70].
- Periodic impulsive noise synchronous with the mains supply, where impulses with a repetition rate of 50 Hz or 100 Hz are generated by power supplies that operate synchronously with the mains cycle. The PSD of this type of impulsive noise reduces with frequency and occurs for a short duration [27].
- Periodic impulsive noise asynchronous with the mains supply that occurs with a repetition rate of 50 Hz or 100 Hz is produced by power supplies that operate synchronously with the mains cycle. The PSD of this type of impulsive noise reduces with frequency and occurs for a short duration [27].
- The asynchronous impulsive noise is characterised by a high PSD that can reach 50 dB above the background noise and also occurs sporadically and in bursts. Switching transients in the PLC network is the primary source of this troublesome noise [25, 27, 28].

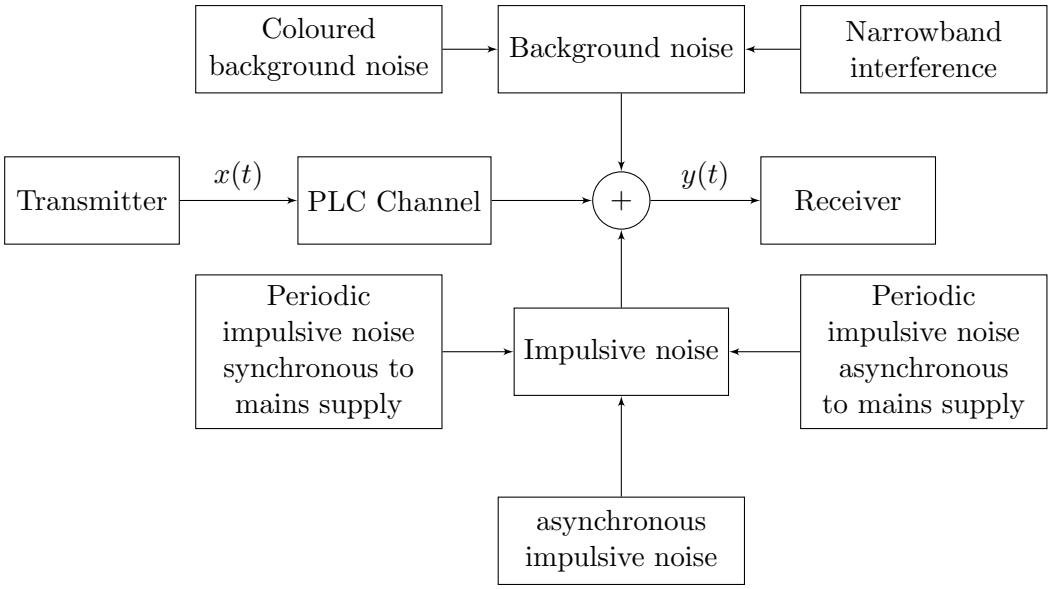

Figure 2.1: PLC Noise Classification

Different models have been proposed for the various noise categories. The Nakagami and Rayleigh distributions have been proposed in [71], for modelling of the background noise. Extensive noise measurements were carried out on narrowband interference in low-voltage indoor networks in [72, 73] with a 3D Markov chain model proposed in [74]. As for the periodic impulsive noise, [75] describes the noise as a cyclostationary Gaussian process given by the combination of simple and typical noise waveforms, whereas in [76], the cyclostationary behaviour of the periodic impulsive noise is observed to exhibit self-similarity.

The spectral density of background noise increases rapidly at low frequencies below 1 MHz, contrary to the attenuation of the transmitted signal, which decreases as frequency increases. As a result, to limit the effect of background noise, a trade-off between path loss and background noise in the transmission frequency band must be identified. In PLC this trade-off is determined to be at a frequency range of 1 MHz -20 MHz, depending on the distance, electrical network topology and loads in the circuit [28]. Transmission schemes such as spread spectrum techniques, discrete modulation tone and orthogonal frequency division multiplexing can help cope with the disturbance caused by narrowband interference [28, 77]. As for the periodic impulsive noise, modelling of the service and inter-arrival time is straightforward due to its deterministic nature [24]. On the contrary, the asynchronous impulsive noise is the most difficult to describe due to the random nature of the time domain characteristics and has been the subject of interest for various research. The main focus is to model the PLC noise characteristics in the frequency band of $1-30$ MHz and as such the review of the widely adopted models that have been proposed for asynchronous impulsive noise are discussed in the following sections.

2.7 PLC Noise Models

The previously proposed models for the PLC impulsive noise are stochastic since characterisation through pure deterministic derivation is a complex task. The models can thus be categorised as either frequency domain or time domain, depending on the method used to conduct the measurement. The former approach captures the average noise spectrum, whereas the latter captures the amplitude, inter-arrival time and duration of the PLC noise impulses. It is the most widely adopted approach in literature and is also employed in this work. This is because the time domain characteristics are essential in determining the strength and occurrence of the impulse noise, which are key in analysing the impact of the PLC noise on the transmitted signal. Fig. 2.2 depicts the time domain characteristics of the impulse noise using rectangular pulse envelopes. The inter-arrival time is denoted by t_{iat} and gives the time between arrival times (t_{arr}) of successive impulses (impulse i and impulse $i+1$) and is obtained as:

$$t_{iat} = t_{arr,i+1} - t_{arr,i} = t_{w,i} + t_d, \tag{2.1}$$

where $t_{w,i}$ is the impulse width of impulse i and t_d is the impulse distance between the departure of impulse i and the arrival of impulse $i+1$, whereas, $A = max\{A_i{}^+, A_i{}^-\}$ is the impulse noise amplitude.

The PLC noise models based on the time domain can also be classified into those generated from independent and identically distributed (i.i.d.) random variables and those that take into account the temporal correlation. The GM model, which is the basis of most models employed in the modelling asynchronous PLC noise, is based on the assumption that the PLC impulsive results form a superposition of a finite number of Gaussian distributions. Depending on the number of impulsive noise states under consideration, various models are proposed. The most popular models are the Middleton Class A (MCA), Bernoulli-Gaussian (BG), Markov Middleton (MM) and Markov Gaussian (MG) models. The MCA and the BG models are based on the identically distributed (i.i.d.) random variables, do not capture the bursty nature of the PLC noise, while the MM and the MG are similar to the MCA and the BG models but with an additional memory term. This minor setback for the models based on the i.i.d. random variables can be addressed through the multi-carrier modulation schemes where discrete Fourier transform is employed to spread the impulse noise on all the sub-carriers in the frequency domain such that the form in which the impulse noise occurs is irrelevant [78].

2.7.1 Bernoulli Gaussian Model

The BG model is commonly employed in describing impulsive noise due to its simplicity and better tractability in comparison to the MCA model [79]. In this model, the Bernoulli process is used to model the occurrence of the PLC noise impulses since only two states are considered impulsive-free (where only the background noise is present) and the impulsive

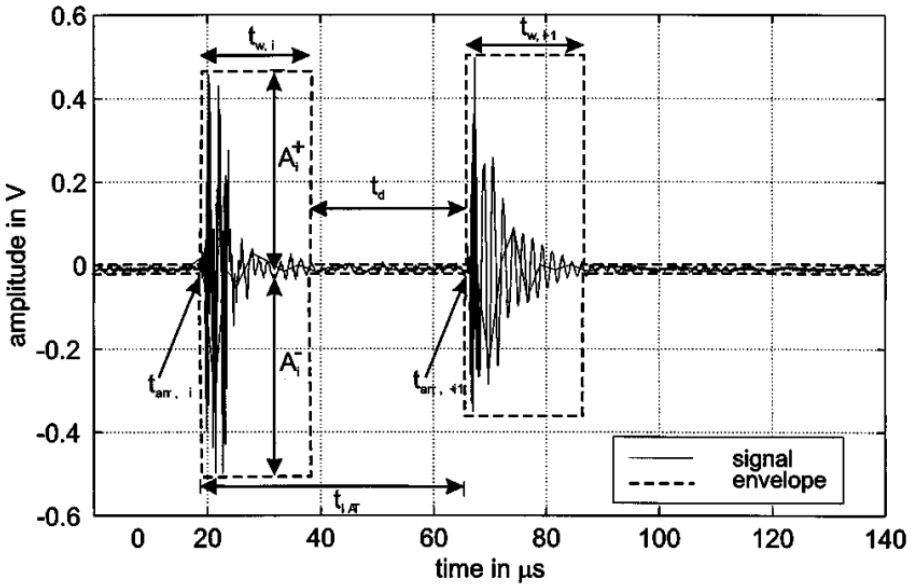

Figure 2.2: PLC Noise Time-domain Characteristics [24]

state, which constitutes both the background and the impulsive noise [29]. The amplitude distribution of the impulsive noise is then assumed to follow the Gaussian distribution. The probability density function (PDF) of the Bernoulli distribution is given by [29, 80]:

$$P(b(x_n)) = \begin{cases} \phi, & \text{for } \; b(x_n) = 1 \\ 1-\phi, & \text{for } \; b(x_n) = 0 \end{cases}$$

where ϕ denotes the probability of occurrence of an impulsive noise state and $1-\phi$ denotes the occurrence probability of an impulse-free state. The BG probability density function (PDF) can then be obtained as [29, 80]:

$$g_{BG}(x_n) = \frac{\phi}{\sqrt{2\pi{\sigma_1}^2}} \exp\left(\frac{-{x_n}^2}{2{\sigma_1}^2}\right) + \frac{(1-\phi)}{\sqrt{2\pi{\sigma_0}^2}} \exp\left(\frac{-{x_n}^2}{2{\sigma_0}^2}\right), \tag{2.2}$$

where the mean of Gaussian distribution is assumed to be zero, whereas, σ_1 and σ_0 in (2.2) denote the variance of the impulsive and impulse-free noise states, respectively.

2.7.2 Middleton Class A Model

The BG model discussed in section 2.7.1 does not guarantee a good fit for the measured data since it is only limited to two states. In addition, to achieve an adequate estimate of the amplitude of the PLC noise, it relies heavily on the accuracy of the impulse noise detection and extraction [81]. In [82–84], the MCA noise model is used to describe the PLC noise, which improves on the BG model by considering a finite number of states that are assumed to follow the Poisson arrival process, given by

$$P_c = \frac{e^{-X} X^c}{c!} \tag{2.3}$$

where X is the impulsive index and denotes the product of the mean length of an impulse noise and the mean number of impulses. The PDF of the MCA model is then obtained as [83, 84]:

$$f_c(m_t) = \sum_{c=o}^{C} \frac{P_c}{\sqrt{2\pi {\sigma_c}^2}} \exp \frac{-{m_t}^2}{2{\sigma_c}^2} \tag{2.4}$$

where P_c denotes the occurrence probability of the c^{th} Gaussian component while m_t denotes the noise sample at time instant t. The Gaussian distribution mean is also assumed to be zero and ${\sigma_c}^2$ is the variance determined as [83, 84]:

$${\sigma_c}^2 = \left({\sigma_0}^2 + {\sigma_1}^2\right) \frac{\frac{c}{X} + \eta}{1 + \eta} \tag{2.5}$$

and η indicates the strength of the impulsive noise component in comparison to the Gaussian noise component, and is given by [83, 84]:

$$\eta = \frac{{\sigma_0}^2}{{\sigma_1}^2}. \tag{2.6}$$

Consequently, as η increases, the level of the impulsive noise in the PLC network decreases. The MCA model has been employed to describe the amplitude distribution of the PLC noise. However, it was determined in [25] to be insufficient in describing the PLC noise since it was originally developed for man-made interference.

2.7.3 Symmetric Alpha Stable Model

This model exhibits heavy tails similar to the tails present in the PLC impulsive noise. It has been determined to provide a better estimate of the PLC impulsive noise amplitude distribution as compared to the MCA model. It is based on the Generalised central limit theorem, where the sum of i.i.d. random variables converges to a normal distribution as the number of samples tends to infinity, whereas it converges to symmetric alpha stable (s α s) distribution when the finite variance limitation drops [85,86]. An alpha stable random variable is denoted by $s\alpha(\theta, \mu, \lambda)$ where $\theta(\theta \geq 0)$ is the scale parameter, μ is the skewness parameter on the values $(-1 \leq \mu \leq 1)$, such that $\mu < 0$ for the left-skewed, $\mu > 0$ for the right-skewed and $\mu = 0$ for a symmetrical distribution. $\alpha(0 < \alpha \leq 2)$ is the stability index and controls tail decays, whereas $\lambda(\lambda \in \mathbb{R})$ represents the shift parameter. The alpha-stable random variable $X \approx s\alpha(\theta, \mu, \lambda)$ is given by its characteristic equation [85, 87]:

$$\eta(\hat{\phi}) = \begin{cases} \exp\left(j\lambda\hat{\phi} - \theta^{\alpha}|\hat{\phi}|^{\alpha}\left(1 + j\mu\sin(\hat{\phi})\tan\frac{\pi\alpha}{2}\right)\right) & \text{if } \alpha \neq 1 \\ \exp\left(j\lambda\hat{\phi} - \theta|\hat{\phi}|\left(1 - j\mu\frac{2}{\pi}\sin(\hat{\phi})\log|\hat{\phi}|\right)\right) & \text{if } \alpha = 1 \end{cases} \tag{2.7}$$

where $\hat{\phi} \in \mathbb{R}$ and

$$\sin(\hat{\phi}) = \begin{cases} 1 & \text{if } \hat{\phi} > 0 \\ 0 & \text{if } \hat{\phi} = 0 \\ -1 & \text{if } \hat{\phi} < 0 \end{cases} \tag{2.8}$$

When $\alpha = 2$ and $\mu = 0$, the symmetric alpha stable distribution reduces to a Gaussian distribution and becomes a Cauchy distribution when $\alpha = 1$ and $\mu = 0$. Another special case of the symmetric alpha stable distribution is the Lèvy distribution that occurs when $\alpha = 0.5$ and $\mu = 1$ [85].

A comprehensive discussion on the use of the symmetric alpha stable distribution in modelling the PLC noise is presented in [85, 88]. Although the symmetric alpha stable model has a better performance as compared to the MCA model in estimating the amplitude distribution of the PLC noise, it was determined in [85] that the parameters that provide the appropriate fit are $\alpha \in [1.5, 2]$ and $B \approx 0$, and as such is a symmetric alpha stable case with no closed form expression for its PDF.

2.7.4 Models with Memory

Thus far, the models discussed do not take into account the bursty nature of PLC noise. In order to incorporate this PLC noise characteristic, studies into the bursty nature of the PLC noise were conducted in [30, 89–91]. The two commonly employed models are the MM and the MG models in [30, 89]. The MG and MM models are similar to the BG and the MCA discussed in sections 2.7.1 and 2.7.2 respectively, but with additional memory terms. The PDF of the MM model is then determined as [30]:

$$P_{mca}(m_t) = \sum_{c=0}^{C} \frac{\hat{P}_c}{\sqrt{2\pi {\sigma_c}^2}} \exp \frac{-{m_t}^2}{2{\sigma_c}^2} \tag{2.9}$$

where

$$\hat{P}_c = \frac{P_c}{\sum_{c=0}^{C}} \tag{2.10}$$

The transition state diagram for the MM model where the number of states is truncated into five terms is shown in Fig. 2.3, where x denotes the time correlation between noise samples and is independent of the MCA parameters. The details on the determination of the x parameters can be found in [30]. As regards the MG model, a two-state Markov process is employed, where the channel is assumed to be in a good state 0, or a bad state 1. A good state represents only the presence of background noise, whereas a bad state denotes the presence of both impulsive and background noise [89, 91]. The MG model PDF for an impulse noise m_t at a time t conditioned on the state s_t of the system is given by [89, 91]:

$$P(m_t \mid s_t = 0) = \frac{1}{2\pi\sigma^2} \exp\left(\frac{-|\ m_t\ |^2}{2\sigma^2}\right) \tag{2.11}$$

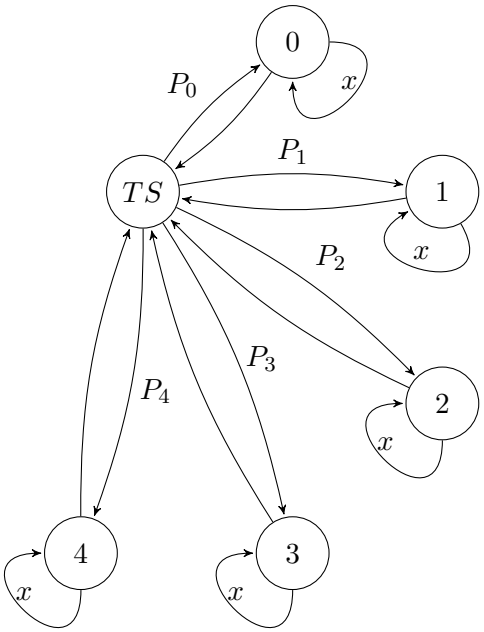

Figure 2.3: Markov-Middleton Model

$$P(m_t \mid s_t = 1) = \frac{1}{2\pi Q\sigma^2} \exp\left(\frac{-\mid m_t \mid^2}{2Q\sigma^2}\right) \tag{2.12}$$

assuming that m_t is a complex circularly-symmetrical Gaussian random variable that varies depending on s_t and Q is the ratio of the impulsive to the impulse-free noise power in the PLC channel. The BG model discussed in section 2.7.1 assumes that the occurrence of impulsive noise state (bad state) follows a stationary Bernoulli process [89], such that:

$$P_1 = P(s_t = 1) \tag{2.13}$$

In the MG model, the occurrence of the bad state for each of the realisation process is assumed to follow a stationary first order Markov process [89, 91], given by:

$$P(s_t + 1) = P(s_1) \prod_{t=1}^{T} P(s_t + 1 \mid s_t) \tag{2.14}$$

The transition probabilities of the channel state is the given by:

$$P_{ij} = P(s_t + 1 = j \mid s_t = i)) \qquad \text{for } \; i, j \in [1, 0] \tag{2.15}$$

Thus, the probability of an impulse noise event to be at a given state at time t is determined as [89, 91]:

$$P_0 = P(s_t = 0) = \frac{P_{10}}{P_{01} + P_{10}} \tag{2.16}$$

$$P_1 = P(s_t = 1) = \frac{P_{01}}{P_{01} + P_{10}} \tag{2.17}$$

and the number of impulses for a given state in the PLC noise process is obtained in 2.18 and 2.19 respectively as:

$$M_0 = \frac{1}{P01} \tag{2.18}$$

$$M_1 = \frac{1}{P10} \tag{2.19}$$

The difference between the MG and the BG model stems from an additional memory parameter r in addition to P_1 in the BG model given by [89]:

$$r = \frac{1}{P_{10} + P_{01}} \tag{2.20}$$

If $r = 1$, the channel is memoryless, for $r < 1$, the channel possesses an oscillatory memory, whereas $r > 1$ indicates that the channel has persistent memory [89]. The state transition for the MG model is depicted in Fig. 2.4.

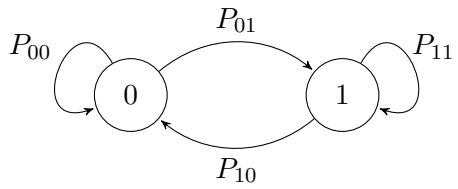

Figure 2.4: Markov Gaussian Model

2.7.5 Gilbert Elliot Model

This model describes the inter-arrival and service time distribution of the PLC impulsive noise using two states: the impulsive state x_1 and the impulse-free state x_0. The probability of transitioning to either state is assumed to be memoryless and thus independent of the current state. As such, the presence or absence of an impulse noise event at a future time $t + 1$ is independent of the occurrence of an impulse noise event at a time t and can be represented as [33, 92]:

$$P\left[x(t+1) = x_1 \mid x(t) = x_0\right] = P\left[x(t+1) = x_1 \mid x(t) = x_1 = y\right], \tag{2.21}$$

where $x(t)$ is the state of the system at time t. It follows that if the PLC noise process is in state x_0 at time $t + 1$, then:

$$P\left[x(t+1) = x_0 \mid x(t) = x_0\right] = P\left[x(t+1) = x_0 \mid x(t) = x_1 = 1 - y\right] \tag{2.22}$$

Figure 2.5 illustrates the state transitions for the Gilbert Elliot model where x_{ij} represent the transition for state x_i to state x_j.

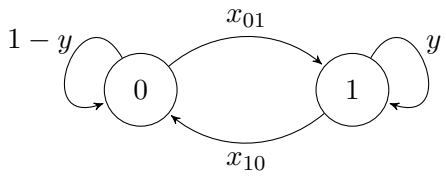

Figure 2.5: Gibert Elliot Model

2.7.6 Zimmerman and Dostert Noise Model

The inter-arrival time and the duration of PLC impulsive noise have been determined to often correspond to a superposition of several exponential distributions unlike the exponential distribution employed in the Gilbert Elliot model in Section 2.7.5. In order to adequately describe this behaviour, a partitioned Markov Chain approach is employed to model the time series characteristics of the impulsive noise. The impulse noise is assumed to pass through m states which are partitioned into two groups, impulsive corresponding to the impulse duration, and impulse-free states corresponding to the inter-arrival time. Thus, if there are a total of m states in the PLC systems for $M(i = 1, 2, ..., m)$, then; the impulse-free state will constitute $X(i = 1, 2, ..., v)$ whereas the impulsive states will constitute $Y(i = v + 1, v + 2, ..., m)$. Each group comprises transition states in the noise process that are assumed to follow the exponential distribution and the output function $\phi(t)$ at instant t, is given by [24]:

$$\phi(t) = \phi(z(k) = z_i) = \begin{cases} 0, & i \in X \\ 1, & i \in Y \end{cases} \tag{2.23}$$

such that the number of states v, in group X represents cases where no impulse noise event occurs, whereas the number of states $w = m - v$ in group Y, represents the occurrence of an impulse noise event. The transitions from the impulse-free state (X) to the impulsive state (Y) and vice versa can then be described using independent transmission matrices given by [24]:

$$A = \begin{pmatrix} a_{1,1} & 0 & \cdots & 0 & a_{1,v+1} \\ 0 & a_{2,2} & \ddots & \vdots & a_{2,v+1} \\ \vdots & \ddots & \ddots & 0 & \vdots \\ 0 & \cdots & 0 & a_{v,v} & a_{v,v+1} \\ a_{v+1,1} & a_{v+1,2} & \cdots & a_{v+1,v} & 0 \end{pmatrix}$$

$$B = \begin{pmatrix} b_{1,1} & 0 & \cdots & 0 & b_{1,w+1} \\ 0 & b_{2,2} & \ddots & \vdots & b_{2,w+1} \\ \vdots & \ddots & \ddots & 0 & \vdots \\ 0 & \cdots & 0 & b_{w,w} & b_{w,w+1} \\ b_{w+1,1} & b_{w+1,2} & \cdots & b_{w+1,w} & 0 \end{pmatrix}$$

If the impulse duration of an impulse noise event exceeds a specified duration t_w, the complementary probability distribution (CPD) of the impulse noise event is obtained as [24]:

$$CPD_d(n) = \begin{cases} 1 & \text{for } n = 0 \\ \sum_{j=1}^{w} b_{w+1,j}(b_{j,j}^n) & \text{for } n = 1, 2, ... \end{cases} \tag{2.24}$$

whereas the CPD for the impulse-free time span between two impulses greater than a specified time span t_d is determined as [24]:

$$CPD_a(n) = \begin{cases} 1 & \text{for } n = 0 \\ \sum_{j=1}^{v} a_{v+1,j}(a_{j,j}^n) & \text{for } n = 1, 2, ... \end{cases} \tag{2.25}$$

The $CPD_d(n)$ and $CPD_a(n)$ comprise a sum of weighted exponentials, and the elements of A and B can then be derived from the impulse duration and impulse-free time spans between impulses by curve-fitting techniques. Further analysis of this model is discussed in [24]. The partitioned Markov chain transition states can be summarised as shown in Fig. 2.6.

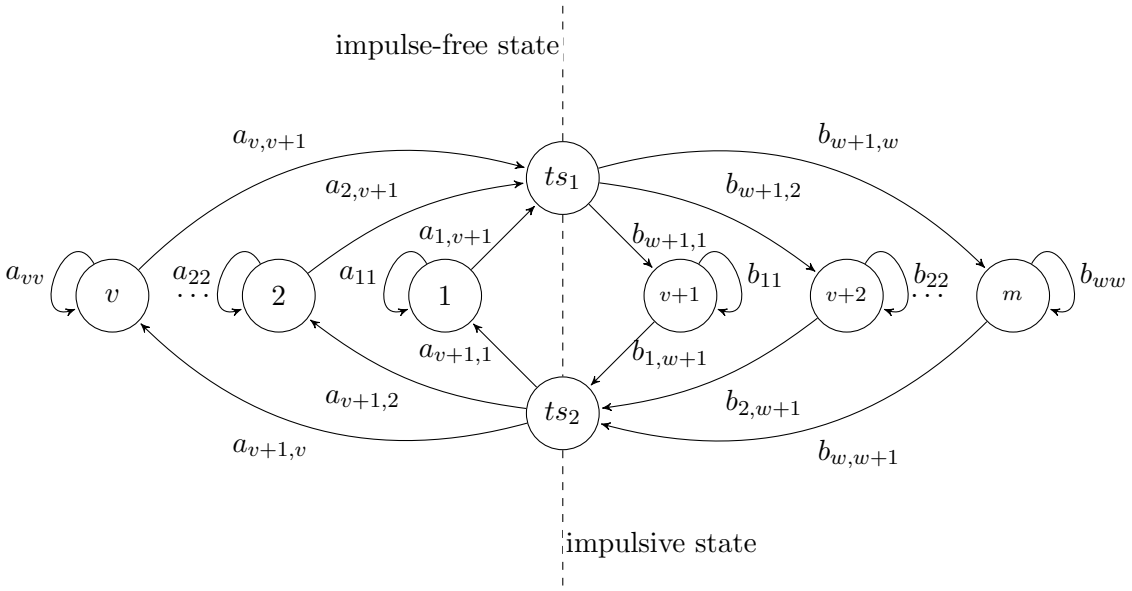

Figure 2.6: Partitioned Markov chain transition state diagram

2.8 Chapter Summary

In this chapter, the PLC network topology is presented, followed by a review of PLC technologies and standards. In addition, the PLC characteristics and classifications of PLC noise are discussed. Previous models proposed for modelling the time-domain characteristics of impulsive noise have been reviewed. The GM model is observed to be widely used for modelling the amplitude distribution of noise, while the PLC noise

is determined to be a superposition of various noise components. The main challenge in these models is determining the mixture weights and the number of Gaussian components for the GM models, as well as the number of exponential distributions in modelling the inter-arrival and duration of the PLC noise. There is, therefore, a need to construct models that are flexible enough to predict the distribution of the PLC characteristics, which is the focus of this work, presented in Chapters 4, 5 and 6. PLC noise measurement and data acquisition are presented in Chapter 3 to enable the development and characterisation of models that improve on the already existing ones.

Chapter 3

PLC Noise Data Acquisition and Measurement Set-up

3.1 Introduction

PLC impulsive noise has been the subject of sustained research through the years, yet still, a standard unified model that describes its characteristics has not been established. This is owing to the adverse effect of this noise on the transmitted signal which may even lead to burst errors resulting in a complete signal loss. As a result, significant efforts have been made to adequately explain PLC impulsive noise characteristics. However, work on the development of a model that fully describes the PLC impulsive noise characteristics to aid in the design of mitigation strategies that will improve the reliability and efficiency of the electrical network is still in progress. Due to the heterogeneous wiring practices, numerous joints and socket outlets in the low-voltage PLC networks, the impulsive noise present in this network is the most troublesome as numerous noise-generating sources are continuously plugged in and out of the electrical network. As such, various frequency and time domain measurement campaigns have been carried out in order to study the PLC noise in low voltage indoor environments [24, 26, 28, 34, 93, 94]. The frequency domain measurements seek to find out the power spectral density of the PLC noise, while the time domain measurements focus investigation the amplitude, duration and inter-arrival time characteristics of the PLC noise.

Preliminary works on the PLC noise measurements were performed in [24], where the PLC noise is categorised into coloured background noise, narrowband interference, periodic impulsive noise and asynchronous impulsive noise. In [26], investigation on the contribution of the various electrical loads is carried out. Further investigations on the PLC noise in indoor networks are performed in [25, 95] where the fluorescent tubes and power switching devices are observed to generate high noise levels at broadband frequencies. In [36], the PLC noise measurements are conducted at the source to establish the correlation between the appliance noise generators and the noise signature. Additional measurement campaigns on narrowband interference and the contribution of the short wave and medium wave transmission stations to the PLC noise are carried out in [72].

For PLC noise measurements to be carried out, couplers are used as an interface between the PLC network and the measurement equipment. The function of the coupler is to filter out the high-voltage low-frequency mains signal while allowing the low-voltage high-frequency communication signals to pass through. Due to the impedance mismatch

characteristics present in the PLC network, couplers have been proposed that match the $50\ \Omega - 75\ \Omega$ [96] impedance of the transmitters and receivers in the PLC system. However, these couplers also introduce noise to the PLC network due to the presence of passive filter components, which contribute to the final noise 'seen' by the measurement equipment [97].. As a result, the noise generated by the PLC couplers is investigated in [97].

The PLC noise models proposed in this work are stochastic in nature, in line with other models discussed in Chapter 2. Measurement campaigns in this work were carried out in various indoor environments, namely: an apartment, post-graduate office, computer laboratory, machines laboratory, second-year laboratory and electronics laboratory.

3.2 Measurement Set-up

Presently, stochastic models are employed in modelling the PLC impulsive noise characteristics, which employ the top-down approach. As a result, extensive measurement campaigns need to be performed in order to develop statistical models that provide an accurate description of the behaviour of the PLC impulsive noise. This work, similar to other stochastic models, employs the top-down approach, in which the parameters for the proposed models are obtained from measurement data for various low-voltage indoor locations. Fig. 3.1 shows the set-up used to perform PLC noise measurements in the $1 - 30$ MHz frequency band.

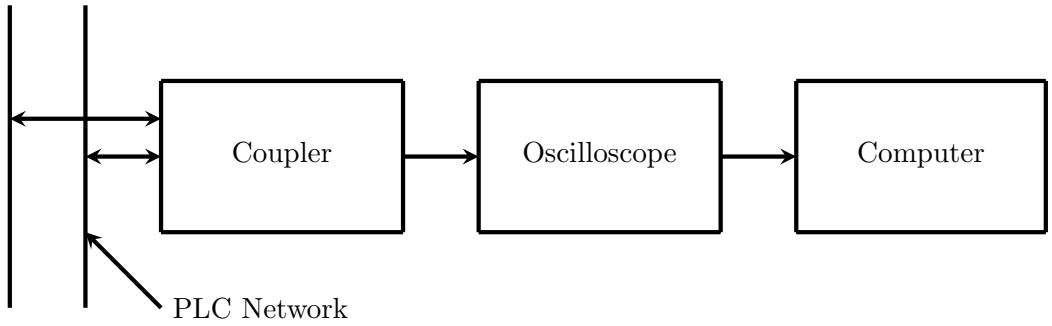

Figure 3.1: PLC Noise Measurement Set-up

In order to filter out low-voltage frequency signals and protect the oscilloscope from damage from the high-voltage mains supply, while allowing high frequency, low voltage communication signals to pass through, a high-pass filter coupler was used as an interface between the oscilloscope and the electrical network. This is achieved by the capacitors, a $1:1$ broadband transformer and Zener diodes present in the coupling circuitry. Galvanic isolation is provided by the transformer, while Zener diodes maintain the output voltage at 5V to protect the equipment from power surges. The series capacitor, on the other hand, prevents the transformer from saturation and filters out the mains signal. It has been established that the passive filter components present in couplers also generate a ringing effect that distorts the time domain characteristics of the impulse signal. This is due to the excitation of resonance points as the PLC noise traverses the coupling circuit [97]. The

schematic diagram for the PLC coupling circuitry is shown in Fig. 3.2.

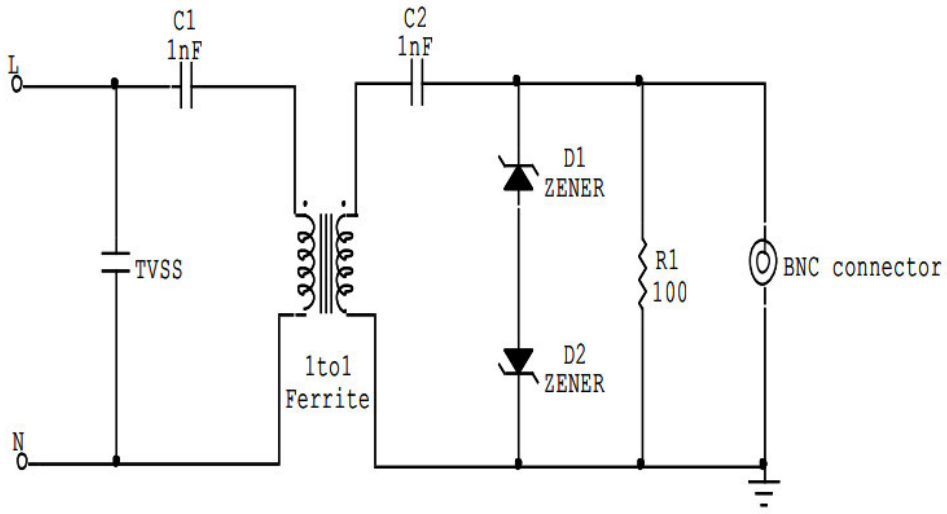

Figure 3.2: PLC Coupling Circuitry [34]

In this work, the PLC noise is measured at the receiver and thus the impact of the coupling circuit is not taken to consideration. For each of the measurements carried out, the Rigol DS2202A was used to perform measurements, where the sampling rate was configured to 1 Giga samples/s, measuring 14 million samples with a window length of 14 ms. The measurement data was the captured in a flash drive and transferred to the computer for analysis and storage of the measured data.

3.3 Measurement Results

The PLC noise is known to vary with location, time and the electrical devices connected to the electrical network. consequently, measurement campaigns were conducted in different locations where the following locations were considered in this study.

- Second-year laboratory (SYL): the loading conditions for the SYL include four air conditioners, thirty-six fluorescent lamps and forty-two workstations each comprising of the following: an electronic trainer board; a function generator; a simple 10 MHz oscilloscope; a DC power supply; a digital multimeter; and a board of passive components. The room dimension for the SYL is approximately 26m by 13m.
- Post-graduate office (PGO): the PGO is connected to the same electrical network as the other offices in the building with a dimension of approximately 10.8m by 4.8m. The PGO consists of two air conditioners, eight fluorescent lights, one heavy duty printer, and eight workstations - each consisting of either a desktop computer with its screen or a laptop computer, and a phone charger.
- Computer laboratory (CL): the CL, with a dimension of 16m by 12m, has the following loads connected to the PLC line: three air conditioners; twenty fluorescent

lights; sixty desktop computers with computer screens. The measurements were conducted as the students carried out their practicals.

- Electronic laboratory (EL): the EL with a dimension of 5m by 5m consists of nine fluorescent lights and two air conditioners. Other appliances connected to this PLC network include electronic trainer boards, function generators, digital multimeter and cathode ray oscilloscopes present in each of the eight work stations.

- Machines laboratory (ML): the ML dimension is 30m by 14.6m and consists of 40 fluorescent lights and four air conditioners liked to the electrical network. Other loads connected to the PLC network include adjustable speed drives, dc generators, ac motors, variac with built-in rectifier, current and voltage transformers, measurement instruments such as voltmeters, ammeters and watt meters, and variable resistors (up to 450 Ω).

- Apartment: with regard to the apartment, the loads connected to the powerline network include light dimmers, a juice blender, an iron box, an electric oven, a microwave, a television, fluorescent lights, an electric kettle and security lights. This measurement was performed between 6:00 and 9:00 p.m. when most of the household's electrical devices had been switched on and functioning.

Measurement campaign was performed between 2:00 pm and 5:00 pm in all the laboratories, during which students conducted their practicals. Except for the various loading conditions, the laboratories at the University of KwaZulu-Natal and the Apartment serve as a representation of the impulsive noise in PLC network. In the sample noise measurement data for the PGO in Figs. 3.3a and 3.3b, the peak to peak ($p-p$) amplitude is approximately $(-0.4 < y < 0.4)V_{p-p}$. However, the occurrence and amplitude distribution of the noise in the observation window are random. As for the EL, sample measurements in Figs. 3.4a and 3.4b have approximately $(-1.5 < y < 1.5)V_{p-p}$ and are higher than that of the PGO. This can be attributed to devices such as silicon-controlled rectifiers (SCR), fluorescent tubes as well as thermostats present in this location, that have been observed to produce high impulsive noise levels at broadband frequencies [25,26,95,98]. In comparison to the ML sample noise measurement in Fig. 3.5b, the sample data in Figs 3.5a shows a lower peak-peak noise level. This can be attributed to the different loads connected to the PLC network at the time of measurement, as well as other internal sources, since motors present in this location, have been determined to cause radio interference [26, 99]. The noise levels of the Apartment in Figs. 3.6a and 3.6b range from approximately $(-0.2 < y < 0.2)V_{p-p}$ with the impulse noise occurring at different times within the observation window. This can be attributed to the electrical appliances that had been plugged in, confirming the time-varying nature of the PLC noise. In regards to the CL, the PLC noise amplitude is also low ranging between $(-0.1 < y < 0.1)V_{p-p}$ in the sample measurement in Fig. 3.7a and less than $(-0.15 < y < 0.15)V_{p-p}$ as shown in Fig. 3.7b. This indicates that the loads connected to the network, mainly computers, do not generate very high noise levels in the $1 - 30$ MHz frequency band. Figs. 3.8a and 3.8b depict the

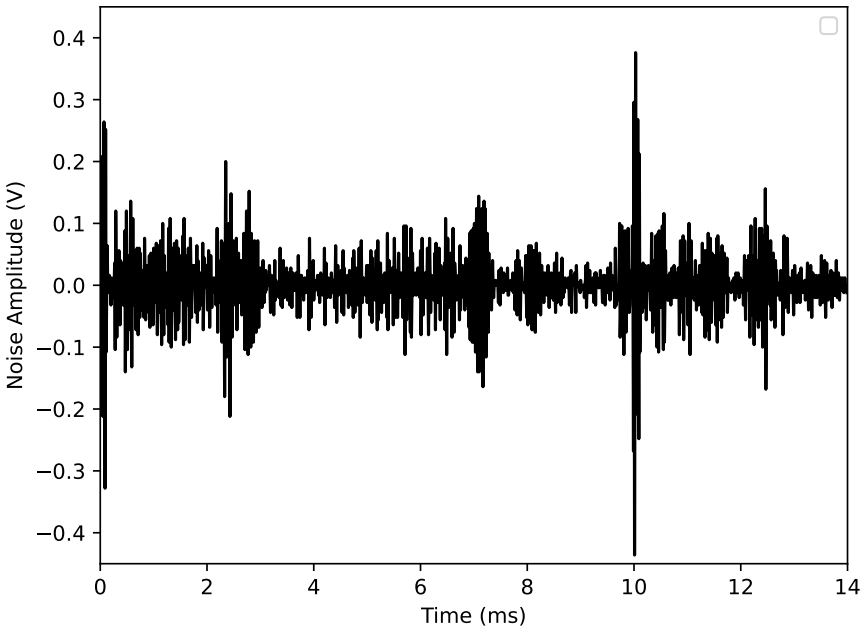

(a) PLC Impulsive Noise Sample

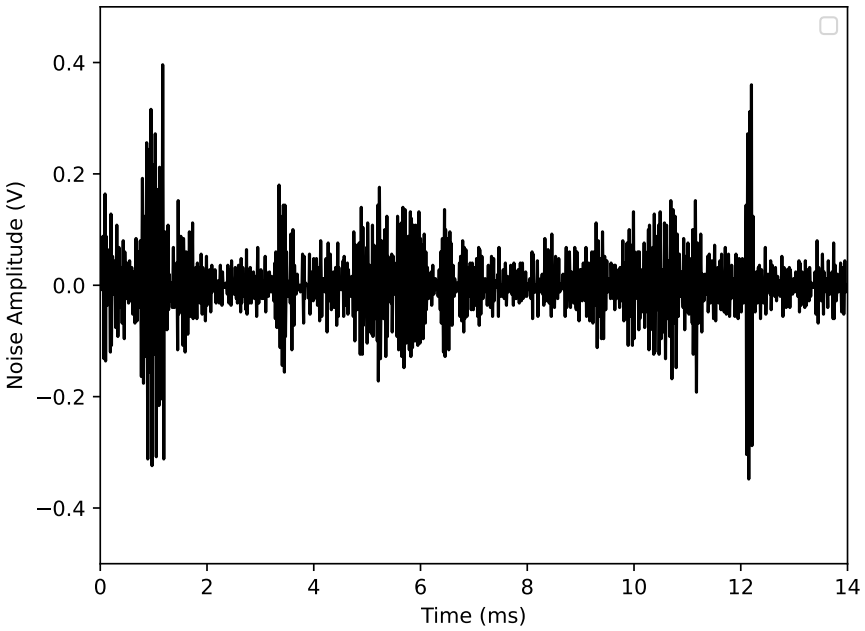

(b) PLC Impulsive Noise Sample

Figure 3.3: Postgraduate Office

SYL sample noise measurement results. It can be observed that in both cases the noise levels range between $(-0.3 < y < 0.3)V_{p-p}$. Although the noise level in this location is lower in comparison to that of the PGO, ML and EL, it is distributed throughout the observation window.

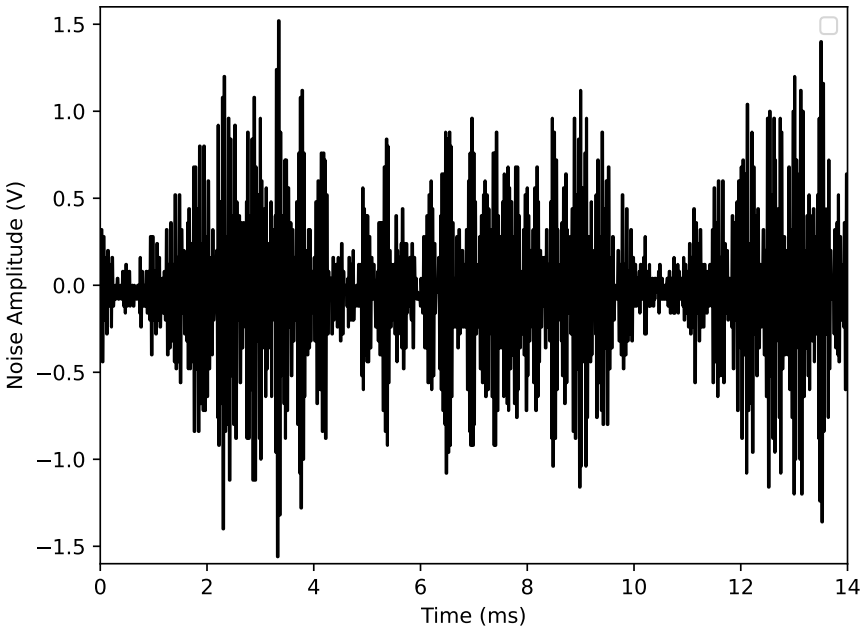

(a) PLC Impulsive Noise Sample

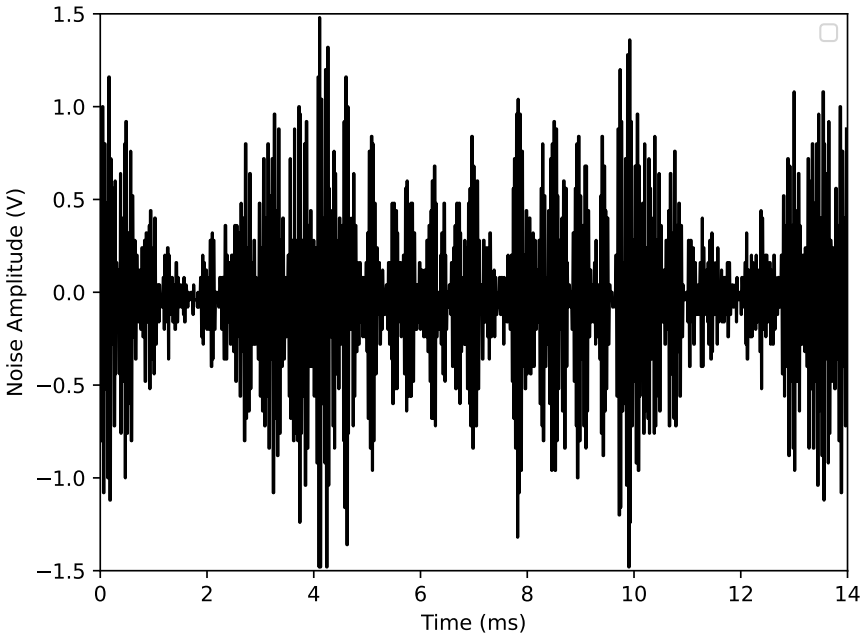

(b) PLC Impulsive Noise Sample

Figure 3.4: Electronic Laboratory

For each sample measurement at each location, the PLC impulsive noise occurrence and amplitude vary. Therefore, developing a statistical model to describe this unpredictable behaviour is a daunting task.

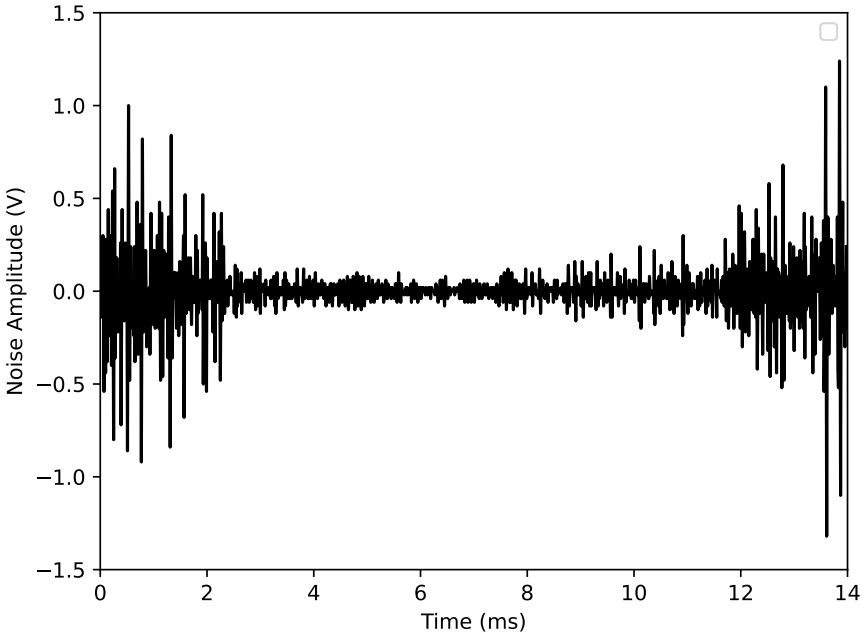

(a) PLC Impulsive Noise Sample

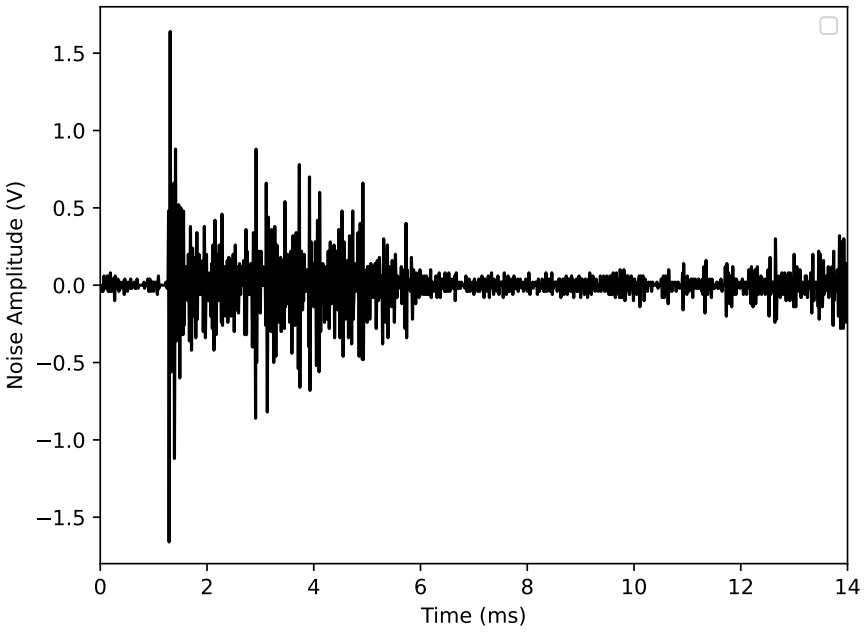

(b) PLC Impulsive Noise Sample

Figure 3.5: Machines Laboratory

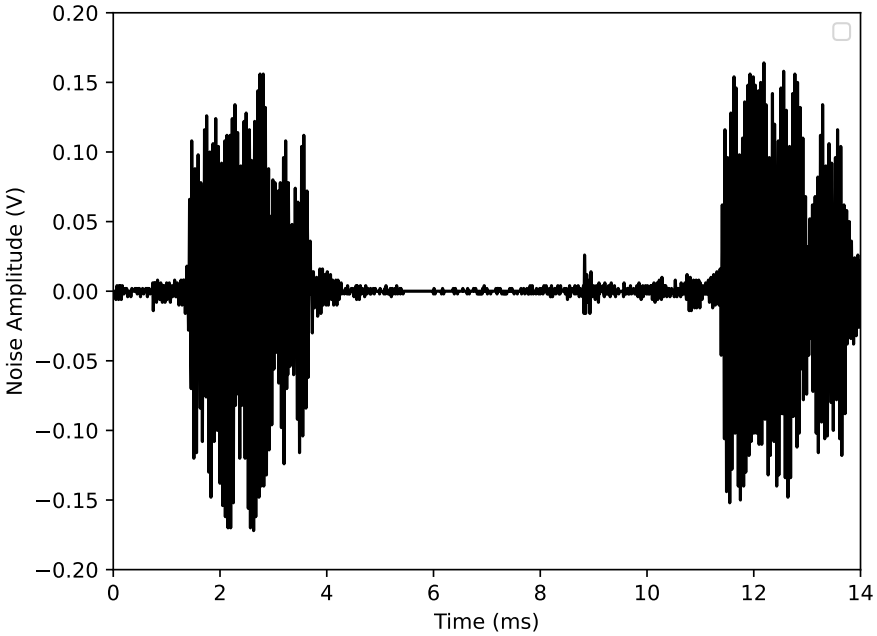

(a) PLC Impulsive Noise Sample

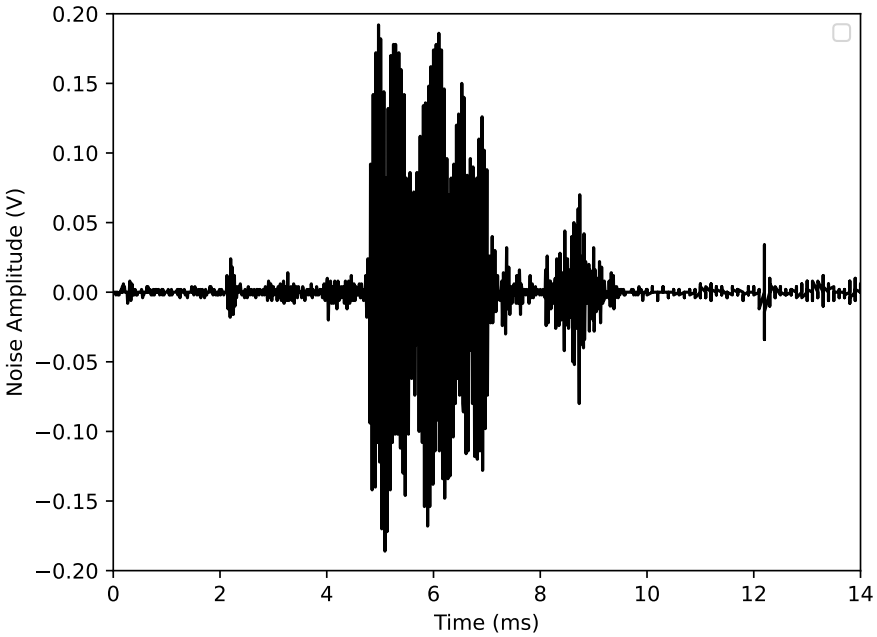

(b) PLC Impulsive Noise Sample

Figure 3.6: Apartment

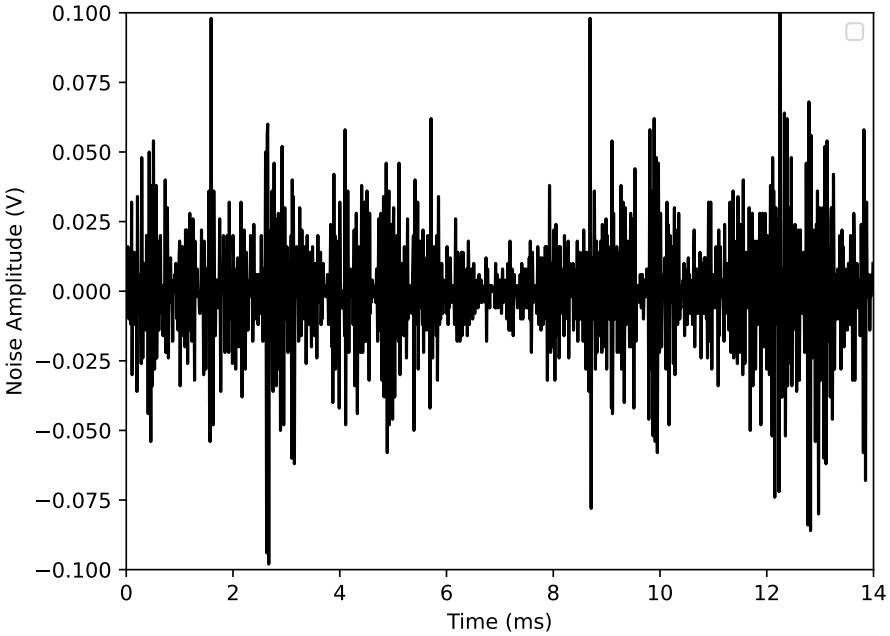

(a) PLC Impulsive Noise Sample

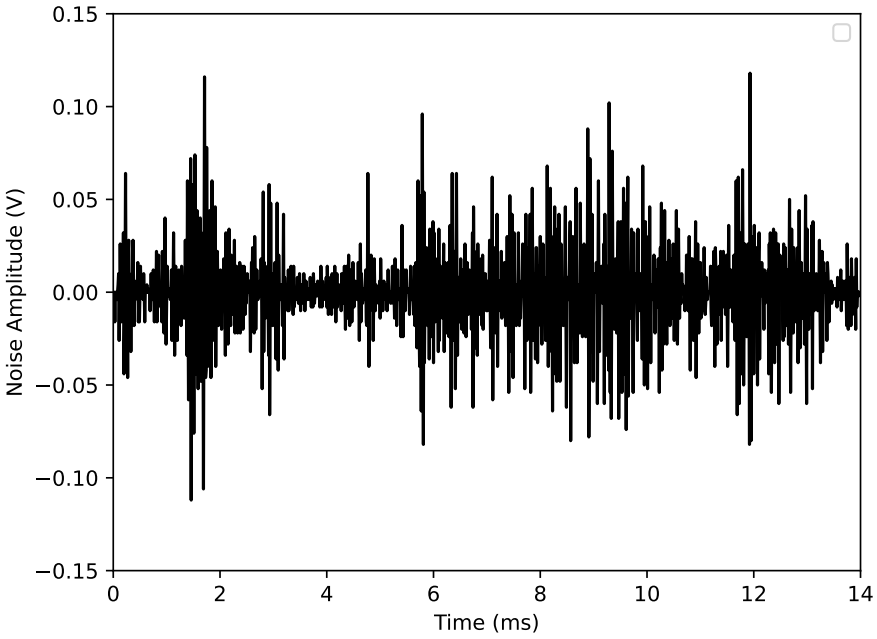

(b) PLC Impulsive Noise Sample

Figure 3.7: Computer Laboratory

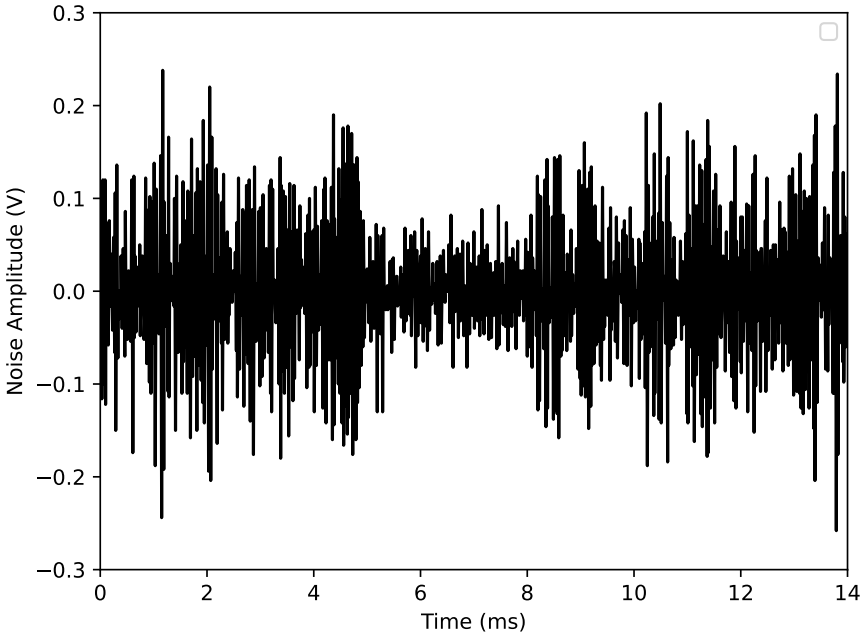

(a) PLC Impulsive Noise Sample

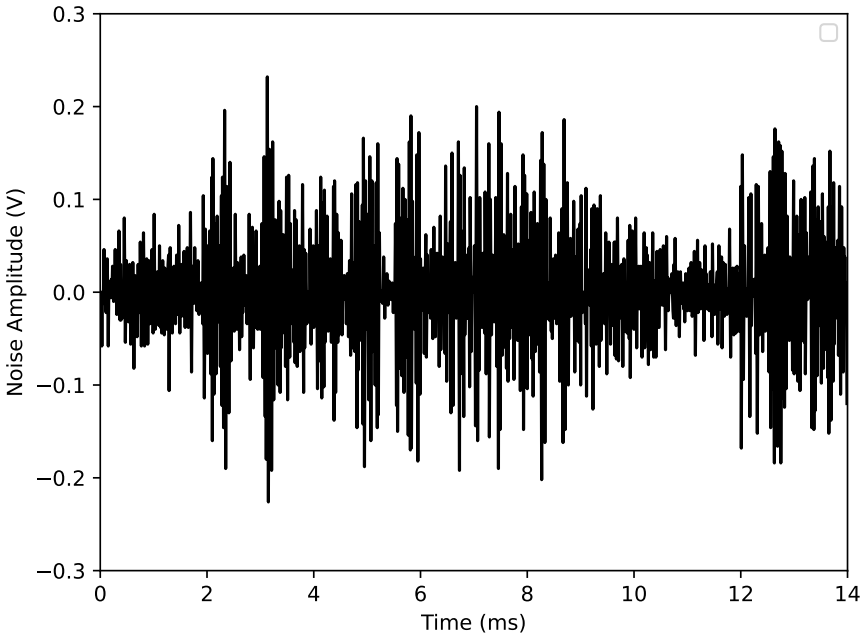

(b) PLC Impulsive Noise Sample

Figure 3.8: Second-year Laboratory

3.4 Chapter Summary

The time domain PLC impulsive noise measurement for various indoor networks has been conducted, and sample measurement data are presented in this chapter. It has been determined that the PLC impulsive noise characteristics — amplitude, inter-arrival times, and duration — are unpredictable. In this work, all the models proposed are stochastic, and thus, the results obtained in this chapter will provide the basis for the development of statistical models as well as validate the models in the subsequent chapters. Chapter 4 begins with modelling the amplitude distribution of the PLC noise.

Chapter 4

Gaussian Mixture Modelling of the PLC Noise Amplitude Distribution

‘

4.1 Introduction

PLC technology can attain data rates of up to 2 Gbps [1] and is developing as a viable option for indoor communication in the broadband communication market [100]. Due to its existing infrastructure, it offers an appealing alternative to other communication networks. However, it is impacted by noise, which is a superposition of numerous heterogeneous components, including narrowband interference, coloured background noise, and impulsive noise. The impulsive noise is further classified as synchronous impulsive noise and asynchronous impulsive noise [24, 71, 101]. According to [102], the most troublesome noise in a broadband PLC is impulsive noise, which may reach up to 50 dB above the thermal noise threshold. Asynchronous impulsive noise, for example, occurs at random in bursts and has significant strength, that may result in signal damage [71]. Therefore, developing a unified statistical model of this noise is an important task.

The amplitude distribution of PLC impulsive noise has been determined to possess heavy tails. As a result, statistical models with comparable heavy tail characteristics were used to model PLC amplitude. This includes the application of symmetric α-stable modelling [85], whereby the characteristic equations are used to describe their distributions and lack a closed-form formulation. The Gaussian mixture (GM) model also exhibits this heavy tail characteristic. As a result, numerous studies employ the GM model to estimate the amplitude distribution of PLC impulsive noise, as well as commonly used models such as the Middleton Class A and Bernoulli Gaussian models. The difference in these models stems from the determination of the mixture weights of the Gaussian components and the number of Gaussian components that the particular model considers. As a result, for the Bernoulli Gaussian model, there are only two states: impulsive and impulse-free, and the occurrence of either state is defined by the Bernoulli distribution. The PLC impulsive noise is considered to have a finite number of states in the Middleton Class A model, hence the mixture weights are generated using the Poisson distribution [84]. Initially intended for man-made interference, the Middleton Class A model was determined to be unsuitable for modelling the PLC impulsive noise distribution [25].

In this work, the heavy tail characteristic of the GM model is also utilised to model the amplitude distribution of PLC noise as seen by the receiver, where machine learning approach is employed to find the model parameters. Machine learning technique finds patterns in data and has been implemented in various domains, including bit error rate estimation [103] [104], and is broadly categorised into two main methods: supervised and unsupervised learning. Unsupervised learning differs from supervised learning in that it utilises training data consisting solely of the input vectors, whereas the latter also includes the corresponding target vectors. Unsupervised learning is utilised in this study, such that the parameters of the model are modified by the training data set to suit the probability density function (PDF) of the measured PLC noise data. The maximum likelihood technique, which is well known for its high accuracy in the determination of GM model parameters, is utilised together with the expectation maximisation (EM) algorithm. The maximum likelihood technique has been employed in other areas of study, such as [105, 106] in image matching and audio-visual scene analysis, respectively. The EM algorithm employed in finding the maximum likelihood parameters is known to be highly sensitive to initial parameters [107–109]. As such, in this work, various models used to initialise the EM algorithm are discussed, and the performance of the two most suitable initialisation techniques for deriving the parameters of the GM models are compared. In addition, the impact of the total number of components comprising the GM on the amplitude distribution of impulsive noise is investigated.

4.2 Gaussian Mixture Model Formulation

Impulsive noise is assumed to be independent and identically distributed random variable in the proposed model, with the PDF generated by the weighted sum of a linear superposition of Gaussian distributions (components) with the total mixing probability equal to one. The discrete-latent variable model is utilised to formulate the GM. For each seen data point d_n, where $n = 1, 2, ...N$, there is a corresponding latent variable z_{nq}, indicating whether the q_{th} mixture component generated that data point for $q = 1, 2, ...Q$ [110]. Thus, the data point d_n can be generated solely by the q_{th} mixture component given by [110, 111]

$$p(d_n \mid z_{dq} = 1) = N(d_n \mid \mu_q, \sigma_q) \tag{4.1}$$

where $N(d_n \mid \mu_q, \sigma_q)$ is the q_{th} Gaussian density given by [112]:

$$N(d_n \mid \mu_q, \sigma_q) = \frac{1}{(2\pi)^{\frac{1}{2}}\sigma_q} \exp - \frac{(d_n - \mu_q)^2}{2\sigma_q^2} \tag{4.2}$$

and σ_q denotes the variance whereas μ_q denotes the mean. Because the latent variable z_{nq} is unknown, a prior distribution is placed such that:

$$p(\mathrm{z}_{nq} = 1) = \pi_q, \tag{4.3}$$

where

$$\pi_q = \begin{cases} 1, & \text{if } d_n \in N(d_n \mid \mu_q, \sigma_q) \\ 0, & \text{otherwise} \end{cases}$$

$$\sum_{q=1}^{Q} \pi_q = 1 \tag{4.4}$$

The value of d_n is generated using the ancestral sampling strategy, which involves computing the joint distribution of the latent variable $p(z_{nq} = 1)$ and the conditional distribution $p(d_n \mid z_{nq} = 1)$ to obtain

$$p(d_n) = \pi_q N(d_n \mid \mu_q, \sigma_q). \tag{4.5}$$

Summing the joint distribution over all possible states of z_{nq} results in the PDF of the Gaussian mixture for data point d_n such that at any given time constant, the noise is a random variable whose PDF is given by

$$p(d_n \mid \theta) = \sum_{q=1}^{Q} \pi_q N(d_n \mid \mu_q, \sigma_q) \tag{4.6}$$

where $\theta := \{\mu_q, \sigma_q, \pi_q : q = 1, 2, ..., Q\}$ is a collection of all parameters of the model. The corresponding posterior probability (responsibility) of z_{nq} given d_n can be determined using Bayes' theorem as follows [110, 111]

$$\begin{aligned} \gamma_{nq} &= p(\mathrm{z}_{nq} = 1 \mid d_n) \\ &= \frac{p(\mathrm{z}_{nq} = 1) p(d_n \mid \mathrm{z}_{nq} = 1)}{\sum_{j=1}^{Q} p(\mathrm{z}_{nj} = 1) p(d_n \mid \mathrm{z}_{nj} = 1)} \\ &= \frac{\pi_q N(d_n \mid \mu_q, \sigma_q)}{\sum_{j=1}^{Q} \pi_j N(d_n \mid \mu_j, \sigma_j)}. \end{aligned} \tag{4.7}$$

Equation (4.7) determines the likelihood that the q_{th} mixture component generated the n_{th} data point. In the GM model, π_q denotes the prior probability and defines the mixing weights, while r_{nq} specifies the posterior probability after d_n has been observed.

4.2.1 Parameter Estimation

The maximum likelihood technique is used to estimate the parameters of the GM, which are derived from the measured impulsive noise dataset. Thus, for a given observation window with noise samples $\{d_1, d_2, ..., d_n\}$, the likelihood function of the Gaussian mixture is determined as follows:

$$p(D \mid \theta) = \prod_{n=1}^{N} p(d_n \mid \theta), \tag{4.8}$$

where N is the total number of observations and $p(d_n \mid \theta)$ denotes the Gaussian density of each individual likelihood. Taking the log of the likelihood function simplifies equation

(5.9), to obtain:

$$\begin{aligned}\log p(D \mid \theta) &= \sum_{n=1}^{N} \log p(d_n \mid \theta) \\ &= \sum_{n=1}^{N} \log \sum_{q=1}^{Q} \pi_q N(d_n \mid \mu_q, \sigma_q)\end{aligned} \tag{4.9}$$

The derivative of equation (4.9) with respect to μ_q is then given by [110]:

$$\frac{\partial \log p(D \mid \theta)}{\partial \mu_q} = \sum_{n=1}^{N} \frac{1}{p(d_n \mid \theta)} \frac{\partial p(d_n \mid \theta)}{\partial \mu_q} \tag{4.10}$$

From equation (4.10) $p(d_n \mid \theta)$ is is given by

$$p(d_n \mid \theta) = \sum_{j=1}^{Q} \pi_j N(d_n \mid \mu_j, \sigma_j) \tag{4.11a}$$

It follows that only the q_{th} mixture component depends on μ_q and therefore:

$$\begin{aligned}\frac{\partial p(d_n \mid \theta)}{\partial \mu_q} &= \pi_q \frac{\partial N(d_n \mid \mu_q, \sigma_q)}{\partial \mu_q} \\ &= \frac{\pi_q}{(2\pi)^{\frac{1}{2}} \sigma_q} \frac{\partial \exp -\frac{(d_n - \mu_q)^2}{2\sigma_q^2}}{\partial \mu_q}\end{aligned} \tag{4.12a}$$

Applying Chain rule to (4.12a) results in,

$$\begin{aligned}\frac{\partial p(d_n \mid \theta)}{\partial \mu_q} &= (d_n - \mu_q)(\sigma_q)^{-1} \frac{\pi_q}{(2\pi)^{\frac{1}{2}} \sigma_q} \exp -\frac{(d_n - \mu_q)^2}{2\sigma_q^2} \\ &= (d_n - \mu_q)(\sigma_q)^{-1} \pi_q N(d_n \mid \mu_q, \sigma_q)\end{aligned} \tag{4.12b}$$

Substituting (4.11a) and (4.12b) to (4.10) results in,

$$\begin{aligned}\frac{\partial \log p(D \mid \theta)}{\partial \mu_q} &= \sum_{n=1}^{N} (d_n - \mu_q)(\sigma_q)^{-1} \frac{\pi_q N(d_n \mid \mu_q, \sigma_q)}{\sum_{j=1}^{Q} \pi_j N(d_n \mid \mu_j, \sigma_j)} \\ &= \sum_{n-1}^{N} \gamma_{nq} (d_n - \mu_q) {\sigma_q}^{-1}\end{aligned} \tag{4.13}$$

The updated mean μ_{qp}, is then determined by setting the derivative in (4.13) to zero yielding:

$$\mu_{qp} = \frac{1}{N_q} \sum_{n=1}^{N} \gamma_{nq} d_n \tag{4.14}$$

where N_q represents the total number of data points assigned to q_{th} mixture component and is given by:

$$N_q = \sum_{n=1}^{N} \gamma_{nq} \tag{4.15}$$

Similarly, the derivatives of (4.9) with respect to σ_q and π_q are determined as [110] [111]:

$$\frac{\partial \log p(D \mid \theta)}{\partial \sigma_q} = \sum_{n=1}^{N} \frac{1}{p(d_n \mid \theta)} \frac{\partial p(d_n \mid \theta)}{\partial \sigma_q} \tag{4.16}$$

$$\frac{\partial \log p(D \mid \theta)}{\partial \pi_q} = \sum_{n=1}^{N} \frac{1}{p(d_n \mid \theta)} \frac{\partial \mid \theta)}{\partial \pi_q} \tag{4.17}$$

and the corresponding updated variance σ_{qp} is then obtained as:

$$\sigma_{qp} = \frac{1}{N_q} \sum_{n=1}^{N} \gamma_{nq} (d_n - \mu_q)^2 \tag{4.18}$$

To determine the partial derivative of the mixture weight π_q, the requirement that all mixture weights must sum up to 1 stated in (4.4) is accounted for by applying the Lagrangian multiplier. The corresponding Lagrangian is given by [110, 111, 113]

$$L = \log p(D \mid \theta) + \lambda \left(\sum_{q=1}^{Q} \pi_q - 1 \right) \tag{4.19}$$

The partial derivatives with respect to π_q and Lagrange multiplier λ are then obtained as:

$$\frac{\partial L}{\partial \pi_q} = \sum_{n=1}^{N} \frac{N(d_n \mid \mu_q, \sigma_q)}{\sum_{j=1}^{Q} \pi_j N(d_n \mid \mu_j, \sigma_j)} + \lambda = \frac{N_q}{\pi_q} + \lambda \tag{4.20}$$

$$\frac{\partial L}{\partial \lambda} = \sum_{q=1}^{Q} \pi_q - 1 \tag{4.21}$$

Setting the partial derivatives derivatives of equations (5.23) and (5.24) and solving for π_q yields the updated mixture weight π_{qp}, given by [114]:

$$\pi_{qp} = \frac{N_q}{N} \tag{4.22}$$

The EM algorithm seeks to maximise the likelihood function with respect to the components' means, variances, and mixture weights. It accomplishes this by iteratively modifying the initial parameters, switching between updating the cluster assignments and parameter estimates. The mean of each component's Gaussian distribution approaches the cluster's mean with each iteration. The EM algorithm for the proposed model is shown in Algorithm 1 [111] [113].

Algorithm 1 EM Algorithm for GM Model

Input: Data $\{d_1, d_2, ..., d_n\}$, number of clusters Q, convergence threshold ϵ
Initialize: Randomly initialize μ_q, σ_q, and π_q
Repeat until convergence:
repeat
    E-step: Compute responsibilities
    for $n \leftarrow 1$ **to** N **do**
        for $q \leftarrow 1$ **to** Q **do**
            $\gamma_{nq} = \frac{\pi_q N(d_n|\mu_q,\sigma_q)}{\sum_{j=1}^{Q} \pi_j N(d_n|\mu_j,\sigma_j)}$
        end for
    end for
    M-step: Compute update parameters
    for $q \leftarrow 1$ **to** Q **do**
        $N_q = \sum_{i=1}^{N} \gamma_{nq}$
        $\mu_{qp} = \frac{1}{N_q} \sum_{n=1}^{N} \gamma_{nq} d_n$
        $\sigma_{qp} = \frac{1}{N_q} \sum_{n=1}^{N} \gamma_{nq} (d_n - \mu_q)^2$
        $\pi_{qp} = \frac{N_q}{N}$
    end for
until Convergence criterion is achieved: $|\log likelihood - \log likelihood_{\text{old}}| < \epsilon$
Output: Learned parameters μ_{qp}, σ_{qp}, and π_{qp}

4.2.1.1 Parameter Initialization

The EM algorithm described in Section 4.2 involves two steps: the E-step, where the posterior probabilities are evaluated from the initial values, and the M-step, where the updated means, mixture weights and variances are determined from the posterior probabilities. While the maximum likelihood solution has identifiability problems (i.e., for any given maximum likelihood solution of a Q-component mixture, there are a total of Q equivalent solutions corresponding to the $Q!$ methods of allocating Q sets of parameters to the Q-components), this problem is not relevant in terms of identifying a good density model because any of the equivalent solutions is as good as any other [111].

The measured time-domain characteristics of noise samples in the low-voltage indoor environment, which are i.i.d. random variables, are used to obtain the parameters of the proposed model. Consequently, at each instant t, an impulsive noise variable d_n exists with a specific amplitude. Figure 4.1 depicts the time-domain amplitude distribution of the measurement data, whereas Figure 4.2 depicts a corresponding sample sequence series with two intervals. The observation window is divided into Q intervals of equal length such that

$$N_q = \frac{d_n - d_0}{Q} \tag{4.23}$$

where $d_N = 1400$ and $d_0 = 0$ from Fig. 4.2 whereas N_q is the length of the q_{th} interval and indicates the total number of samples in the q_{th} interval. The Gaussian mixture component parameters are then derived from each interval. The probability that the average noise

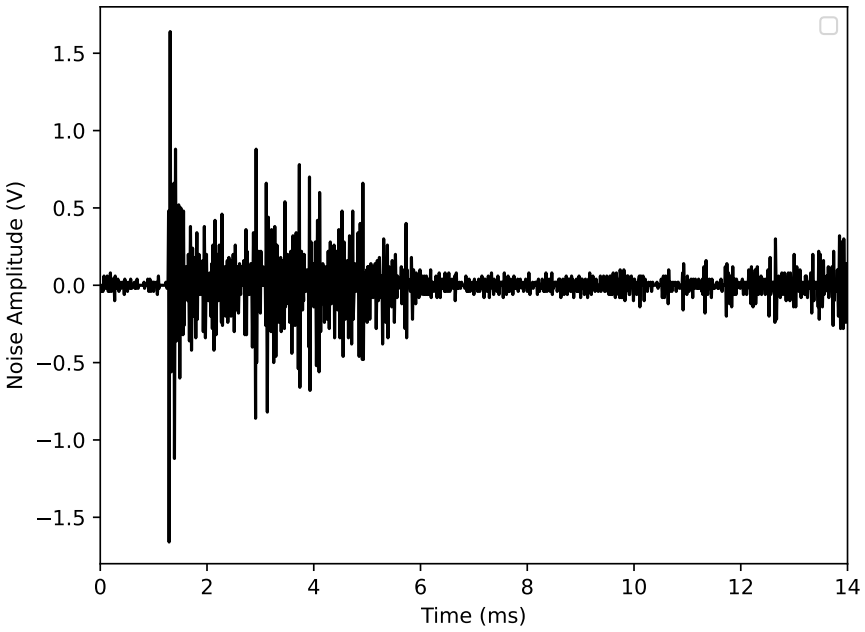

Figure 4.1: PLC Impulsive Noise Sample

level in the observation window is in the q_{th} cluster is then determined as:

$$\pi_q = \frac{N_q}{N} \tag{4.24}$$

The initialization of parameters in the proposed model, consists of the following steps:

1. Divide the data into Q clusters.
2. Compute the initial mixing weights by evaluating the ratio of the number of points in each cluster to the total number of samples.
3. Determine means and variances for the individual components of the Gaussian mixture by computing the mean and variance of each cluster
4. Evaluate the Gaussian distributions for the whole data set using the means and variances found in step 3.

4.2.1.2 Selection of Optimum Parameters

The EM algorithm determines the optimum parameters by examining the convergence of either the parameters or the log-likelihood function [111]. However, in certain instances, the algorithm may fail to converge due to singularities in the likelihood function that arise when the maximum likelihood technique is used to estimate parameters. This happens when one of the component distributions has a mean that is identical to one of the data points. From (4.6), the n_{th} data point contributes to a term in the likelihood function of

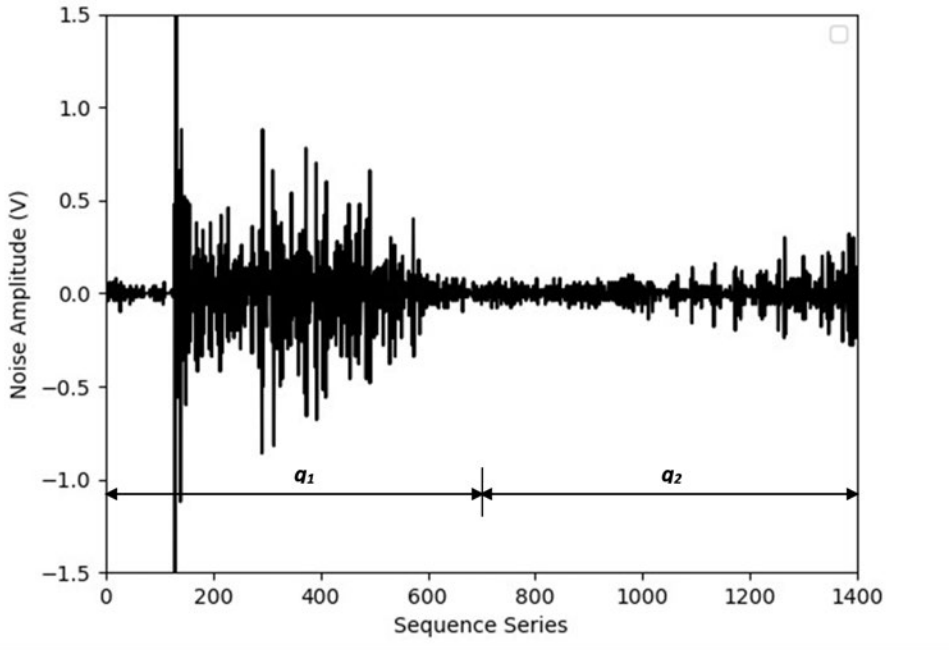

Figure 4.2: PLC Impulsive Noise Sample

the following form:

$$N(d_n \mid \mu_q, \sigma_q) = \frac{1}{(2\pi)^{\frac{1}{2}}\sigma_q} \tag{4.25}$$

Therefore, as $\sigma_q \to 0$, the likelihood function and log-likelihood function both tend to infinity. A Gaussian mixture consists of at least two components. As a result, if one of the component distributions collapses to a single data point, the other component with a finite variance will assign a finite probability to all data points, contributing an increasing additive value to the log-likelihood. To overcome this challenge, regression analysis is proposed for selecting the iteration whose parameters best describe the measured data.

4.3 Error Analysis and Model Calibration

Error analysis was then performed to determine how well the proposed models fit the data where the root mean square error (RMSE) and the χ^2 statistic were employed to determine the goodness of fit of the proposed GM model, and the Pearson's parametric correlation (R) test was utilised to measure the degree of dependency between the GM model and the measured data. Equations (4.26), (4.27) and (4.28) give the formulations for the R, RMSE and the χ^2 statistic respectively [34, 115].

$$R = \frac{\sum_{n=1}^{N}(x_a - \overline{x_a})(x_p - \overline{x_p})}{\sqrt{\sum_{n=1}^{N}(x_a - \overline{x_a})^2 (x_p - \overline{x_p})^2}} \tag{4.26}$$

$$RMSE = \sqrt{\frac{\sum_{n=1}^{N}(x_a - x_p)^2}{N}} \tag{4.27}$$

$$\chi^2 = \sum_{n=1}^{N} \frac{(x_a - x_p)^2}{x_p} \tag{4.28}$$

where x_a is the measured value, x_p is the proposed model value, $\overline{x_a}$ and $\overline{x_p}$ are the means of the measured and proposed model values, and N is the measurement sample size. The Chi-Square test in this study is used to determine the difference between estimated model results and measurement. Thus, the null hypothesis states that the measured data follows the GM distribution, whereas the alternative hypothesis states that the observed data differs from the GM distribution. The significance level is set at 5%, thus a p-value of < 0.05 means the null hypothesis is rejected and thus concludes that the observed data does not fit the GM distribution. Otherwise, if the p-value is > 0.05, the null hypothesis is true, and therefore the measured data is consistent with the proposed model distribution results.

4.4 Results and Discussion

The main characteristics of impulsive noise are the amplitude, width, and inter-arrival time. The proposed model seeks to improve the understanding of PLC noise by investigating the impulsive noise amplitude characteristic. In this chapter, the measurement data used to validate the proposed model is obtained from four different locations: CL, PGO, Apartment and ML. The measured data is divided into three categories based on peak-to-peak (p-p) voltage: low, medium, and very impulsive. The low, medium, and highly impulsive noise ranges are $(0 \leqslant y \leqslant 0.25\ V_{p-p})$, $(0.25 < y \leqslant 2)\ V_{p-p}$, and $(y > 2)\ V_{p-p}$, where the impulsive noise in CL was determined to be low, whereas the PGO and the Apartment fall under the medium impulsive category. The PLC in the ML, on the other hand, was found to be highly impulsive. The PDF for each category was estimated using two components ($q = 2$), three components ($q = 3$), and four components ($q = 4$) GM model.

The performance of each GM model is analysed using the correlation coefficient, RMSE and the χ^2 statistic for each measured data. In Fig. 4.3, the $q = 4$ Gaussian mixture exhibits a fair correlation with the measured data. The correlation coefficient values range from 0.9857 to 0.9897, with the maximum correlation observed for the four-component Gaussian mixture model. Consequently, there is a strong correlation between the estimated and observed data, with all values higher than 0.98. As the number of components decreases, the peak height increases, as observed in Fig. 4.3. Table 4.1 presents a summary of correlation coefficients and RMSE values. The four-component GM model outperforms the other two models with an RMSE of 0.1716 as compared to 0.1842 and 0.1821 for the two and three-component GM models in Measurement 1. Figure 4.4 shows that the projected density contour closely follows the measured data at $q = 4$ and $q = 3$. When

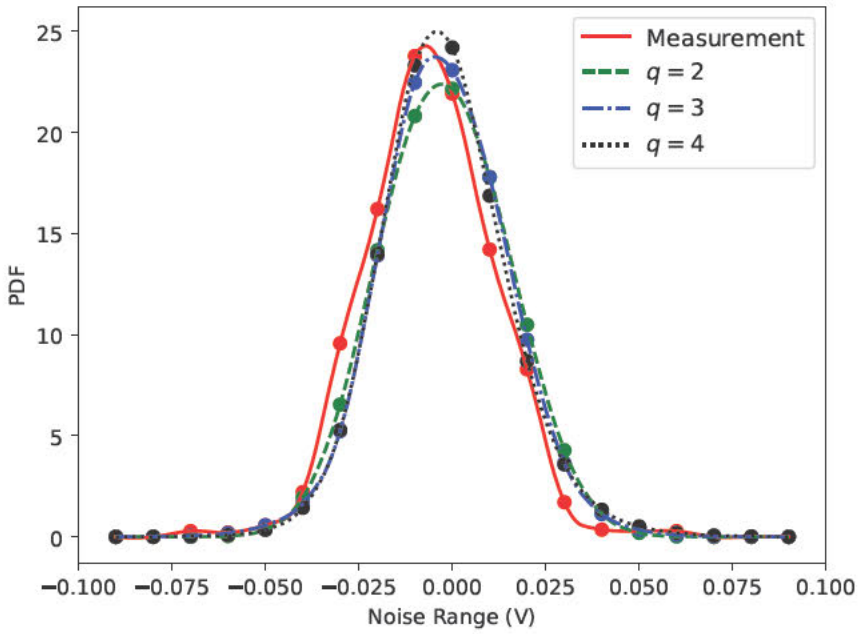

Figure 4.3: Low Impulsiveness: Measurement #1

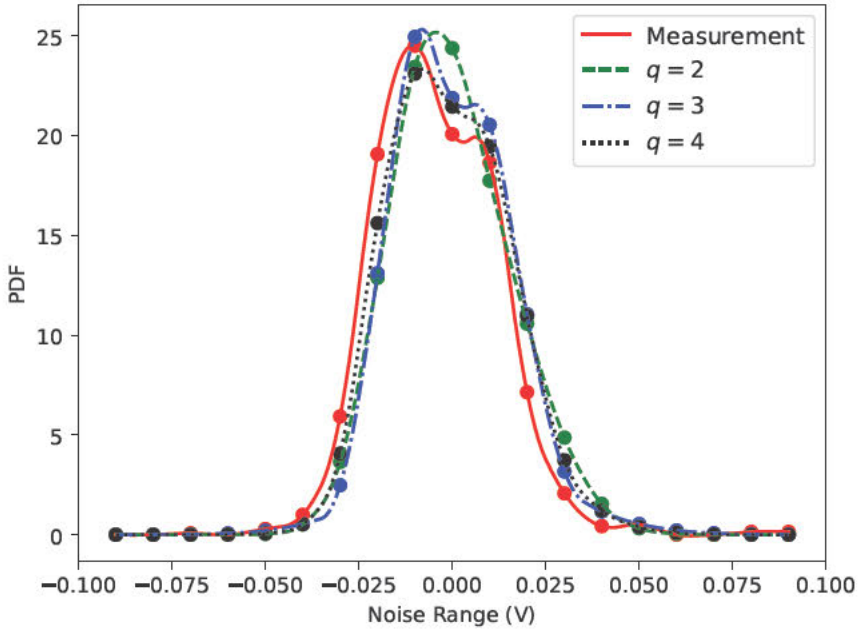

Figure 4.4: Low Impulsiveness: Measurement #2

$q = 2$, there is no notch between the two peaks, as in the three- and four-component GM models. It can be observed from Table 4.1 that for measurement 2, the two-component GM has a lower correlation than the other models, with a value of 0.9761. In terms of accuracy, the RMSE values range from 0.1653 to 0.2463, with $q = 4$ having the lowest RMSE value. All of the models in this case are highly correlated with the measured data.

Table 4.1: Low Impulsiveness

Computer Lab						
	Measurement #1			**Measurement #2**		
Model	$q = 2$	$q = 3$	$q = 4$	$q = 2$	$q = 3$	$q = 4$
R	0.9857	0.986	0.9897	0.9761	0.9801	0.9893
RMSE	0.1842	0.1821	0.156	0.2463	0.2246	0.1653

In both cases, the three-component GM model correlation coefficient and RMSE values are between that of $q = 2$ and $q = 4$. From Figs. 4.3 and 4.4, it can be observed that the measured PDF for the CL is free of outliers induced by high-amplitude impulse noise. The computers in this location use switched-mode power supplies, which have been linked to low-amplitude impulsive noise [25]. Fluorescent lights in the CL, on the contrary, have been linked to higher impulse noise levels [25, 95], resulting in increased amplitude.

In the medium impulsive noise category, the GM models at $q = 2$, $q = 3$, and $q = 4$ overlap, as depicted in Fig. 4.5 and Fig. 4.6. The likelihood function for each q-component GM model yields the same density distribution in this case. Furthermore, the correlation coefficients are equal for $q = 2$ with $R = 0.9718$ and $q = 4$ with $R = 0.9726$ for the two measurement data, as summarised in Table 4.2. The correlation coefficient differs slightly at $q = 3$. This could be due to the presence of impulsive noise with similar amplitude levels when the measurement is made in the same location. However, the RMSE values vary, with the RMSE values for Measurement 1 ranging between 0.1875 and 0.1849, whereas for Measurement 2, the values are between 0.1935 and 0.1908. Table 4.2 summarises the correlation coefficients and RMSE values for medium impulsive noise.

Table 4.2: Medium Impulsive

Post-Graduate Office						
	Measurement #1			**Measurement #2**		
Model	$q = 2$	$q = 3$	$q = 4$	$q = 2$	$q = 3$	$q = 4$
R	0.9718	0.9725	0.9726	0.9718	0.9723	0.9726
RMSE	0.1875	0.1852	0.1849	0.1935	0.1918	0.1908
Apartment						
Measurement						
Model	$q = 2$	$q = 3$	$q = 4$			
R	0.9877	0.9828	0.9871			
RMSE	0.2875	0.3400	0.2950			

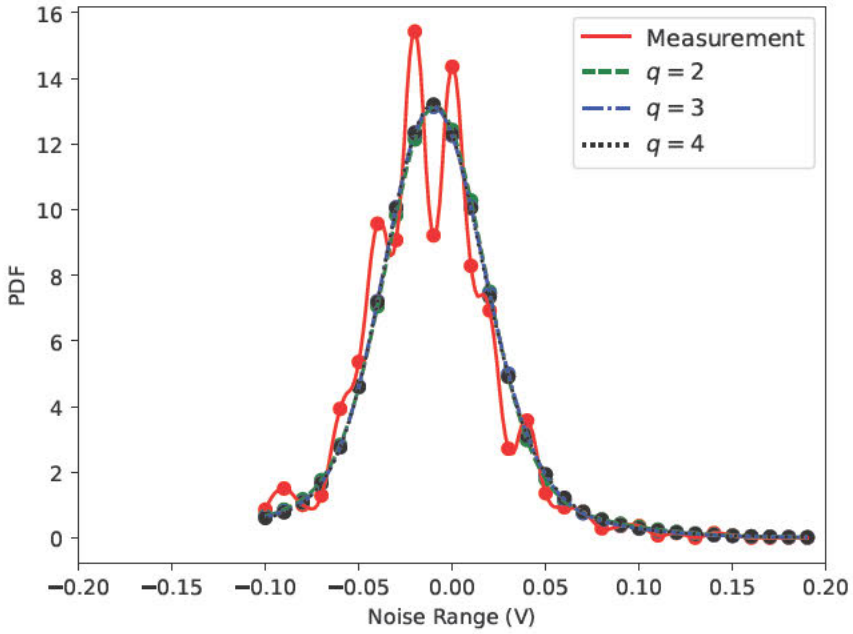

Figure 4.5: Medium Impulsive: Measurement #1

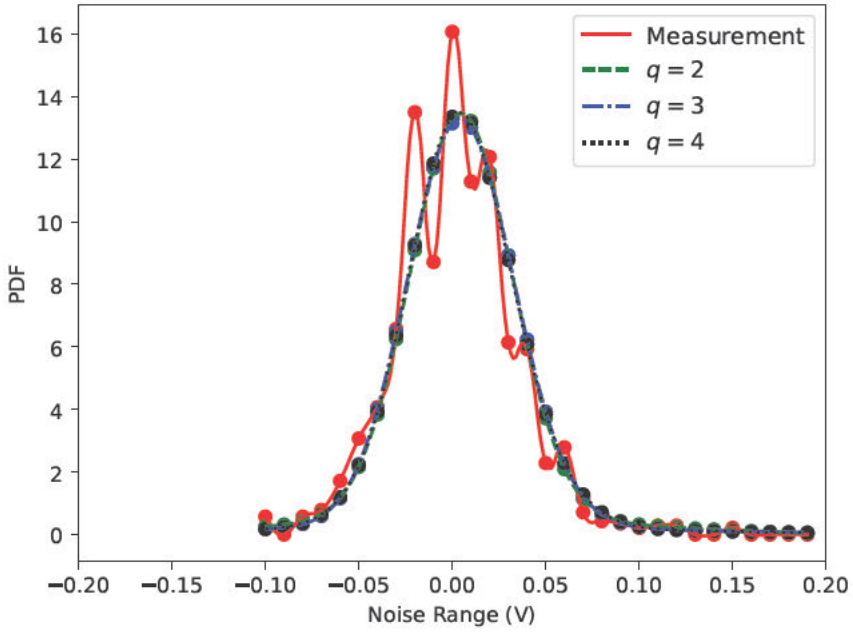

Figure 4.6: Medium Impulsive: Measurement #2

Fig. 4.7 shows the density distribution of impulsive noise measured in an apartment. In this case, there is a singularity where one of the several component models has collapsed. Thus, the GM density increased with each iteration. The parameters were determined through regression analysis, and the iteration with the best maximum likelihood estimates was used to model the PDF. It was observed that the two-component GM model yields

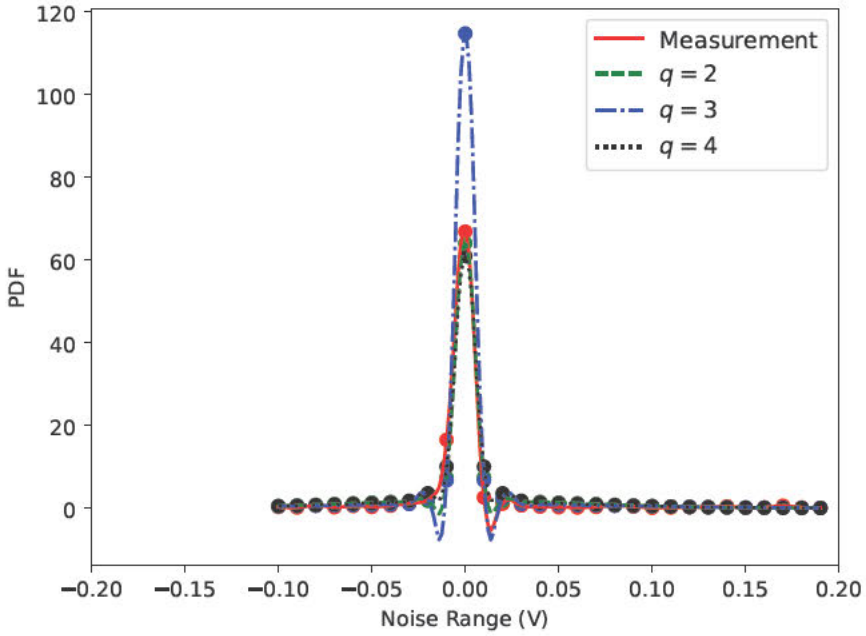

Figure 4.7: Apartment: Medium Impulsive

the best estimate with a correlation coefficient of 0.9877, followed by the $q = 4$ component model with $R = 0.9871$, whereas the $q = 3$ model has the lowest correlation coefficient of 0.9828. All of the R-values are, however, high, which indicates a significant correlation between the measured data and the GM model densities. Fig. 4.5 and Fig. 4.6 show spikes at peaks in measured amplitude distributions from the PGO. Fluorescent lights, electric kettles, heavy-duty printers, and air conditioning units, among other appliances, generate high levels of impulsive noise due to silicon-controlled rectifiers, rectifier diodes, and other

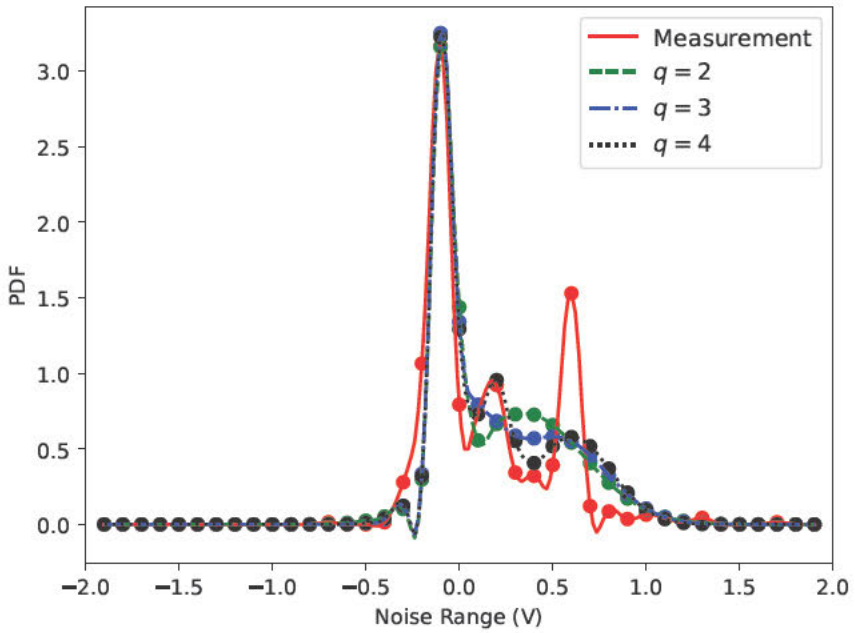

Figure 4.8: Highly Impulsive: Measurement #1

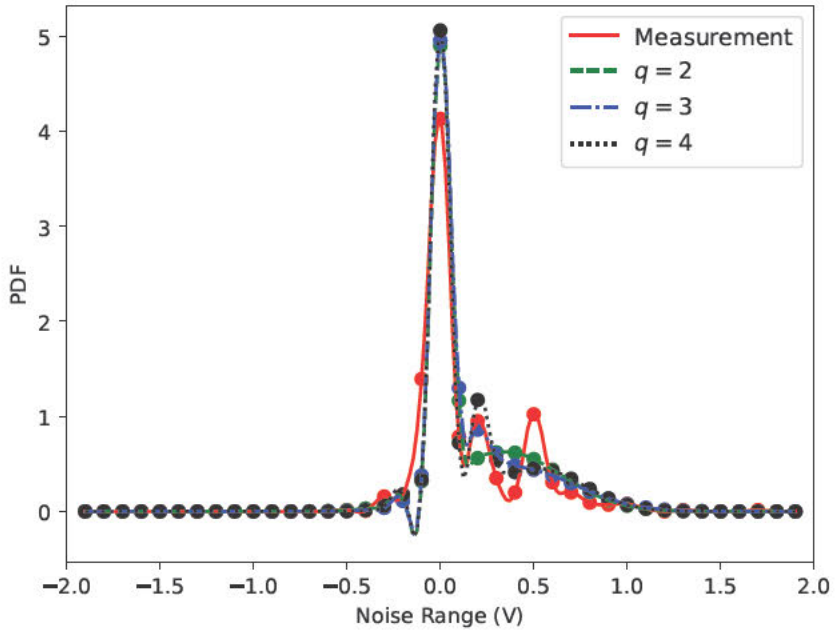

Figure 4.9: Highly Impulsive: Measurement #2

power-electronic switching devices [25, 100]. Figures 4.7, 4.8 and 4.9 show measurements from an Apartment and ML, demonstrating similar observations.

Fig. 4.8 and 4.9 depicts the results for the highly impulsive category. The PDF is observed to possess a number of peaks, with the highest peak occurring at zero. In Fig.4.8,

Table 4.3: Highly Impulsive

Machines Lab						
	Measurement #1			Measurement #2		
Model	$q = 2$	$q = 3$	$q = 4$	$q = 2$	$q = 3$	$q = 4$
R	0.916	0.9282	0.9334	0.9531	0.9571	0.9586
RMSE	0.0427	0.0397	0.0382	0.0378	0.0362	0.0355

the shape of the PDF is better defined at the $q = 4$ model, followed by the $q = 3$ model. There are two peaks at $q = 2$, with the second peak not occurring near the mean of the second component distribution. The R-values in this case, increase as the number of components in the Gaussian mixture increases, as shown in Table 4.3, with the maximum correlation coefficient at $q = 4$. The RMSE values, on the other hand, decrease as the number of components increases, with measurement 2 having the lowest RMSE value of 0.3550. A higher number of components in this category results in a better fit. This can be attributed to the multi-modal characteristic observed. The model density distribution becomes more defined and closer to the measured density as q increases.

The χ^2 statistical test results for the low, medium and highly impulsive categories are summarised in Table 4.4. The CL χ^2 values are observed to be below the critical values for both Measurements 1 and 2. As the number of components in the GM model increases, the χ^2 value reduces. The $q = 4$ GM model offers a better fit than the $q = 3$ and $q = 2$ models. Furthermore, the p-values are greater than 0.05, indicating that the data fits the proposed model. The PGO data has χ^2 values ranging from 7.522 to 7.9027, which are less than the crucial value of 36.4150, supporting the null hypothesis. The p-values are greater than 0.05, indicating that the data is consistent with the GM distribution. It can also be seen that a better fit is obtained as q increases. The apartment data showed a strong correlation and low RMSE values. However, the χ^2 values for the $q = 2$ and $q = 4$ models were lower than the crucial threshold, supporting the null hypothesis.

Table 4.4: χ^2 Test

Computer Lab					
	Model	χ^2	**P value**	**df**	**Critical Value**
Measurement #1	$q = 2$	9.4927	0.6603	12	21.0260
	$q = 3$	7.1429	0.8480		
	$q = 4$	6.9873	0.8584		
Measurement #2	$q = 2$	10.9882	0.3588	10	18.3070
	$q = 3$	10.5123	0.3967		
	$q = 4$	5.5325	0.8528		
Post-Graduate Office					
	Model	χ^2	**P value**	**df**	**Critical Value**
Measurement #1	$q = 2$	7.9027	0.9991	24	36.4150
	$q = 3$	7.6701	0.9998		
	$q = 4$	7.5227	0.9998		
Measurement #2	$q = 2$	6.6179	0.9996	24	36.4150
	$q = 3$	7.8061	0.9992		
	$q = 4$	7.7434	0.9993		
Apartment					
	Model	χ^2	**P value**	**df**	**Critical Value**
Measurement #1	$q = 2$	33.8929	0.2851	30	43.7729
	$q = 3$	44.6812	0.0413		
	$q = 4$	30.0886	0.4611		
Machines Lab					
	Model	χ^2	**P value**	**df**	**Critical Value**
Measurement #1	$q = 2$	5.6529	0.9952	17	27.5871
	$q = 3$	4.9463	0.9979		
	$q = 4$	5.2042	0.9971		
Measurement #2	$q = 2$	5.2649	0.9969	17	27.5871
	$q = 3$	4.7111	0.9984		
	$q = 4$	5.0569	0.9976		

4.5 K-means Initialisation

As previously discussed, the EM approach is well recognised for its excellent accuracy and plays an important role in mixture model parameter estimation, and it is commonly used to generate maximum likelihood estimates [107–109]. It has been shown, however, that the EM algorithm's final parameter estimations are heavily dependent on its initial values and are susceptible to locally optimum solutions [107–109] since there are no known true solutions or global optimums. Thus, poor starting values may lead to poor parameter estimation, which can lead to poor performance in density estimation, clustering, and other mixed model applications [109]. As a result, appropriate initial parameter estimations to initialise the EM algorithm are required.

The agglomerative hierarchical clustering (AHC), sum scores, iteratively constrained EM algorithm (ICEM), random initialization, and the K-means approach are some of the initialization procedures for the EM algorithm that have been proposed [107]. The AHC method begins with a hierarchical cluster analysis, followed by splitting the number of clusters chosen. These clusters are then used to determine the starting parameters of the EM algorithm. This method is suited for data that is organised hierarchically although the accuracy of classifications based on this type of cluster analysis has been disputed by some researchers [107]. In regards to the sum scores strategy, data is split into clusters with an equal number of samples after computing the total score of each data point. The cluster settings are then utilised to initialise the EM. Although this method is quick and simple to apply, the clusters will be inaccurate if they are not sorted by increasing means [107]. As for the ICEM algorithm strategy, it entails executing a series of successively limited EM algorithms to narrow the search space for the global optimum. The premise is that the random value with the greatest likelihood will yield a better solution than the other random values used to initialise the EM method. However, because of the number of initial-stage EM algorithm that are run, this technique has a longer calculation time. Furthermore, the number of iterations in the first stage of the EM must be specified, which may or may not be sufficient for particular likelihood functions.

The dataset is divided into C clusters (components) each with the same amount of observations. As a result, all components will have the same weight in the combination in the random initialisation approach. The initial means and variances from the samples in the specified clusters are then analysed [107]. The random initialisation approach is used in Section 4.2.1 to predict the amplitude distribution for low-voltage PLC impulsive noise. Although random initialisation has been demonstrated to perform as well as or better than alternative initialisation approaches, the considerable prevalence of local optimal solutions in mixed models is a challenge [107]. This is because any two solutions produced by this procedure are likely to produce different results [107]. As a result, finding a solution involves a large number of random starts, which may be problematic because there is no known method for identifying the sufficient number of random starts required to get the optimal initialization. The K-means method divides the dataset into a number of clusters

and then assigns each data point to the cluster with the shortest sum of square distances from the cluster centre. As a result, data points with comparable features are clustered together in the same cluster.

In this section an alternative initialisation method based on the K-means technique is proposed to estimate the initial parameters of the EM algorithm, as it has been found to be a useful method of initialising, particularly the GM model, as it provides parameter estimates that are close to the final values, reducing the number of iterations and, as a result, the computation time [109].

4.5.1 K-means Formulation

Let Q be the number of clusters in a dataset D defined in Section 4.2. For each data point d_n, there is a corresponding set of binary indicator variables $z_{nq} \in \{0, 1\}$ that specifies which cluster a data point has been assigned to. As a result, $z_{nq} = 1$ when data point d_n belongs to cluster q, and zero otherwise. Thereafter, random samples equal to the number of clusters Q are selected and considered as the centres of each cluster denoted by ϕ_q for $\{q = 1, 2, ..., Q\}$. The data points are then assigned to clusters based on the minimal sum of square distance (R) between the data point and the cluster centre, defined by [111]:

$$R = \sum_{n=1}^{N} \sum_{q=1}^{Q} z_{nq} || \ d_n - \phi_q \ ||^2 \tag{4.29}$$

The means of the samples within each cluster are then determined, resulting in 'new' cluster centres, and the procedure is reiterated until convergence. As a result, each cluster has a number of samples that possess comparable properties. The K-means clustering can be summarised as follows:

1. Randomly select n samples $d_1, d_,..., d_n$, corresponding to the set number of clusters. These will be the cluster centres for the whole data set.

2. Determine the sum of the squares of the distances of each data point to the cluster centres, and assign the data point to the closest cluster.

3. Evaluate the sample mean of each cluster. This gives rise to the new cluster centre.

4. Check for convergence of the parameters. If the convergence criterion is satisfied stop the iteration otherwise return to Step 2.

The final values of the K-means algorithm, that is, the mean, variance and the number of samples in each cluster are then used to initialise the EM algorithm.

4.5.2 Results and Discussion

The previous section addressed the effect of the number of components on the PLC impulsive noise amplitude distribution density. The fit of the GM model for measurement improved as the number of components increased. Furthermore, a Gaussian MM with more components captured multiple peaks in the PLC noise amplitude distribution density better. However, the fitting accuracy between the 2, 3, and 4-component GM model was minimal. As a result, the two-component GM model (the most basic form of the GM) is used to assess the performance of the GM model when the K-means clustering methodology is employed to initialise the parameters of the EM algorithm in this study. The performance of K-means initialised Gaussian MM (KGMM) was compared to the Gaussian MM initialised using the random initialisation approach (RGMM), as proposed in [114].

Figs. 4.10, 4.11 and 4.12 depict the amplitude distribution of PLC impulsive noise in the Apartment, PGO, and ML, respectively. Except for the Apartment, where the RGMM peak is greater than that of the KGMM, the KGMM and RGMM curves are observed to superimpose in all cases. It can be observed in Fig. 4.10 that both models exhibit heavy tails, with the RGMM capturing the peak of the measured distribution. It is also observed that the PDF curve is fairly smooth, with only one peak at zero. In the PGO PDF curve, however, the measured amplitude distribution contains spikes. This can be attributed to the loads such as heavy-duty printers, fluorescent lights, and air conditioners connected to the powerline network, which contain rectifier diodes, silicon-controlled rectifiers, and other power-switching devices that have been found to generate high impulsive noise levels [25].

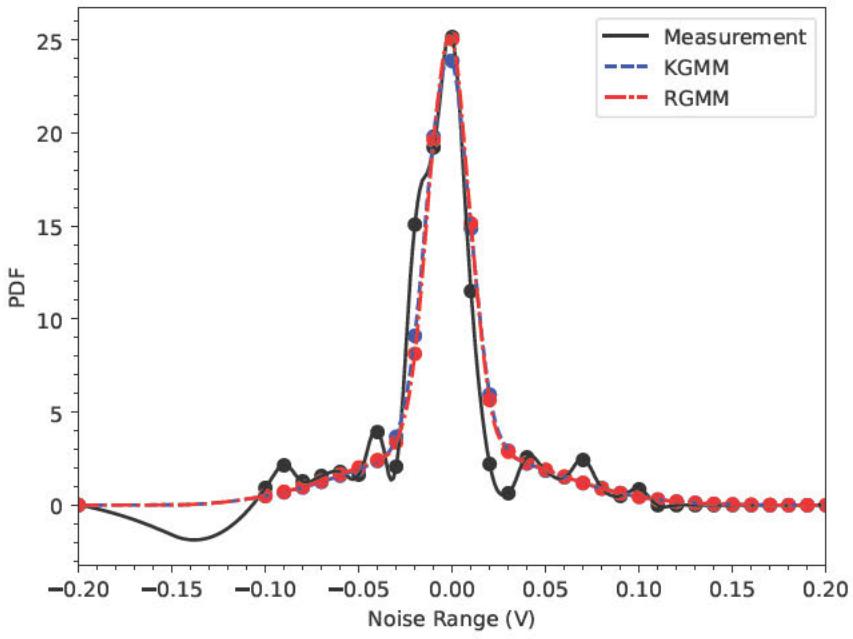

Figure 4.10: PLC Noise Data-Apartment

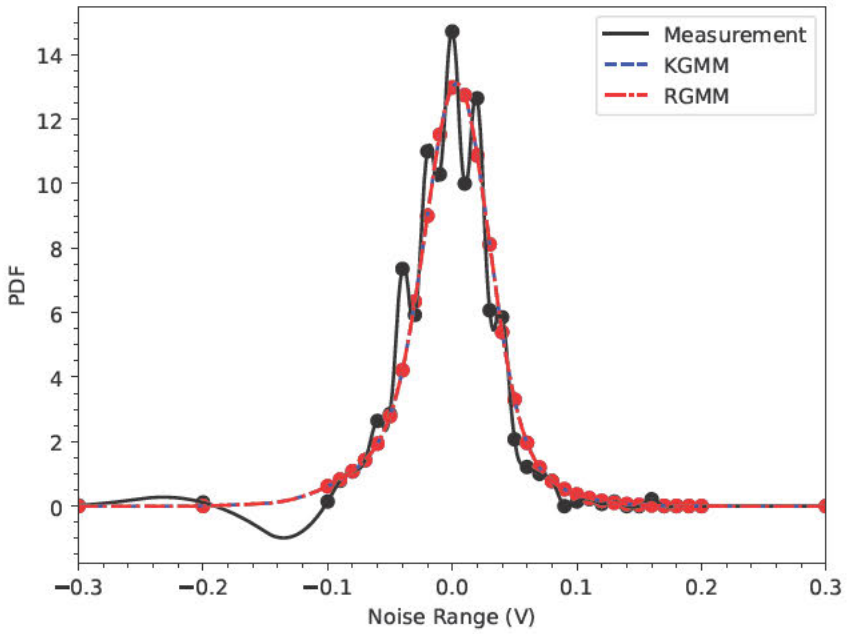

Figure 4.11: PLC Noise Data-Postgraduate Office

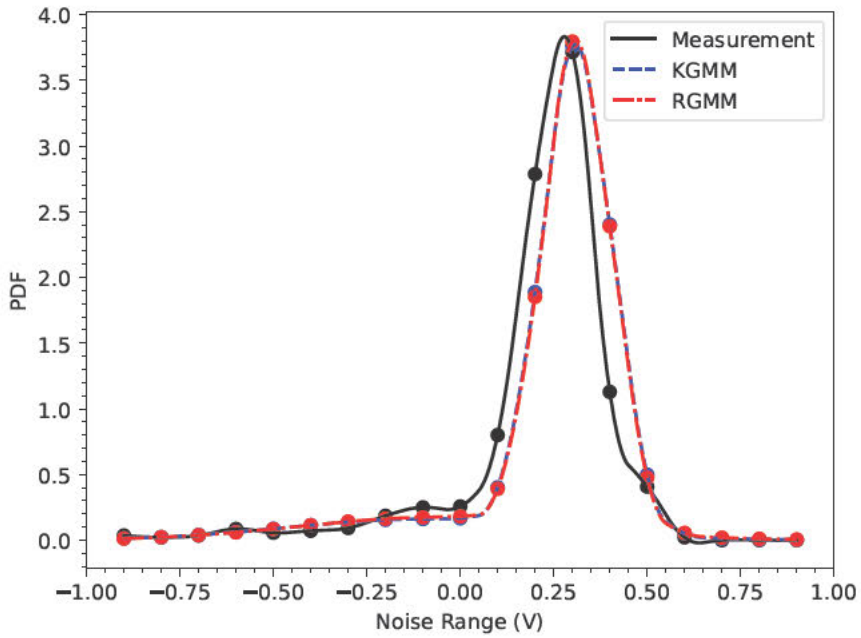

Figure 4.12: PLC Noise Data-Machines Laboratory

The ML measurement PDF is seen to have a smooth curve with a peak at $0.25V$.

Pearson's parametric correlation (4.26) and RMSE (4.27) tests were employed to assess the models' dependence and the goodness-of-fit in relation to the measurements in this study. The GM model is found to provide a good fit for all of the data under consideration.

Table 4.5 provides an overview of the performance analysis. For the Apartment and ML data, the KGMM outperforms the RGMM; however, the RGMM is more accurate for the PGO. In all locations, the Gaussian MM adequately estimates the PLC impulsive noise amplitude density, with the RMSE ranging between 0.0426 and 0.2484 for both initialization strategies. The performance difference between the K-means and random initialization approaches proposed in [114] is between 0.08 and 0.3%.

Table 4.5: Performance Analysis

	KGMM		**RGMM**	
	R	**RMSE**	**R**	**RMSE**
Apartment	0.9721	0.2358	0.9690	0.2484
Postgraduate Office	0.9749	0.1817	0.9752	0.1829
Machines Laboratory	0.9451	0.0426	0.9443	0.0429

4.6 Chapter Summary

In this chapter, the impulsive noise is determined to exhibit a very unpredictable behaviour in terms of amplitude, 'burstiness' and inter-arrival time. The estimated PDF accuracy is observed to improve with the increases in the number of Gaussian mixture components for each noise category. Except for the $k = 3$ component distribution of the measured PLC noise data for the Apartment, the proposed GM model distribution fairly fits measured data. This illustrates how singularity negatively affects the GM model performance, and hence, an alternative parameter estimation strategy can be used to enhance model performance. Furthermore, the GM model amplitude distribution of PLC noise is analysed using two initialization methods: the K-means algorithm and the random initialization technique. The K-means technique is observed to perform better than random initialization, although the difference is insignificant. As such, either initialisation method can be used to estimate Gaussian MM parameters.

Chapter 5

Application of Variational Bayesian Model for PLC Noise Modelling

5.1 Introduction

The key tasks in the GM model deployment are determining the model parameters and selecting the optimal number of components in the GM. The maximum likelihood estimate [116] approach presented in the previous chapter is the most often employed in statistical parameter estimation. This approach selects specific values for the model parameters that correspond to the local maximum of the likelihood function [116, 117]. The maximum likelihood estimates for missing data in parametric models are then determined using a two-step process referred to as expectation-maximization (EM). One problem with this technique is the occurrence of singularities in the likelihood function, which means that the maximum likelihood is not well-defined. This happens when one of the component parameters has the same value as one of the data points, resulting in infinite density at the data point's position [114, 117]. Furthermore, the maximum likelihood framework is known for its tendency to overfit data, which is made worse for complex models including high-dimensional data [117]. Another limitation is that it cannot be used to optimise the model structure since it prefers complex models such that as the number of parameters increases, a better fit is obtained [116, 117].

In order to mitigate the challenges encountered by the maximum likelihood technique, this chapter presents a Variational Bayesian (VB) framework that incorporates random parameters for the GM model. A fully Bayesian model considers a finite or infinite class of models rather than concentrating on a single model [116]. The posterior probability of each model is then determined given the dataset. The posteriors of each individual model are then averaged and weighted to provide predictions for the test data. The Bayesian framework prevents over-fitting and has high generalisation capabilities by integrating the parameters, [116,118]. Furthermore, complex models are automatically penalised by being assigned a lower posterior probability resulting in optimum structures [116].

This chapter employs the VB framework for modelling PLC impulsive noise. The PLC noise is viewed as a superposition of noise components, and hence the GM model is utilised to model the amplitude distribution. The GM model's parameters, namely the mixture weights, means, and precision, are calculated via Bayesian inference and are thus allocated conjugate prior distributions. The variational expectation maximisation framework is then used to calculate the optimal number of components in each measurement data set as well

as the estimated posterior distribution.

5.2 Variational Bayesian Gaussian Mixture Modelling

The amplitude distribution of the PLC noise is considered to be independent and identically distributed (i.i.d.) in this approach, and is represented by a one-dimensional GM with K components. Thus, all the component parameters of the GM, including the means $\mu = [\mu_1, ..., \mu_k]$, precisions $\phi = [\phi_1, ..., \phi_k]$, and mixture weights $\pi = [\pi_1, ..., \pi_k]$, may be collectively expressed as $\theta := \{\pi, \mu, \phi\}$. Let y_n be the observed PLC noise amplitude at a particular time, where N is the number of samples at a given observation window, and that for each data point y_n, there is a latent variable z_n for $z = 1, .., N$ that indicates which component generated the n_{th} data point. Thus, the likelihood of data point x_n is defined by [111, 119].

$$p(x_n \mid \theta) = \sum_{k=1}^{K} \pi_k \left(\frac{\phi_k}{2\pi}\right)^{\frac{1}{2}} \exp\left(-\frac{\phi_k}{2}(x_n - \mu_k)^2\right) \tag{5.1}$$

where the mixing probabilities are subject to the constraint:

$$\sum_{k=1}^{K} \pi_k = 1 \tag{5.2}$$

and $0 \leqslant \pi_k \leqslant 1$. However, the mixture weights, means and precisions of the component Gaussian distributions are unknown. As such, the VB framework introduces prior distributions to the latent variables and parameters that have the same functional form as the Gaussian likelihood function. Consequently, the conjugate prior to the multinomial distribution $p(z_n \mid \pi)$ is Dirichlet given by [111, 119]:

$$p(\pi) = Dir(\pi \mid \lambda_0) = C(\lambda_0) \prod_{k=1}^{K} {\pi_k}^{\lambda_o - 1} \tag{5.3}$$

where λ_0, is the initial number of samples in each Gaussian component and is chosen to be the same for all the components in the GM and $C(\lambda_0)$ is the normalization constant for the Dirichlet distribution and is given by:

$$C(\lambda_0) = \frac{\Gamma(\sum_{k=1}^{K} \lambda_k)}{\prod_{k=1}^{K} \Gamma(\lambda_k)} \tag{5.4}$$

Similarly, the conjugate prior distribution over the means and precision is a Normal-Gamma distribution obtained as [111, 119]:

$$p(\mu, \phi) = \prod_{k=1}^{K} N(\mu_k \mid t_0, (s_0\phi_k)^{-1}) G(\phi_k \mid \alpha_0, \beta_0) \tag{5.5}$$

where t_0, s_0 are the initial hyper-parameters for the means, whereas α_0 and β_0, are the initial hyper-parameter values for the precision and the $G(\phi_k \mid \alpha_0, \beta_0)$ can be expressed as [119, 120]:

$$G(\phi_k \mid \alpha_0, \beta_0) = \frac{\phi_k^{\alpha_0 - 1} exp(-\frac{\phi_k}{\beta_0})}{{\beta_0}^{\alpha_0}\Gamma(\beta_0)} \tag{5.6}$$

Since the measured data is assumed to be i.i.d., the joint distribution of all the random variables conditioned on the number of clusters K can be determined as [111, 119, 120]:

$$p(X, Z, \pi, \mu, \phi) = p(\mu, \phi) \prod_{n=1}^{N} p(\pi) p(X \mid Z, \mu, \phi) p(Z \mid \pi) \tag{5.7}$$

where:

$$p(Z \mid \pi) = \prod_{n=1}^{N} \prod_{k=1}^{K} \pi_k^{z_{nk}} \tag{5.8}$$

and $p(\mu, \phi)$ in (6.4) can be re-written as [121]:

$$\begin{aligned} p(\mu, \phi) = \prod_{k=1}^{K} & \left(\frac{s_0 \phi_k}{2\pi} \right)^{\frac{1}{2}} \\ & \exp\left(\left(-\frac{s_0 \phi_k}{2} (\mu_k - t_0)^2 \right) \left(\frac{\phi_k^{\alpha - 1} \exp(-\frac{\phi_k}{\beta_0})}{{\beta_0}^{\alpha_0}\Gamma(\beta_0)} \right) \right) \end{aligned} \tag{5.9}$$

In order to determine the marginal likelihood (model evidence) $p(X)$, the joint distribution in (5.7) is marginalised with respect to π, Z, μ, ϕ.
The main tasks in the application of the GM model are to determine the true posterior distribution and to evaluate the possible number of components. The application of a fully Bayesian treatment implies that the posterior distribution is obtained as [111, 119]:

$$p(Z, \pi, \mu, \phi \mid X) = \frac{p(Z, \pi, \mu, \phi, X)}{p(X)} \tag{5.10}$$

It can be observed that solving for (5.10) involves a computationally intensive evaluation of multi-integrals for which expectations are analytically intractable. As such, the variational Bayes method is used to infer the posterior distribution for the mixture weights, means and precision where an approximate joint variational distribution $q(Z, \pi, \mu, \phi)$ is introduced.

5.2.1 Variational Approximation Framework

Let the set of all the latent variables and parameters be denoted by $\eta = [Z, \pi, \mu, \phi]$. Thus, the joint variational distribution will be given by $q(\eta)$ and the marginal log-likelihood of the observed data can be obtained as [111, 118]:

$$\log p(X) = \log \int p(X, \eta) d\eta \tag{5.11}$$

Multiplying both the numerator and denominator of (5.11) by $q(\eta)$, the marginal log-likelihood becomes:

$$\log p(X) = \log \int q(\eta) \frac{p(X,\eta)}{q(\eta)} d\eta \tag{5.12}$$

In order to find a solution $q(\eta)$ that provides a tight lower bound to the true posterior distribution, the Jensen's inequality is applied. Therefore, (5.12) becomes [111, 118]:

$$\begin{aligned} \log p(X) &= \log \int q(\eta) \left(\frac{p(X,\eta)}{q(\eta)} \right) d\eta \\ &\geq \int q(\eta) \log \left(\frac{p(X,\eta)}{q(\eta)} \right) d\eta = L_q(\eta) \end{aligned} \tag{5.13}$$

where $L_q(\eta)$ denotes the lower bound (or the negative free energy) of the marginal log-likelihood which can also be expressed as:

$$L_q(\eta) = \mathbb{E}_q(\log p(X,\eta) - \mathbb{E}_q(\log q(\eta)) \tag{5.14}$$

where $\mathbb{E}_q(.)$ denotes the expectation over all the variables. To measure the distance between the true posterior distribution and the approximate variational posterior distribution, the Kullback-Leibler(KL) divergence is employed. As such, the KL divergence between $p(\eta \mid X)$ and $q(\eta)$ is given by:

$$KL(q(\eta) \mid\mid p(\eta \mid X)) = \int q(\eta) \log \left(\frac{q(\eta)}{p(\eta \mid X)} \right) d\eta \tag{5.15}$$

From the product rule of probability, $p(\eta \mid X)$ can be defined as:

$$p(\eta \mid X) = \frac{p(X,\eta)}{p(X)} \tag{5.16}$$

Substituting (5.16) in (5.15), the KL divergence becomes [111]:

$$\begin{aligned} KL(q(\eta) \mid\mid p(\eta \mid X)) &= - \int q(\eta) \log \left(\frac{p(X,\eta)}{q(\eta)} \right) d\eta \\ &\quad + \log p(X) \\ &= - (\mathbb{E}_q(\log p(X,\eta) - \mathbb{E}_q(\log q(\eta)) \\ &\quad + \log p(X) \end{aligned} \tag{5.17}$$

Therefore,

$$KL(q(\eta) \mid\mid p(\eta \mid X)) = -L_q(\eta) + \log p(X) \tag{5.18}$$

Consequently, the variational log-likelihood can be obtained as:

$$\begin{aligned} \log p(X) &= L_q(\eta) + KL(q(\eta) \mid\mid p(\eta \mid X)) \\ &= \int q(\eta) \log \left(\frac{p(X,\eta)}{q(\eta)} \right) d\eta - \\ &\quad \int q(\eta) \log \left(\frac{p(\eta \mid X)}{q(\eta)} \right) d\eta \end{aligned} \tag{5.19}$$

Since the marginal log-likelihood $\log p(X)$ is independent of $q(\eta)$, maximizing the lower bound is equal to minimizing the KL divergence which occurs when $q(\eta) = p(X, \eta)$ and hence $KL(q(\eta) \,||\, p(\eta \mid X)) = 0$ [111]. Therefore, the main objective in variational Bayes is to minimise the KL divergence given by (5.18), which is equivalent to the maximization of the lower bound. As such, the lower bound will be as close as possible to the true posterior. Assuming that the approximating joint distribution factorises over the parameters and latent variables, $q(\eta)$ becomes [111, 120]:

$$q(Z, \pi, \mu, \phi) = q(Z)q(\pi)q(\mu, \phi) \tag{5.20}$$

where $q(Z)$, $q(\pi)$ and $q(\mu, \phi)$ are given by:

$$q(Z) = \prod_{k=1}^{K} \prod_{n=1}^{N} \gamma_{nk}{}^{z_{nk}} \tag{5.21}$$

$$q(\pi) = \Gamma(\sum_{k=1}^{K} \lambda_k) \prod_{k=1}^{K} \frac{\pi_k{}^{\lambda_k - 1}}{\Gamma(\lambda_k)} \tag{5.22}$$

$$q(\mu, \phi) = \prod_{k=1}^{K} N(\mu_k \mid t_k, (s_k \phi_k)^{-1}) G(\phi_k \mid \alpha_k, \beta_k) \tag{5.23}$$

Accordingly, the evidence lower bound in (5.14) can be determined as a functional over the parameters as [111, 120]:

$$L_q(\eta) = \mathbb{E}_q \left(\log \frac{p(Z, \pi, \mu, \phi, X)}{q(Z)q(\pi)q(\mu, \phi)} \right) \tag{5.24}$$

The explicit hyper-parameter values are then derived from estimating the log of the joint distribution and the lower bound optimised using a coordinate ascent algorithm analogous to the expectation-maximization.

5.2.2 Lower Bound Maximization

The log of the joint distribution can be obtained as [111, 120]:

$$\begin{aligned} \log p(Z, \pi, \mu, \phi, X) = &\log p(Z \mid \pi) + \log p(\pi) + \\ &\log p(\mu, \phi) + \log p(X \mid Z, \mu, \phi) \end{aligned} \tag{5.25}$$

Considering only the terms in the joint distribution that are associated with the latent variable and absorbing those independent of Z into the additive normalization constant, the optimal solution for the latent variables $q(Z)$ can be determined as:

$$\begin{aligned} \log q^{+}(Z) = &\mathbb{E}_{\pi}(\log p(Z \mid \pi) + \mathbb{E}_{\mu,\phi}(\log p(X \mid Z, \mu, \phi)) \\ &+ constant \end{aligned} \tag{5.26}$$

Substituting for $p(Z \mid \pi)$ and $p(X \mid Z, \mu, \phi)$, equation (5.26) can be further simplified as [111]:

$$\log q^{+}(Z) = \sum_{n=1}^{N} \sum_{k=1}^{K} z_{nk} \log \tau_{nk} + constant \tag{5.27}$$

where:

$$\begin{aligned} \log \tau_{nk} = \mathbb{E}_{\pi,\mu\phi} \left(\log \pi_k + \frac{1}{2} \left(\log \phi_k - \log 2\pi \right) \right) \\ - \mathbb{E}_{\pi,\mu\phi} \left(\frac{\phi_k}{2} (x_n - t_k)^2 \right) \end{aligned} \tag{5.28}$$

Evaluating (5.28) yields [119, 120]:

$$\tau_{nk} = \exp \left(\widehat{\pi_k} + \frac{\widehat{\phi_k}}{2} - \frac{1}{2} \left(\frac{1}{s_k} + \alpha_k \beta_k (x_n - t_k)^2 \right) \right) \tag{5.29}$$

where:

$$\mathbb{E}(\log \pi_k) = \psi(\lambda_k) - \psi(\bar{\lambda}) = \widehat{\pi_k} \tag{5.30}$$

$$\mathbb{E}(\log \phi_k) = \psi(\alpha_k) + \log(\beta_k) = \widehat{\phi_k} \tag{5.31}$$

$\mathbb{E}(\mu_k) = t_k$, $\mathbb{E}({\mu_k}^2) = {t_k}^2 \alpha_k \beta_k + \frac{1}{s_k}$ and $\bar{\lambda}$ is given by [111, 120]:

$$\bar{\lambda} = \sum_{k=1}^{K} \lambda_k \tag{5.32}$$

$\psi(.)$ represents the digamma function defined by $\psi(y) = \frac{d \log \Gamma(y)}{dy}$. Thus, the normalized $q^{+}(Z)$ can be obtained as:

$$q^{+}(Z) = \prod_{n=1}^{N} \prod_{k=1}^{K} {\gamma_{nk}^{+}}^{z_{nk}} \tag{5.33}$$

where γ_{nk}^{+} are the responsibilities for the variational approximation and are given by:

$$\gamma_{nk}^{+} = \frac{\tau_{nk}}{\sum_{j=1}^{K} \tau_{nj}} \tag{5.34}$$

For a discrete distribution, $\mathbb{E}(z_{nk}) = \gamma_{nk}^{+}$ [111]. To characterize the new posterior parameters, the following quantities are computed from the responsibilities:

$$N_k = \sum_{n=1}^{N} \gamma_{nk}^{+} \tag{5.35}$$

$$x_k^{+} = \frac{1}{N_k} \sum_{n=1}^{N} \gamma_{nk}^{+} x_n \tag{5.36}$$

$$s_k^{+} = \frac{1}{N_k} \sum_{n=1}^{N} \gamma_{nk}^{+} (x_n - x_k^{+})^2 \tag{5.37}$$

where (5.35), (5.36) and (5.37) represent the number of data points in component K, weighted data values and the weighted squared data values respectively. Similarly, considering only the terms in the joint distribution that are associated with the mixture weights and absorbing those independent into the additive normalization constant, the optimal solution for the mixture weights can then be obtained from (5.25) as:

$$\begin{aligned}\log q^{+}(\pi) =& \mathbb{E}_{\pi}\left(\log p(\pi) + \log p(Z \mid \pi)\right) + constant \\ =& \sum_{k=1}^{K}\left((N_k + \lambda_0)\log \pi_k - \log \pi_k\right)\end{aligned} \tag{5.38}$$

Hence, $q^{+}(\pi)$ is a Dirichlet distribution given by:

$$q^{+}(\pi) = Dir(\pi \mid \lambda) \tag{5.39}$$

and λ is a hyper-parameter given by:

$$\lambda_k = \lambda_0 + N_k \tag{5.40}$$

Solving for the optimal solution for the means and precision:

$$\begin{aligned}\log q(\mu, \phi) =& \mathbb{E}_{\mu,\phi}\left(\log p(X \mid Z, \mu, \phi) + \log p(\mu, \phi)\right) \\ &+ constant\end{aligned} \tag{5.41}$$

The corresponding hyper-parameters for the means (t_k, s_k) and precision (α_k, β_k), can then be given by [119, 120]:

$$t_k = \frac{1}{s_k}(t_0 s_0 + x_k^{+} N_k) \tag{5.42}$$

$$s_k = s_0 + N_k \tag{5.43}$$

$$\alpha_k = \alpha_0 + \frac{N_k}{2} \tag{5.44}$$

$$\frac{1}{\beta_k} = \frac{1}{\beta_0} + \frac{1}{2}\left(N_k {s_k}^{+} + \frac{s_0 N_k}{s_k}(x_k^{+} - t_0)^2\right) \tag{5.45}$$

The detailed derivations for the updated equations are illustrated in the Appendix A. In order to obtain the best family of variational distributions that maximize the lower bound, the variational expectation maximization (VEM) algorithm is employed and involves five steps as follows [116, 119]:

1. Initialize the mixing weights π by the number of clusters which also is a hyper-parameter. Then initialize means and precision from the measured data X. Consequently, compute the initial hyper-parameters a_0, b_0, α_0, β_0 and v_k for the prior distributions.

2. Variational expectation step: Evaluate the posterior probability γ_{nk} using the current hyper-parameters.

$$\gamma_{nk}^{+} = \frac{\tau_{nk}}{\sum_{j=1}^{K} \tau_{nj}} \tag{5.46}$$

where:

$$\tau_{nk} = \exp\left(\widehat{\pi_k} + \frac{\widehat{\phi_k}}{2} - \frac{1}{2}\left(\frac{1}{s_k} + \alpha_k \beta_k (x_n - t_k)^2\right)\right) \tag{5.47}$$

3. Variational maximization step: Re-evaluate the posterior hyper-parameters in two stages:

   – Compute the intermediate variables;

$$N_k = \sum_{n=1}^{N} \gamma_{nk}^{+} \tag{5.48}$$

$$x_k^{+} = \frac{1}{N_k} \sum_{n=1}^{N} \gamma_{nk}^{+} x_n \tag{5.49}$$

$$s_k^{+} = \frac{1}{N_k} \sum_{n=1}^{N} \gamma_{nk}^{+} (x_n - x_k^{+})^2 \tag{5.50}$$

   – Evaluate the new hyper-parameter values ;

$$\lambda_k = \lambda_0 + N_k \tag{5.51}$$

$$t_k = \frac{1}{s_k}(t_0 s_0 + x_k^{+} N_k) \tag{5.52}$$

$$s_k = s_0 + N_k, \tag{5.53}$$

$$\alpha_k = \alpha_0 + \frac{N_k}{2} \tag{5.54}$$

$$\frac{1}{\beta_k} = \frac{1}{\beta_0} + \frac{1}{2}\left(N_k s_k^{+} + \frac{s_0 N_k}{s_k}(x_k^{+} - t_0)^2\right) \tag{5.55}$$

4. Evaluate the average log-likelihood at iteration t as [118]:

$$\log_t p(X \mid \theta) = \frac{1}{N} \sum_{n=1}^{N} \log p_t(x_n \mid \theta) \tag{5.56}$$

5. Check for convergence of the log-likelihood by comparing the variation ϵ in the normalized log-likelihood. If the difference falls below a pre-defined value (0.01%), the process terminates otherwise return to step 2 [118].

$$\epsilon > \frac{\log_t p(X \mid \theta) - \log_{t-1} p(X \mid \theta)}{\log_t p(X \mid \theta)} \tag{5.57}$$

5.2.3 Model Order Selection

In machine learning techniques, determining the number of components needed in a mixture model is important because an excessive or insufficient number of components can lead to over- or underfitting of the measured data. Consequently, it leads to poor generalisation or prevents the model from assigning a high probability to data that is randomly selected from the same distribution as the training set [117, 118]. Consequently, extensive research in regards to modelling the PLC impulsive noise using mixture models with different number of components have been performed. In [31], the Middleton Class A model was modelled using a GM of up to five components. It was observed that the accuracy of the model also increases as the number of components increases. Comparable outcomes were also observed in [114], where the PLC impulsive noise was modelled using the GM model, which uses the maximum likelihood estimation approach to establish the optimal parameters. The two-, three-, and four-component GM models that were employed in this case automatically prune out the components that do not contribute to the GM by reducing their mixture weights to zero. Additional work on the number of components required to simulate the GM was conducted in [113], where the bit error rate of bursty impulsive noise in low-voltage PLC networks was estimated using the mutual information theory framework.

The most popular technique for estimating parameters in machine learning is the maximum likelihood framework [111], which selects a particular model parameter value that corresponds to a local maximum of the likelihood function. The maximum likelihood solutions are then obtained using the expectation-maximisation approach, and the result is that it does not provide guidance for determining the optimal number of components. This is because higher values enable the model to achieve a better fit to the training data and, as a result, assign higher likelihood function values to the observed data set.

The VB technique, provides a method for determining the number of components when training the model similar to the Bayesian Information Criterion (BIC). Let M represent a large number of model structures, and K represent the optimal model for a fixed number of components, where $K \in [2, M]$. Let $p(K)$ represent the prior distribution of the number of components, then [120]:

$$p(Z, \pi, \mu, \phi, X, M) = \prod_{K=1}^{M} p(Z, \pi, \mu, \phi, X \mid K) p(K) \tag{5.58}$$

where $p(Z, \pi, \mu, \phi, X \mid K)$ denotes the joint distribution defined in (5.7) since it is dependent on a fixed number of components K. From the VB methodology, the posterior distribution will be given by:

$$q(Z, \pi, \mu, \phi, K) = q(Z, \pi, \mu, \phi) q(K) \tag{5.59}$$

where the updates for $q(Z, \pi, \mu, \phi, K)$ conditioned on a specific K have already been defined in Section 5.2.1. Thus, it can be observed that the normalised posterior distribution $q(K)$

can be obtained as [119, 120]:

$$q(K) = \frac{\exp(Lq(\eta m)p(K))}{\sum_{K'}^{M} Lq(\eta m')p(K')} \tag{5.60}$$

where $Lq(\eta m)$ is the optimal lower bound for the K_{th} component mixture model. Choosing a uniform prior distribution $p(K) = \frac{1}{M}$, the the optimal posterior distribution becomes [119, 120]:

$$q(K) = \frac{\exp Lq(\eta m)}{\sum_{K'}^{M} Lq(\eta m')} \tag{5.61}$$

The lower bound in (5.24) can be re-expressed as [111, 119, 120] :

$$\begin{aligned} L_q(\eta) = \mathbb{E}_q \left(\log \frac{p(Z, \pi, \mu, \phi, X)}{q(Z)} \right) - \\ KL\left(q(\mu, \phi) \mid\mid p(\mu, \phi)\right) - KL\left(q(\pi) \mid\mid p(\pi)\right) \end{aligned} \tag{5.62}$$

Thus, the VB criterion in (5.62) compares to the BIC, where the first term corresponds to the average log-likelihood and the second and third terms correspond to the KL divergence between the approximate posterior and prior distributions. The KL divergence, therefore, acts as a penalty term that penalises complex models while the lower bound can be used exactly as a model selection criterion. The parameter posterior sharply peaks at the most likely values, which are also the ML values θ^+, as the number of samples increases. Consequently, as $N \to \infty$, the penalty term reduces to $\frac{h}{2} \log N$, where h is the number of parameters in the model and the lower bound becomes equivalent to the BIC given by [119, 122]:

$$BIC_{(K)} = \log p(X \mid \theta^+) - \frac{h}{2} \log N \tag{5.63}$$

Hence, the BIC emerges as a limiting case of the VB framework and in the case of the univariate GM model, the $BIC_{(m)}$ becomes [119]:

$$BIC_{(K)} = \sum_{n=1}^{N} \log \left(\sum_{k=1}^{K} \pi_k N(x_n \mid \mu_k, \phi_k) \right) - \frac{3K}{2} \log N \tag{5.64}$$

The number of components with the highest value of $BIC_{(K)}$ corresponds to the required value of K.

5.3 Results

Measurement results from various locations under varying loading situations were used to validate the VB model. Two data sets were used for each location, which include the ML, EL and the CL, to determine the PLC noise levels as well as their distribution over time. The optimum number of components must be established before using the VB framework to estimate the posterior distribution, which offers a tight lower bound, in order to choose the optimal model that fits the data. Performance analysis is then carried out to evaluate

the proposed model's significance and accuracy as well as compare its performance with the maximum likelihood estimation method.

5.3.1 Selection of Number of Components

The VB model provides a mechanism for determining the appropriate number of components, as stated in Section 5.2, where the lower bound is regarded as the Bayesian information criteria, while the KL divergence works as a penalty term penalising complex models. As the number of components increases, so does the KL distance between the priors and posteriors, causing the lower bound to diminish. In contrast, when the average log-likelihood increases, the lower bound also increases, resulting in a higher lower bound value. As a result, for a model to have a higher lower bound, its average log-likelihood must be greater than the KL distance. As a result, the VB criterion selects the simplest model, which implies the one with the fewest components that yet fits the measured data well. The most suitable model will thus be the one with the highest lower bound after accounting for model complexity, which indicates a high average log-likelihood and consequently a more appropriate fit.

Figures 5.1a and 5.1b show the optimal model selection results for EL sampled data. The value of the lower limit is observed to reduce as the number of components increases, with the two-component GM model yielding the highest lower bound. This is due to a lower increase in average log-likelihood as model complexity increases, as compared to the increase in KL distance. Figs. 5.2a and 5.2b indicate that the three-component mixture model has the highest lower bound value in both scenarios. On the other hand, it can be observed from Figure 5.2a, that the five-component GM has the lowest lower bound value. This can be attributed to a slight increase in the average likelihood, with a significant increase in the penalty term. In regards to Fig. 5.2b, the lower bound peaks at the three-component model and reduces with increasing model complexity. The maximum lower bounds for the PLC noise samples collected from the CL can be observed to occur at the two-component mixture model for the first data and the four-component model for the second data as shown in Figs. 5.3a and 5.3b respectively.

5.3.2 Impulsive Noise Amplitude Distribution

The optimum number of components for each location was determined in Section 5.3.1. The PLC noise amplitude distribution is then modelled using both the VB and maximum likelihood GM models. The model's predictions are then compared with the measured data. Figs 5.8 and 5.9 depict spikes in the probability density function (PDF) measurement data for the EL. In this scenario, the VB and maximum likelihood models are observed to superimpose and possess the same heavy tails as the measurement PDF. This may be due to the fact that as the number of samples increases, the VB inference converges to the maximum likelihood estimate [111].

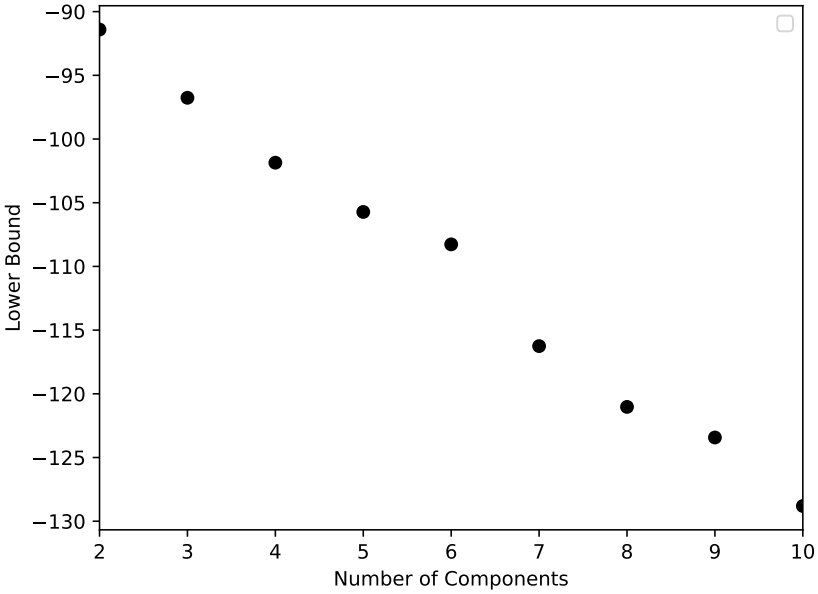

(a) Model order selection for data-1.

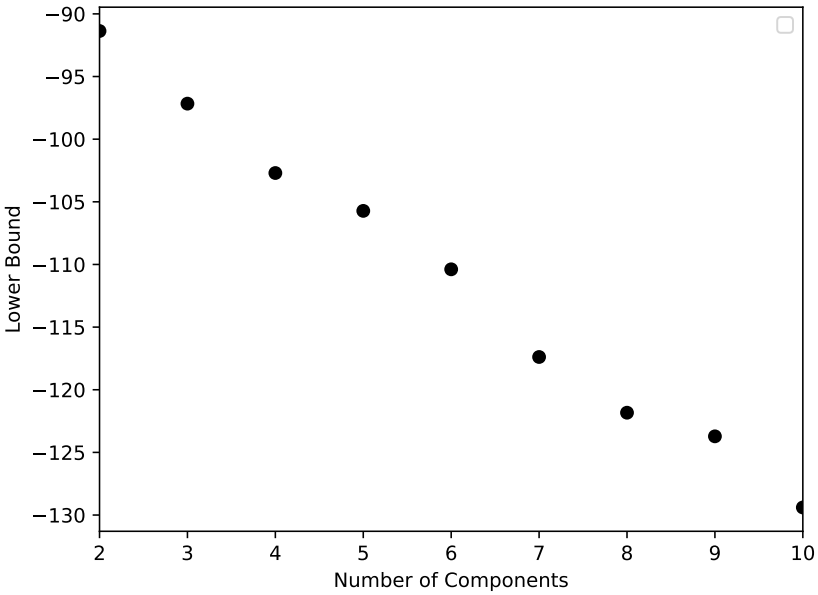

(b) Model order selection for data-2.

Figure 5.1: Electronic Laboratory.

Figures 5.4 and 5.5 present the PDF results for the ML model. The measured impulsive noise PDF is observed to possess a number of peaks, with the highest peak occurring at zero. The ML estimate presents the highest peak among the three PDFs, though the VB peak at zero is lower than the measurement data. In regards to the other peaks, the maximum likelihood estimate is observed to closely follow the measurement result when compared to the VB. This is owing to the maximum likelihood model's high level of flexibility. Furthermore, the VB model provides an approximation rather than an

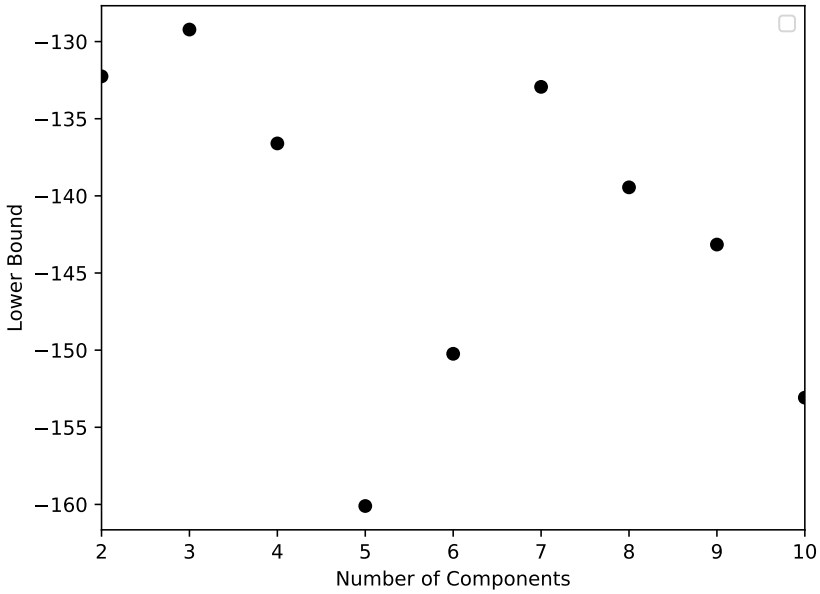

(a) Model order selection for data-1.

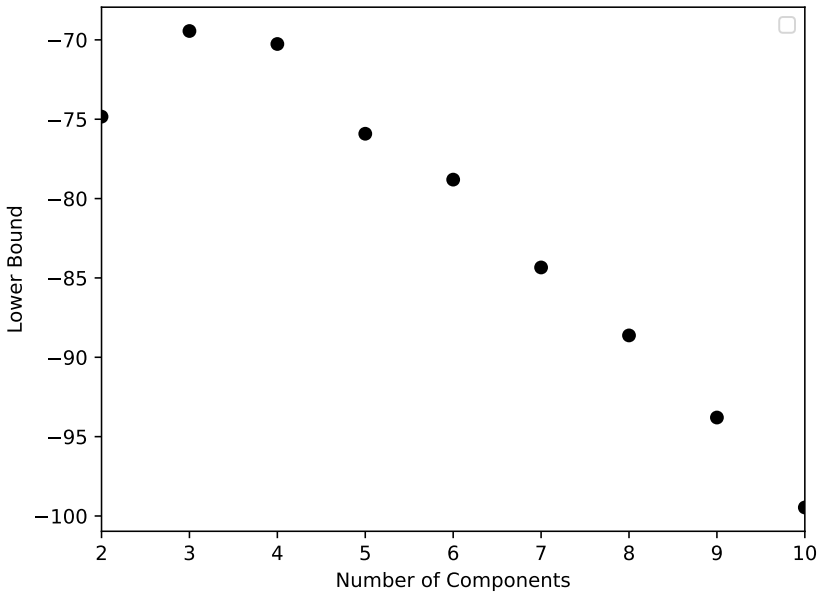

(b) Model order selection for data-2.

Figure 5.2: Machines Laboratory.

exact solution, resulting in the tightest lower bound for the measurement.

Figs. 5.6 and 5.7 depict the CL PLC noise amplitude distribution where the peak-to-peak voltage is low ranging between $(-0.1 \leqslant x \leqslant 0.1)V$. In Fig. 5.6, the VB and the maximum likelihood estimates peak at almost the same point and are lower than the peak of the measurement data. However, in Fig. 5.7, the maximum likelihood estimate has the highest peak width and the smallest width of the curve. The VB, though having a lower peak, has a wider curve that follows closely with the measured data. In both cases,

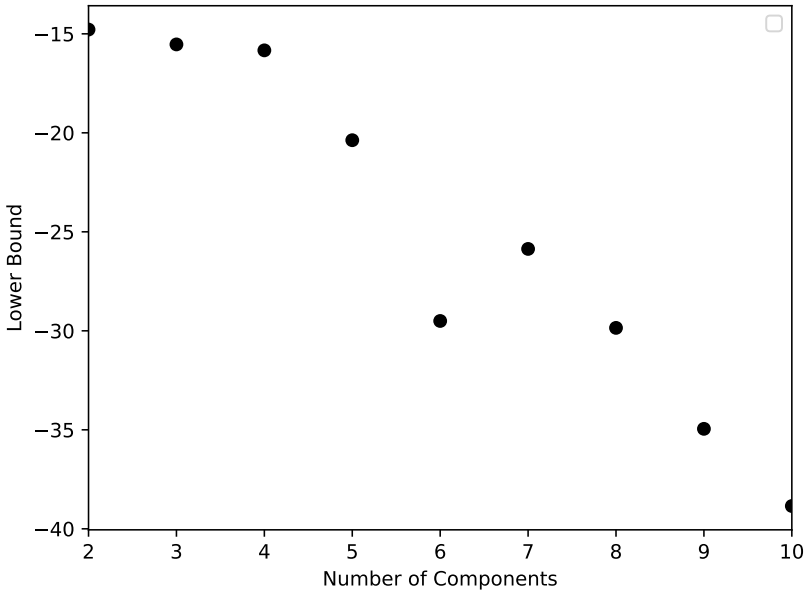

(a) Model order selection for data-1.

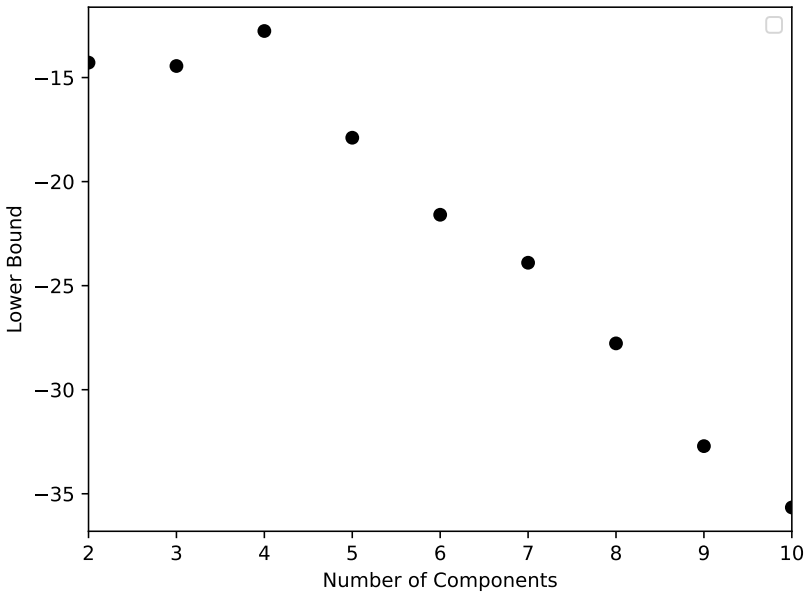

(b) Model order selection for data-2.

Figure 5.3: Computer Laboratory.

the PDF is smooth and is characterised by low amplitude and thus can be interpreted as background noise.

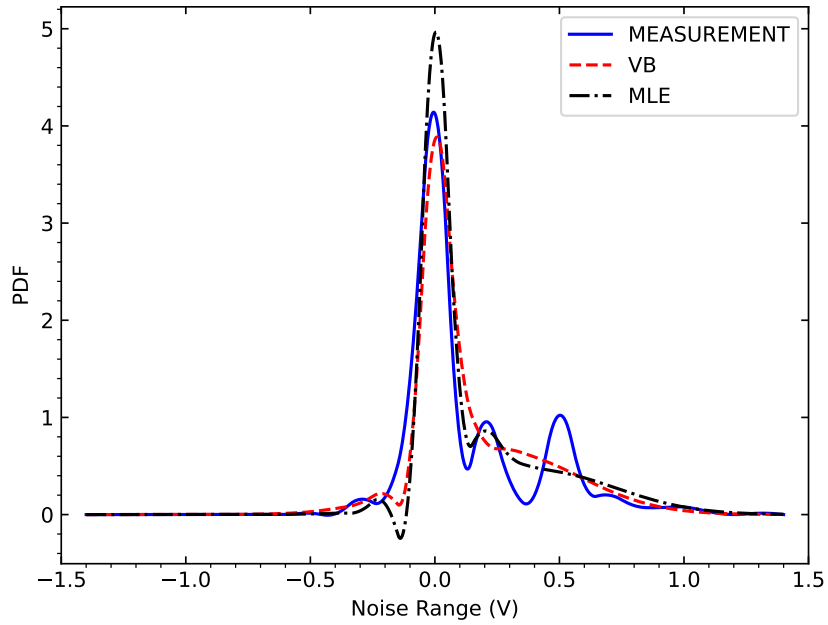

Figure 5.4: ML PLC Noise Distribution (data-1).

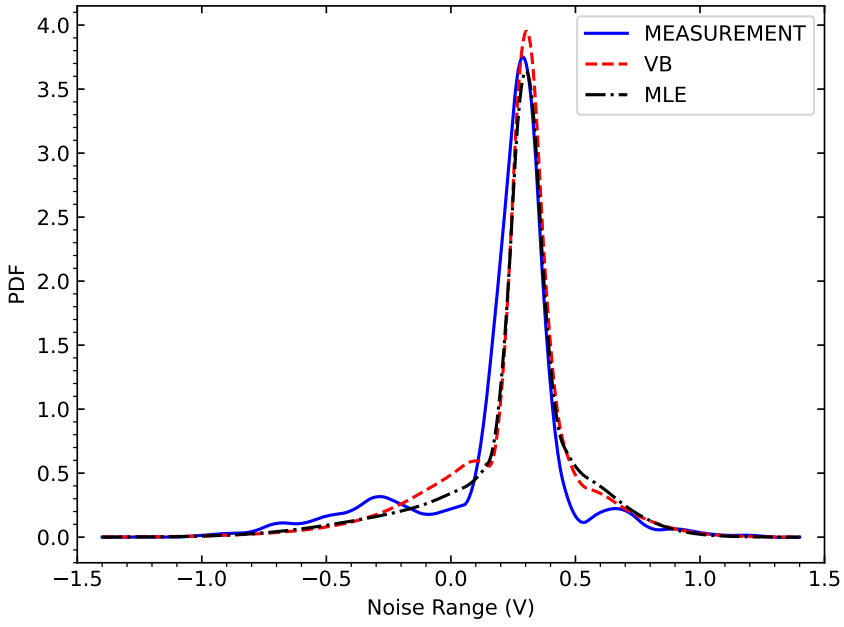

Figure 5.5: ML PLC Noise Distribution (data-2).

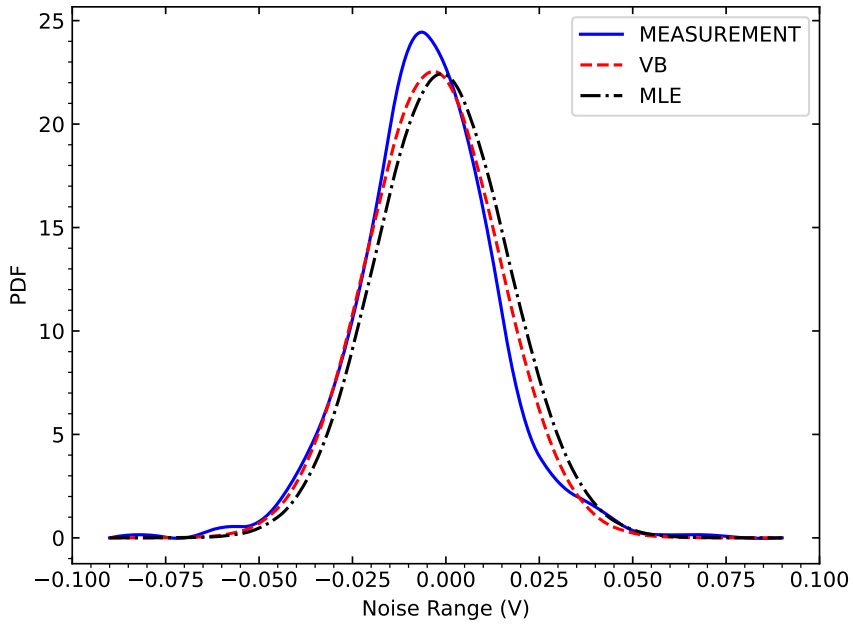

Figure 5.6: CL PLC Noise Distribution (data-1).

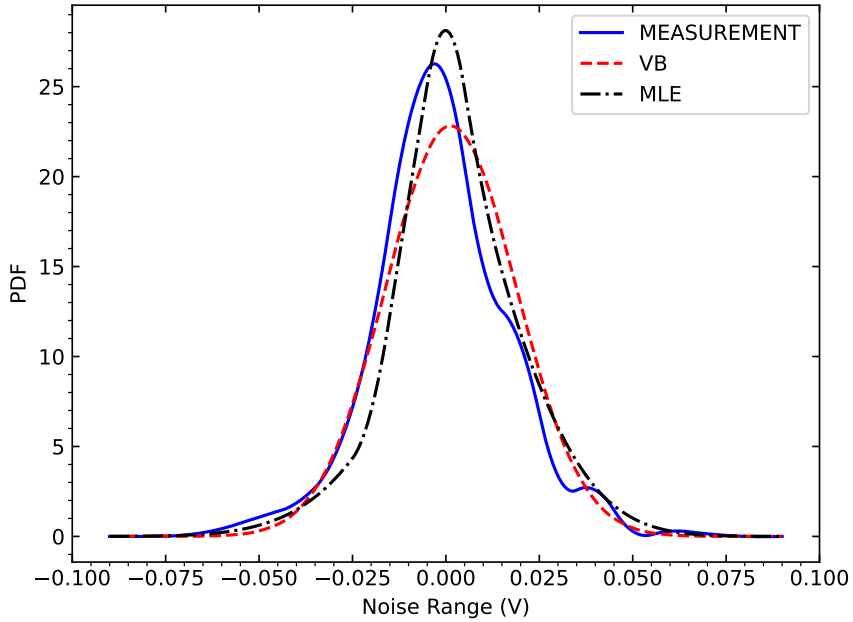

Figure 5.7: CL PLC Noise Distribution (data-2).

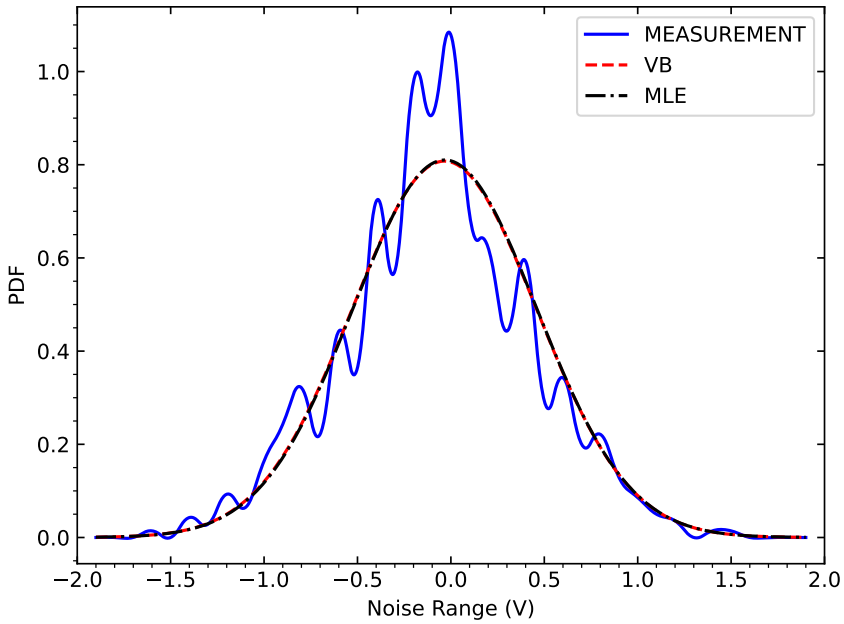

Figure 5.8: EL PLC Noise Distribution (data-1).

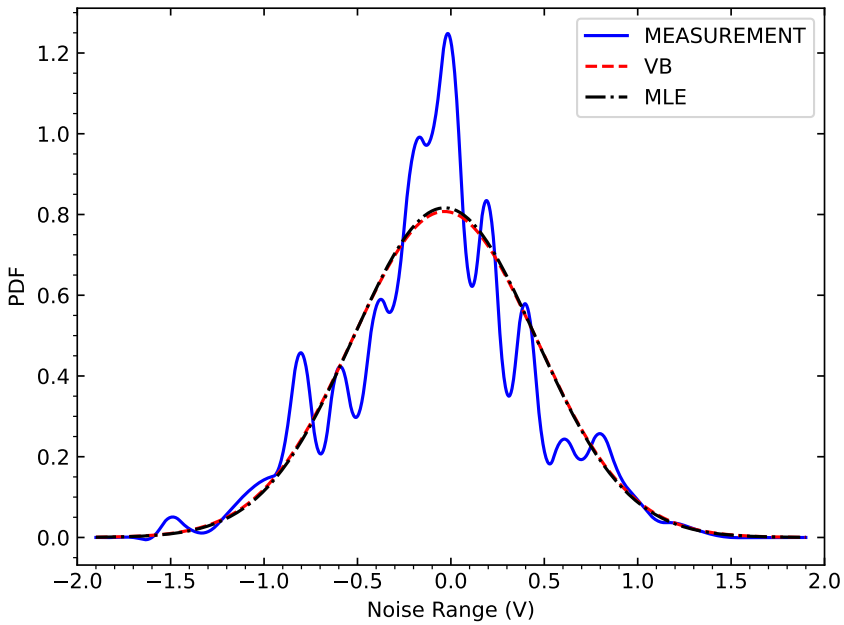

Figure 5.9: EL PLC Noise Distribution (data-2).

5.3.3 Perform Analysis

This study employs Pearson's parametric correlation (R) test to evaluate the degree of dependence between the observed data and the proposed model. The formulations defined

in (4.27), (4.28) for RMSE, correlation coefficient and the χ^2 statistic which was set to a significance level of 0.05 are used to validate the proposed model. The performance results are summarised Table 5.1. From Table 5.1, it can be observed that all measured data have correlation coefficients above 0.95, indicating that there is an adequate correlation between the maximum likelihood model, VB model, and the data. All of the χ^2 values are below the threshold values, and the RMSE values range from 0.0146 to 0.2554, indicating that the proposed model and the maximum likelihood (MLE) model both fit the data well. As a result, there is no significant difference between the density distribution obtained from the measured data and the VB model PDF. All of the models exhibit 95% confidence level consistent with the observed data. As a result, the amplitude distribution of the PLC noise can be effectively modelled using the VB model.

5.4 Discussion of Results

The sampled data acquired from various locations at the University of KwaZulu-Natal shows that the number of components required to represent the indoor PLC noise amplitude distribution ranges between two and four. It has been shown that as the number of components increases, so does the model's accuracy, with complex models outperforming simpler models when many peaks are present in the measurement. Fig. 5.4 shows that the maximum likelihood estimate model outperforms the VB model in capturing multiple peaks. This is because the maximum likelihood technique has a high degree of flexibility. However, the VB model is found to provide a good generalisation of the amplitude distribution of PLC noise in the ML.

The PLC noise perceived by the receiver is a combination of noise from numerous sources within the PLC network. In this scenario, PLC noise is considered to be independent and identically distributed, with a Gaussian distribution. Thus, the VB criterion aims to determine the optimal number of components that may have contributed to the observed noise. The noise amplitude distribution of the ML data shows three peaks in Figs. 5.4 and 5.5. This number of peaks corresponds to the expected value of the VB criterion, with the highest lower bound occurring at the three-component GM model. The four components chosen for the PLC noise amplitude distribution in the CL may be due to an overlap between the several components that make up the GM. Although

Table 5.1: Performance Analysis

			VB			**MLE**			
		K	**R**	**RMSE**	χ^2	**R**	**RMSE**	χ^2	**Critical Value**
EL	**Data-1**	2	0.9749	0.0146	0.6399	0.9557	0.0193	0.6511	43.773
	Data-2	2	0.9544	0.0202	0.5746	0.9548	0.02	0.5674	43.773
ML	**Data-1**	3	0.9503	0.0389	16.1014	0.9572	0.0362	6.793	31.4104
	Data-2	3	0.958	0.0349	2.361	0.9684	0.0303	1.8832	35.1725
CL	**Data-1**	2	0.9946	0.1125	8.1073	0.9835	0.1963	9.5279	27.5871
	Data-2	4	0.9724	0.2554	9.2498	0.9792	0.2225	7.8809	26.2962

the measured amplitude distribution for the EL has higher levels of impulsive noise and outliers, the two-component GM model is determined to be the best fit. In [114], it was observed that when the PDF of the amplitude noise has outliers, the likelihood of the model changes minimally as model complexity increases.

Comparable results were also observed in [123], where the first two to three components were found to accurately predict the PDF of the PLC impulsive noise amplitude using the Middleton Class A model. In [124], an extension of the Middleton Class A model with four terms was investigated, whereas in [31], five components were employed to approximate the PLC impulsive noise amplitude distribution with the Middleton Class A model. It was confirmed that increasing the number of components in the mixture results in a more accurate approximation. The same is observed in [114], where the two-, three-, and four-component GM components were applied in the modelling of the PLC impulsive noise where the ML technique was employed in parameter determination. In this study, the VB criterion has been utilised to determine the number of components required to adequately estimate the PDF of the PLC impulsive noise amplitude for a particular observation window from various locations under varying loading conditions. The two-, three-, and four-component GM models are shown to be sufficient for simulating the PLC impulsive noise amplitude distribution. In this study, the VB criterion has been utilised to determine the number of components required to adequately estimate the PDF of the PLC impulsive noise amplitude for a particular observation window from various locations under varying loading conditions. The two-, three-, and four-component GM models are shown to be sufficient for simulating the PLC impulsive noise amplitude distribution.

The measurement PDFs observed in the EL in Figs. 5.8 and 5.9 are seen to exhibit outliers. Similarly, the ML is characterised by high impulsive noise levels with multiple peaks, as shown in Figs. 5.4 and 5.5. As earlier mentioned, this may be attributed to the SCRs coupled with fluorescent lights that have been seen to contribute to high impulsive noise levels in broadband PLC. On the other hand, the CL exhibits low and smooth amplitude distribution levels as compared to those present in the EL and ML, as seen in Figs. 5.6 and 5.7. This is due to the computers at this location, which form the highest loads connected to the PLC network that utilise switched-mode power supplies, which have been observed to emit low-amplitude impulsive noise [25]. The time series analysis of the impulsive noise further confirms that the PLC noise amplitude PDF for the CL in Fig. 3.7a and 3.7b is lower than that for the EL and ML in Figs. 3.4a-3.5b, respectively.

5.5 Chapter Summary

The amplitude characteristic of the PLC impulsive noise, which is the main source of decreased performance and reliability of the PLC channel, has been modelled using the VB GM model. The proposed model provides a tractable and suitable estimation of the amplitude distribution of the PLC noise and does not suffer from the singularity present in the ML framework. Additionally, the proposed model provides a mechanism for model-

order selection as well as parameter estimation which are crucial in the application of the GM for modelling of the PLC noise. Although, the ML estimate model provides higher accuracy levels, the VB model provides a good generalization of the measurement data. It is, however, limited due to the fact that it provides an approximate solution rather than the exact solution since the aim is to maximise the lower bound. Despite this minor setback, the performance analysis results indicate that the VB model provides a good correlation as well as a high level of significance to the measured PLC noise data.

Chapter 6

PLC Impulsive Noise Analysis and Modelling: Queueing Theory Approach

6.1 Introduction

The type of impulsive noise determines the extent of distortion of the signal transmitted. Thus, impulsive noise in the electrical network is commonly classified as either a single-impulse (SI) or burst-impulse (BI) noise event depending on the duration, frequency content and shape of the impulse. However, no restriction is placed on the shape of the pulse [24,28,125]. The SI noise events are often similar in shape to a damped sinusoid, while a BI noise event takes the form of superimposed damped sinusoids [24,34]. Extensive research has been conducted on the amplitude distribution of the asynchronous impulsive noise in chapter 4 and chapter 5, hence, the primary focus of this chapter is to model the impulsive noise events service and inter-arrival time distribution.

Impulsive noise levels vary based on the electrical devices plugged into the PLC network. As a result, each indoor environment will display distinct PLC impulsive noise behaviour. The impulsive noise sources on the PLC channel are numerous and can thus be deemed infinite due to the numerous electrical devices that have been built and are still under development. The demand for electrical power is endless as there are electrical devices that require power to operate, and must therefore be fully plugged in for extended periods. Furthermore, while some of the PLC network's electrical devices are unplugged, others are connected. As a result, the PLC impulsive noise can be viewed as an infinite queue. The time series analysis of the occurrence and duration of the impulsive noise events can fully be described as a queueing system. The main parameters of a queueing system are the inter-arrival and service time distributions, the number of servers, the system capacity, the size of the sources that generate impulsive noise, and the queue discipline. These characteristics can be represented by the Kendall notation as $X/Y/Z/D/E/F$. If the queue discipline is first-in-first-out, and the system capacity and size of the sources are infinite, as is the case with PLC, the last three terms are omitted as they are automatically implied. Consequently, a PLC queueing system can be represented as an $X/Y/Z$ queue, denoting the inter-arrival time, service time and the number of servers, respectively.

The Markov chain model has been widely utilised in analysing the PLC impulsive

noise temporal correlation. In [33], the exponential distribution is employed in modelling the impulse noise inter-arrival time and the service time, where the Markov chain with two states is employed. From the impulsive noise measurements conducted in the PLC communication networks, it has been established that the durations and the inter-arrival time of the impulses result from a superposition of a number of exponential distributions [24]. As such, further analysis is performed in [24, 27], where a partitioned Markov Chain approach is employed to model the impulsive noise duration and inter-arrival time distribution. In this case, the impulse noise is divided into two groups, impulse-free and impulsive states, each group comprising transition states that are exponentially distributed. To find the elements of the transition matrices, curve fitting techniques are employed. The complementary probability distributions of the impulsive and the impulse-free times are then determined as the sum of weighted exponentials. The Hidden Markov Model was utilised to describe PLC impulsive noise in [126]. However, since the state transition could not be observed directly, a different set of stochastic processes was used to determine the impulse noise inter-arrival time and duration in the PLC network. To represent the burst events present in the PLC noise, a Markov Middleton model was employed in [30,126]. In the models discussed, the transitional probabilities for the various states are not observable and the limiting distributions were not taken into consideration. As such, the connection between the Markov Chain and the PLC statistical properties is investigated in [34]. The methods discussed in [27, 30, 33, 125, 126] also do not take into account the type of noise whether single-impulse or burst-impulse. Further, the duration and inter-arrival time distribution for the various impulsive noise events are modelled in [34], where the log-normal, Gamma and Weibull distributions are proposed for the duration, and exponential distribution is proposed for the inter-arrival times.

In this work, an alternative method based on the queueing theory approach is proposed for modelling the inter-arrival and service time distributions of impulsive noise in the PLC network. The queueing theory approach fully describes the PLC impulsive noise time series characteristics including the interconnection between the PLC noise characteristics and the Markov Chain. The Erlang-k distribution is employed in this work in modelling both the service and inter-arrival time characteristics for the single-impulse (SI) and burst-impulse (BI) noise events. The appropriate number of stages corresponding to the number of exponentials is determined from the mean and the variance of the measured data.

6.2 Proposed Queueing Models for PLC

Let the PLC impulse noise events arrive at time instants t_m $(m = 0, 1, 2, ...)$ and that the service time for the m_{th} impulse noise event be s_m $(m = 1, 2, ...)$. Assuming that the inter-arrival and service times are independently and identically distributed (i.i.d) according to the Erlang-k distribution given by (6.1)and (6.2) respectively as [127, 128]:

$$a(m) = \frac{k\phi(k\phi m)^{k-1}\exp(-k\phi m)}{(k-1)!} \tag{6.1}$$

$$s(m) = \frac{k\psi(k\psi m)^{k-1}\exp(-k\psi m)}{(k-1)!} \tag{6.2}$$

whose means and variance for the inter-arrival times defined by [127, 128]:

$$E[M] = \frac{1}{\phi} \tag{6.3}$$

$$Var[M] = \frac{1}{k\phi^2} \tag{6.4}$$

The service time means and variance are similarly defined as in (6.3) and (6.4), with the ϕ replaced by ψ. The $\frac{1}{\phi}$ and $\frac{1}{\psi}$ thus denote the mean arrival time and mean service time of the impulse noise events respectively. k is limited to be a positive integer ranging from $1 \leq k \leq \infty$ and represents the degree of variation of the data to the mean. From (6.1) and (6.2), it can be shown that when $k = 1$, the Erlang distribution is reduced to an exponential distribution given by [35, 127]:

$$a(m) = \phi\exp(-\phi m), \qquad m \geq 0 \tag{6.5}$$

$$s(m) = \psi\exp(-\psi m), \qquad m \geq 1 \tag{6.6}$$

for the inter-arrival and service time distribution respectively. As $k \to \infty$ the variance $\to$ zero, the Erlang-k distribution becomes deterministic. Accordingly, the Erlang-k distribution becomes more symmetrical and more closely centred around its mean as k increases. Since the Erlang distribution is comprised of k i.i.d exponential distributions, each having a mean of $\frac{1}{k\phi}$ for inter-arrival times or $\frac{1}{k\psi}$ for service times, k can also be considered as the number of exponentials in the Erlang distribution. [37, 127]. Due to its relationship with the exponential distribution, the Erlang model is more flexible in fitting the distribution to actual data as compared to the exponential distribution and is thus beneficial in queueing analysis. Four queue models can therefore be derived from the Erlang-k distribution for modelling the PLC impulsive noise events namely; $M/M/1$, $M/E_k/1$, $E_j/M/1$ and $E_j/E_k/1$ queues due to their memoryless property and are considered in this work.

In order to ascertain that the queue models proposed are tractable, it is of paramount importance to determine if a steady state exists for the PLC impulsive-noise events under study. To achieve this the traffic intensity is determined and is defined by [37, 127, 128]:

$$\theta = \frac{\phi}{\psi} \tag{6.7}$$

If $\theta < 1$, then a steady state exists where the occurrence of an impulse noise event at a future time t_m as $t_m \to \infty$ is independent of the original state of the system. Consequently, the arrival or service process of the impulse noise events can return to any state with a probability of 1 with a mean return time $< \infty$. $\theta = 1$ indicates that the arrival and service process of the PLC impulsive noise events returns to any state with a probability of 1 both

with a mean return time of ∞. Accordingly, the PLC system queue will increase over time and the queue will grow indefinitely. For $\theta > 1$, the probability of the arrival and service process returning to the finite states is zero for the impulse-noise events, resulting in an infinite queue [37, 127, 128].

6.2.1 M/M/1 Queue

For the $M/M/1$ queue, the exponential distribution is employed in modelling the impulse noise events inter-arrival and service time distribution in the PLC network. Equations (6.5) and (6.6) respectively, define the density distribution (PDF) of the inter-arrival and service times. The birth-death process can then be used to model the steady-state probabilities of the $M/M/1$ queue as in [37]. As such, the rate at which the impulse noise events arrive and depart at the PLC network is equal as $t \to \infty$.

6.2.2 M/E_k/1 Queue

The arrival process of the PLC impulse noise events are assumed to follow an exponential distribution in the $M/E_k/1$ model, whereas the impulse noise events are considered to pass through k stages each with a rate $k\psi$ before departing the PLC network and hence the service time follows the Erlang-k distribution. It follows that if there are m impulsive noise events in the system, and the impulsive noise currently at the receiver is in stage $j(j = 1, 2, ..., k)$ where k is the initial stage of service and $j = 1$ is the final stage of service such that when stage 1 is completed, the impulse noise event leaves the electrical network, then state of the PLC system can be completely described by (m, j). Thus, for a system in state m, j, there are $m - 1$ impulse noise events in the queue, each requiring k stages, as well as an impulse noise event at the receiver having j additional stages yet to be completed. Therefore, the total count for the number of stages in the PLC system will be $(m - 1)k + j$. Accordingly, the state of the service process can be regarded as Markovian and to derive the queue parameters, the knowledge of the number of impulse noise events and the current stage of service is sufficient. Consequently, (6.5) and (6.2), respectively, give the density functions of the inter-arrival time and the service times.

6.2.3 E_j/M/1 Queue

The assumption in this model is that the impulsive noise event passes through k stages prior to entering the PLC network, with each stage having a mean of $\frac{1}{k\phi}$, while the service time distribution follows a Poisson process. This model can similarly be described as a bivariate Markov process (m, j), with the first variable representing the number of impulse noise events in the PLC system and the second variable representing the number of completed stages as $\{(0, 0); (1, 1), (1, 2), ..., (1, k); (2, 1), (2, 2), ..., (2, k); ....\}$ [127]. In this case, m represents the number of PLC impulsive noise events, each with k completed stages, and j represents the number of completed stages corresponding to the arrival of

the next impulse noise event. The inter-arrival time PDF is thus obtained from (6.1), whereas (6.6) gives the density distribution of the service time.

6.2.4 $E_j/E_k/1$ Queue

The arrival and service process in this queue involves k stages, in which the PLC impulsive noise events traverse k stages before entering the PLC network and another k stages before leaving the PLC system. As a result, the arrival process is analogous to the $E_j/M/1$ queue model, while the service time is similar to the $M/E_k/1$ queue model. The inter-arrival and service time distributions are subsequently determined using (6.1) and (6.2) respectively.

6.3 Results and Discussion

The impulsive noise measurement data in Section 3.2 was categorised into SI and BI noise events, since their effect on the transmitted signal varies, with BI noise events resulting in more severe effects. A single impulse noise event is made up of one or two noise impulses while for the PLC noise to be considered as a burst, it should comprise the occurrence of at least 3 single impulse noise events occurring consecutively [24, 35]. Figs. 6.1 and 6.2 show samples of a SI and BI noise event derived from the SYL noise measurement data in Fig. 3.8a.

In order to determine the density distribution of the inter-arrival and the service time, the parameters of the model first need to be determined. These parameters also provide guidance as to which density distribution is applicable to the data under consideration. Thus, the queue parameters, for the exponential and the Erlang-k distribution are summarised in Table 6.1. It is observed that for the SI noise events, the number of i.i.d exponential distributions (k) in the Erlang-k model is one. As such, the exponential distribution is selected to model the impulsive noise inter-arrival times in all the data under consideration. This indicates that there is a high variation in the inter-arrival times and can be attributed to the burst impulse noise events that last for longer durations with varying service times. The service time distribution of the SI noise events can be modelled using both the exponential and the Erlang-k distribution in all locations except for the CL, where only the exponential distribution is applicable. As for the burst impulse noise events service time and inter-arrival time distributions, both the Erlang-k and the exponential distributions are applicable in the modelling of the data in the various locations. It is again observed from Table 6.1 that the mean service time in all the sample data under consideration is less than the mean inter-arrival time. Consequently, the PLC impulsive noise events can achieve a steady-state equilibrium.

The proposed models in Section 6.2 were then validated through the sample PLC impulsive noise measurement data in Section 3.2. It is observed from Fig. 6.3 that the SI noise events inter-arrival times are adequately modelled using the exponential distribution while for the BI events, the Erlang-k distribution provides a better fit. This can be

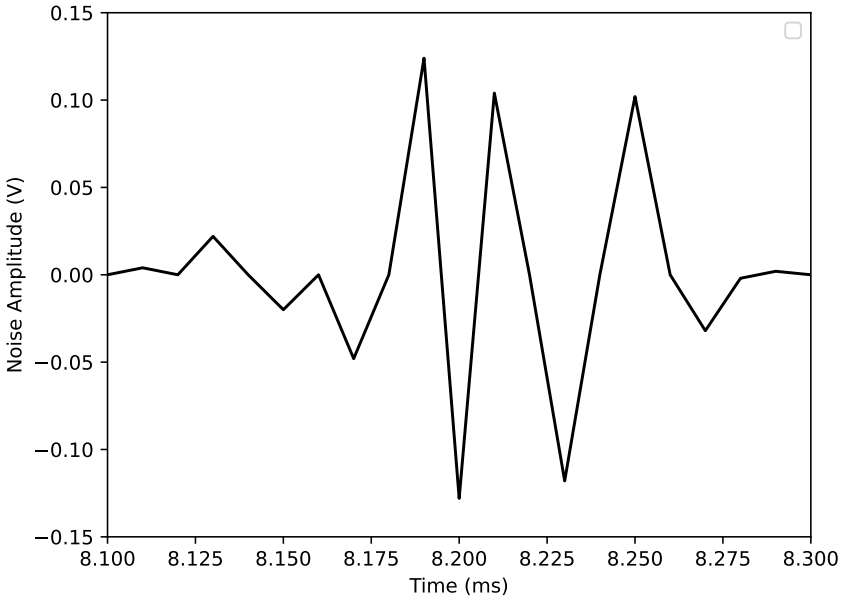

Figure 6.1: Sample Single-impulse Noise Event

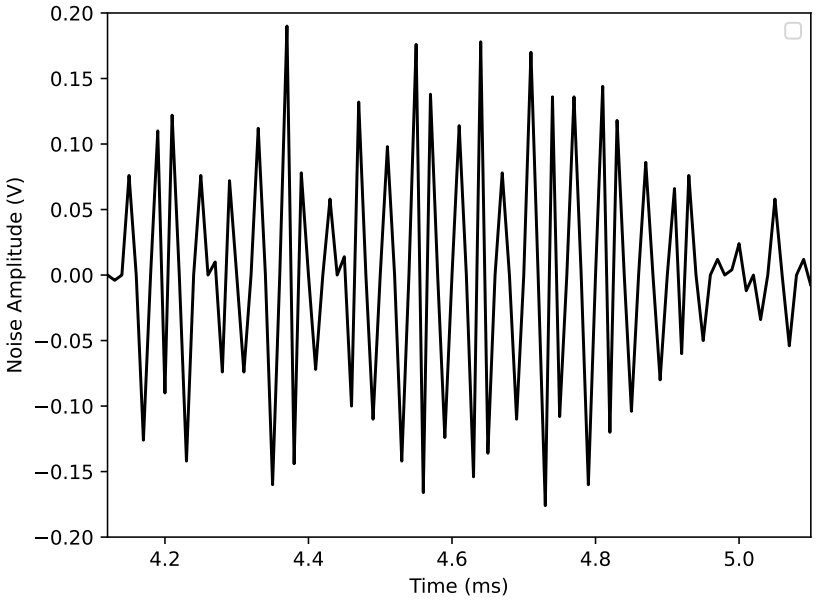

Figure 6.2: Sample Burst-impulse Noise Event

attributed to the fact that the burst events last for longer durations that are also random and for a single-impulse event following a burst, will have a high variation. As regards to the SI noise events service time distribution, there is less variation and thus, the Erlang distribution provides a better fit as shown in Fig. 6.4a and 6.4b, though the number of exponential distributions needs for each data sample is different. However, the exponential distribution provides a suitable fit to the CL measurement data as shown in Fig. 6.4c. The BI noise events have been found to comprise the largest percentage of the impulsive noise

Table 6.1: Queue Model Parameters

	Single-impulse Events	
	Inter-arrival time	**Service time**
	Second-year Laboratory	
Mean	0.3563	0.119
Variance	0.3208	0.0088
K	1	2
	Postgraduate Office	
Mean	0.4943	0.1376
Variance	0.3418	0.0054
K	1	4
	Computer Laboratory	
Mean	1.0154	0.1471
Variance	1.7583	0.0157
K	1	1
	Burst-impulse Events	
	Inter-arrival time	**Service time**
	Second-year Laboratory	
Mean	0.995	0.8538
Variance	0.3227	0.3236
K	3	2
	Postgraduate Office	
Mean	1.0085	0.5893
Variance	0.4705	5.1984
K	2	2
	Computer Laboratory	
Mean	0.6917	0.6005
Variance	0.0886	0.0488
K	5	7

with up to 80% in the indoor PLC networks [34]. Although the BI noise events inter-arrival time varies, the degree of variation is not as significant as that of the SI noise events. Consequently, in all the various locations, the Erlang-k distribution may be employed to model the inter-arrival times and is observed to adequately capture the measured data as compared to the exponential distribution with the value of k ranging from 2 to 5 as shown in Figs. 6.5. Moreover, the occurrence of the BI noise events are observed to have a higher variance in the SYL and the PGO in Figs. 6.5a and 6.5b, which have higher noise levels, in comparison with the CL where $k = 5$ for the Erlang distribution as depicted in Fig. 6.5c. Figure 6.6 depicts the burst impulse noise event service time distribution in various indoor locations. The burst impulse noise events have a considerable variation for the SYL and the PGO, with the Erlang-2 distribution observed to adequately fit to the measurement data. The exponential distribution is also observed to provide an adequate fit the measurement data as depicted in Figs. 6.6a and 6.6b. This is due to the high noise levels in these locations, which cause greater fluctuation. The Erlang-k distribution, on the

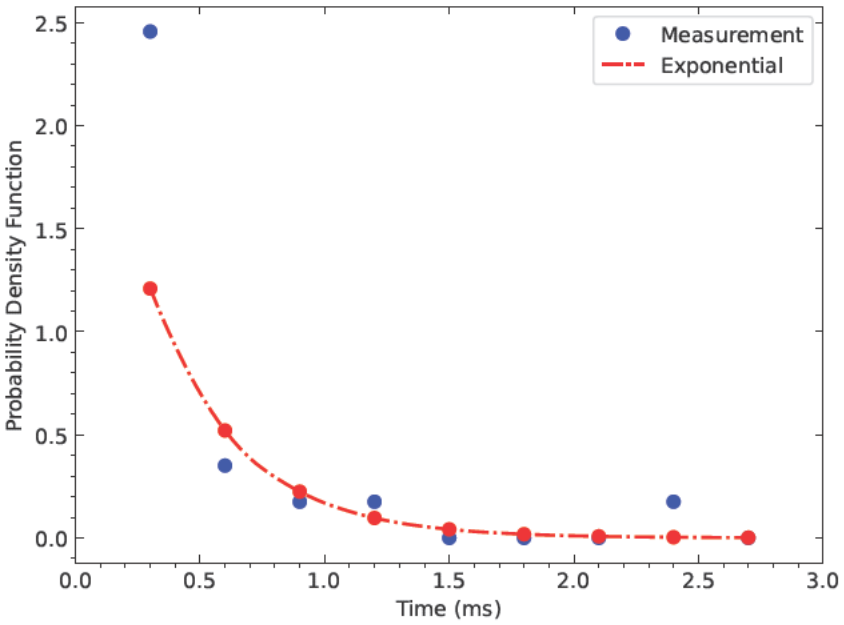

(a) Second-year Laboratory

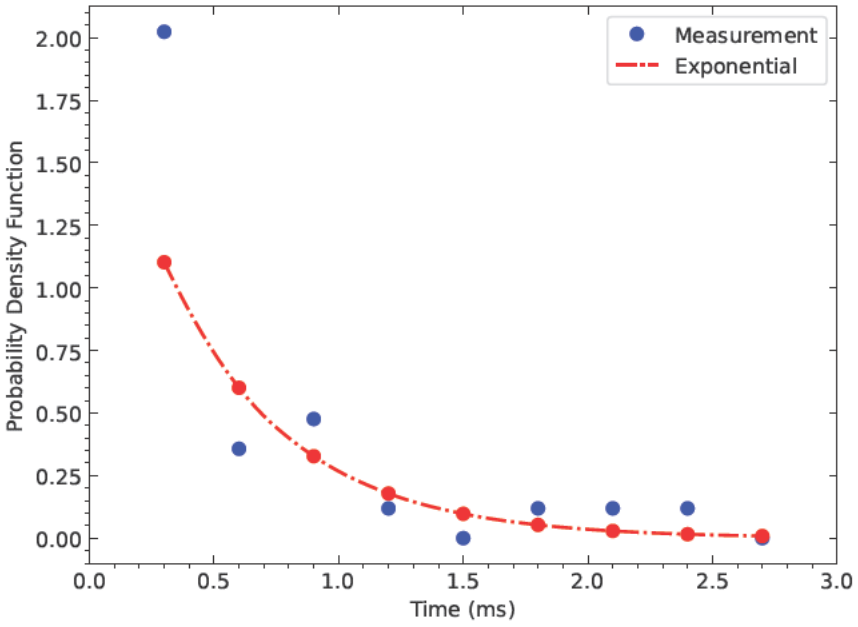

(b) Postgraduate Office

Figure 6.3: Single-impulse Noise Events Inter-arrival Time Distribution

other hand, provides a suitable fit where the measured distribution is found to approach a normal distribution in the CL where the noise levels are lower.

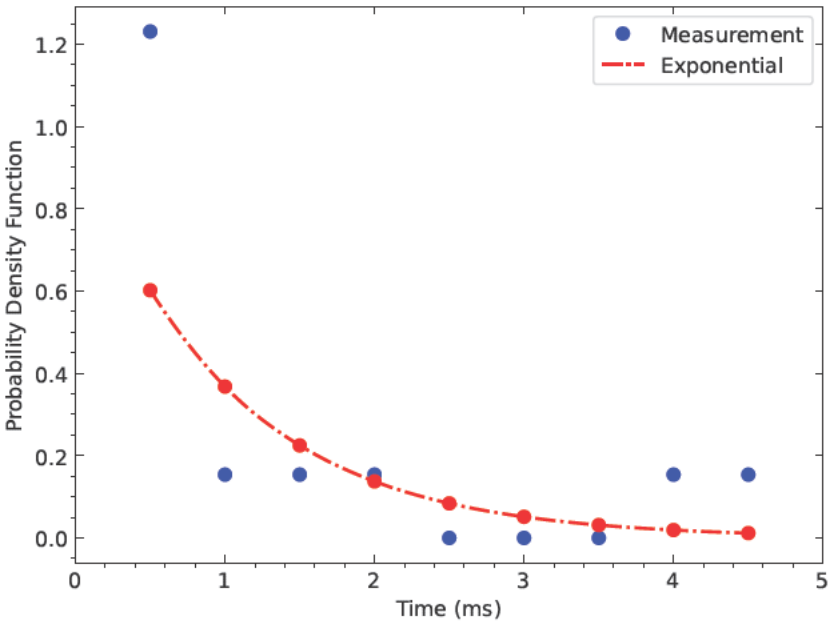

(c) Computer Laboratory

Figure 6.3: Single-impulse Noise Events Inter-arrival Time Distribution

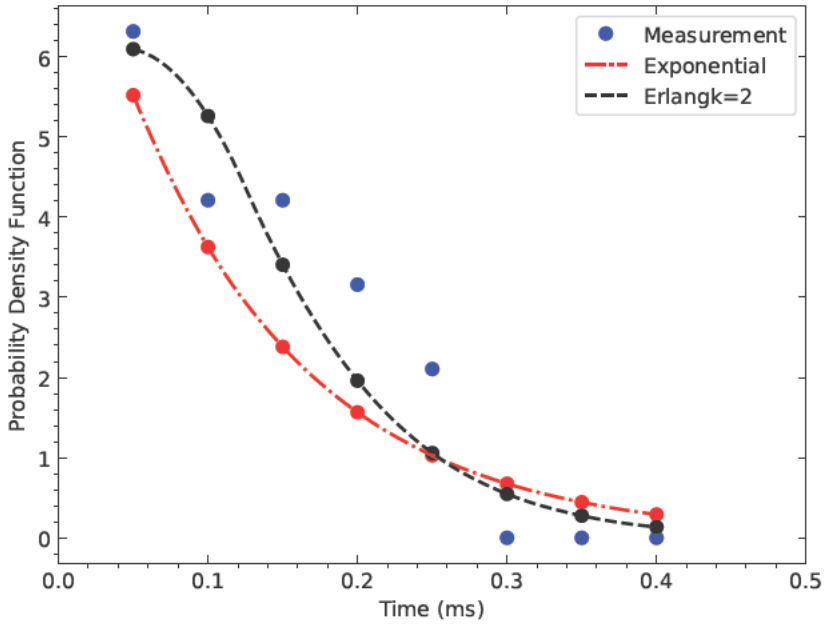

(a) Second-year Laboratory

Figure 6.4: Single-impulse Noise Events Service Time Distribution

6.3.1 Model Validation

Error analysis was then performed to determine how well the proposed models fit the data where the RMSE (4.27) and the χ^2 statistic (4.28), were employed to determine the

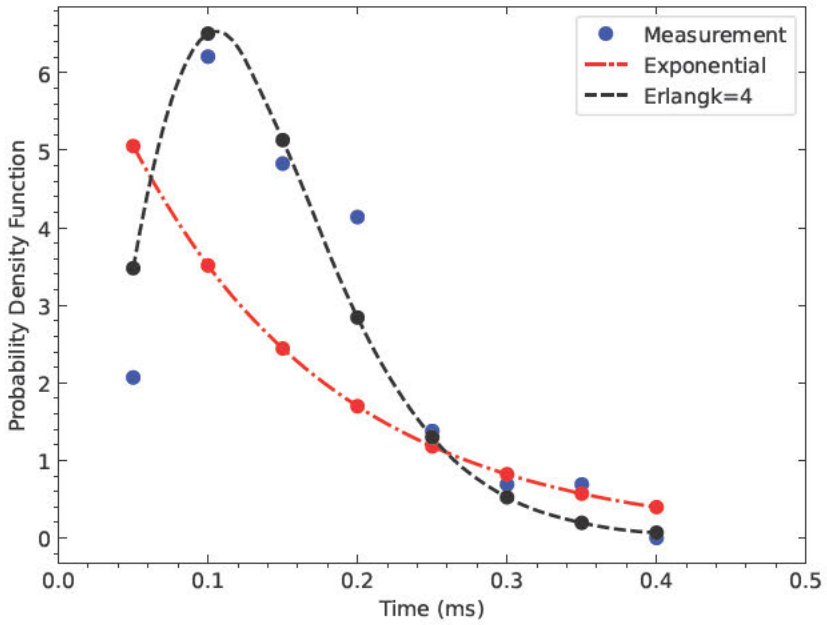

(b) Postgraduate Office

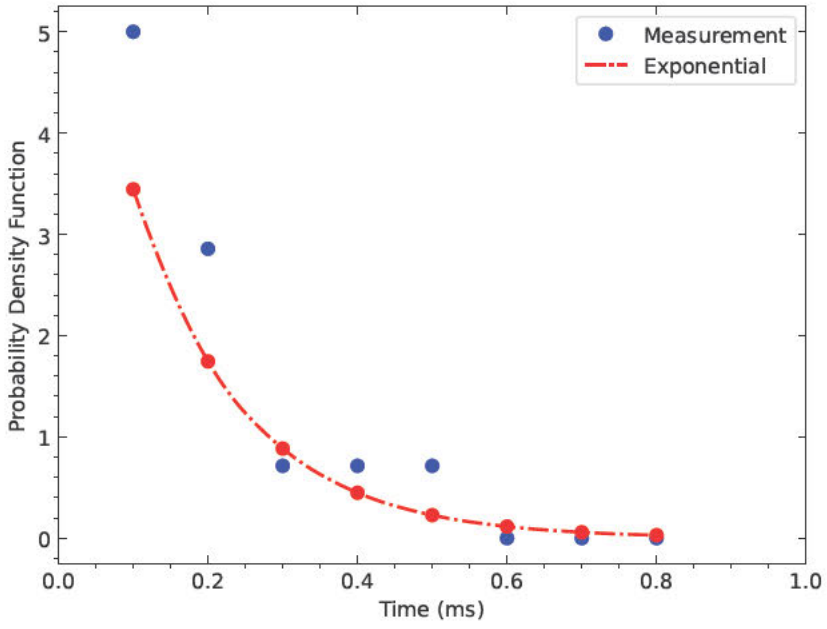

(c) Computer Laboratory

Figure 6.4: Single-impulse Noise Events Service Time Distribution

goodness of fit of the proposed queue models where a 5% threshold of significance level (SL) was set for the χ^2 statistic.

Table 6.2 gives a summary the performance of the proposed models. The Erlang-k and the Exponential distributions proposed for modelling the various measurement data under

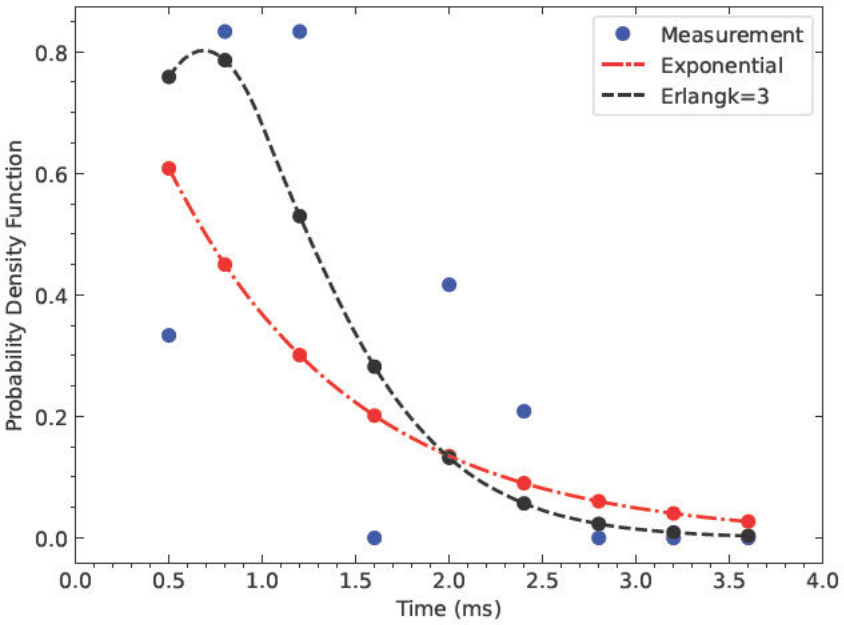

(a) Second-year Laboratory

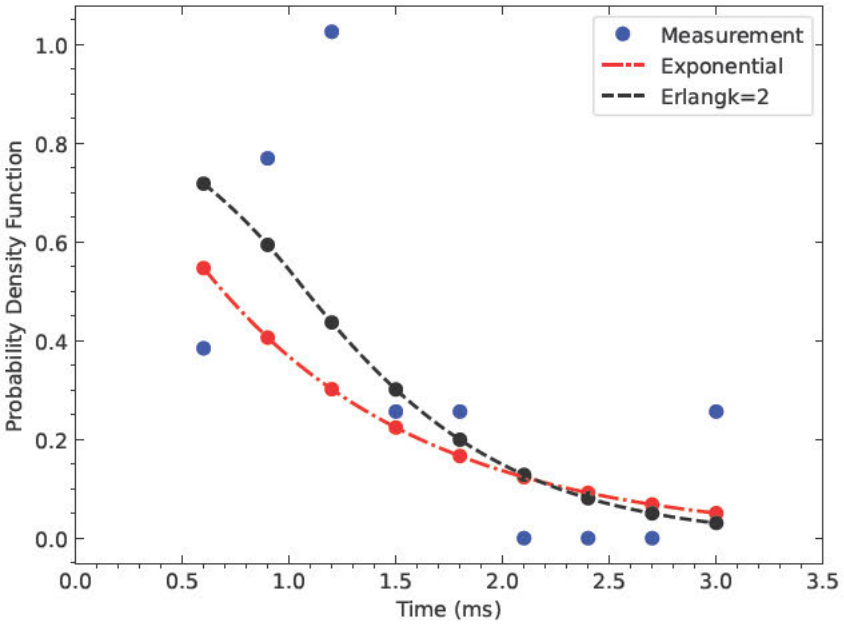

(b) Postgraduate Office

Figure 6.5: Burst-impulse Noise Events Inter-arrival Time Distribution

consideration are determined to be statistically significant. The Erlang-k distribution is found to provide better accuracy as shown by the lower RMSE and χ^2 values compared to the exponential distribution. This is due to the flexibility of the Erlang-k model where the value of k varies depending on the measurement data under consideration. The results of the model parameters and performance analysis indicate that the SI noise events for

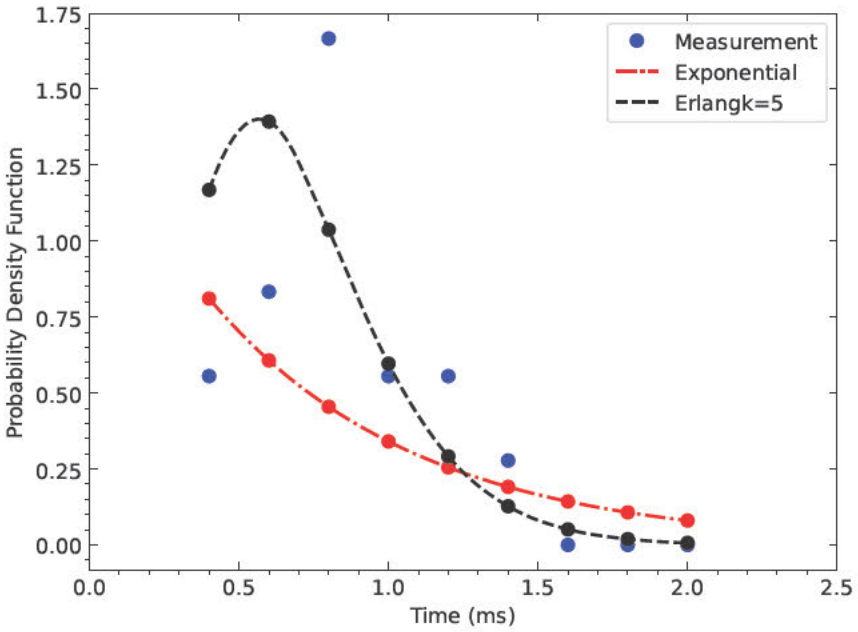

(c) Computer Laboratory

Figure 6.5: Burst-impulse Noise Events Inter-arrival Time Distribution

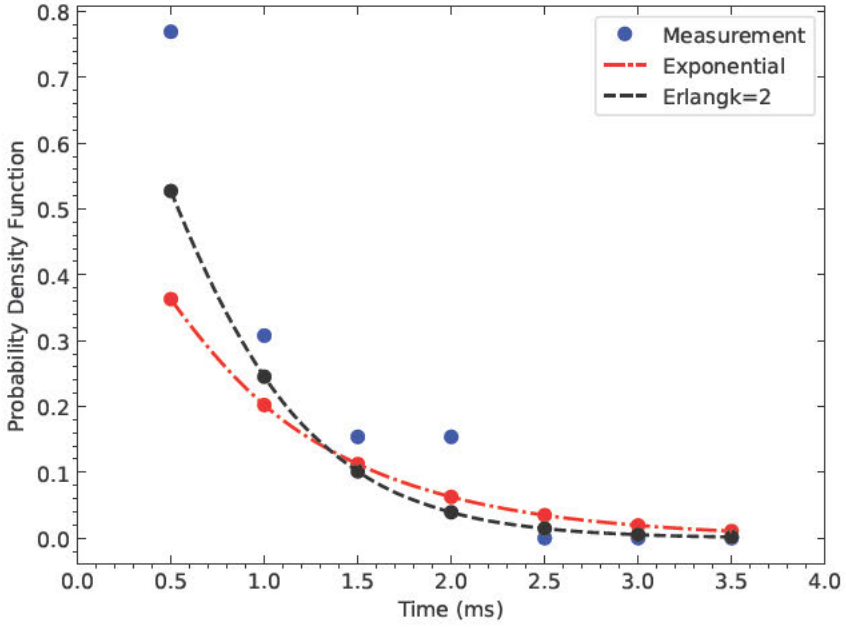

(a) Second-year Laboratory

Figure 6.6: Burst-impulse Noise Events Service Time Distribution

the SYL, PGO, and CL can be effectively modelled using the $M/E_2/1$, $M/E_4/1$ and $M/M/1$ queue models, respectively. Accordingly, the exponential distribution adequately models SI noise events inter-arrival times. As regards to the BI noise events, the $E_3/E_2/1$,

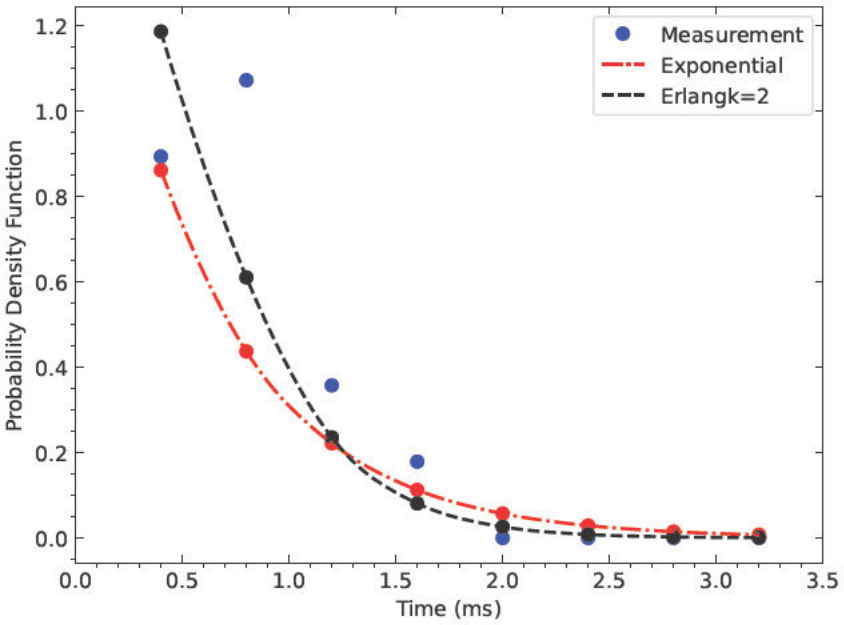

(b) Postgraduate Office

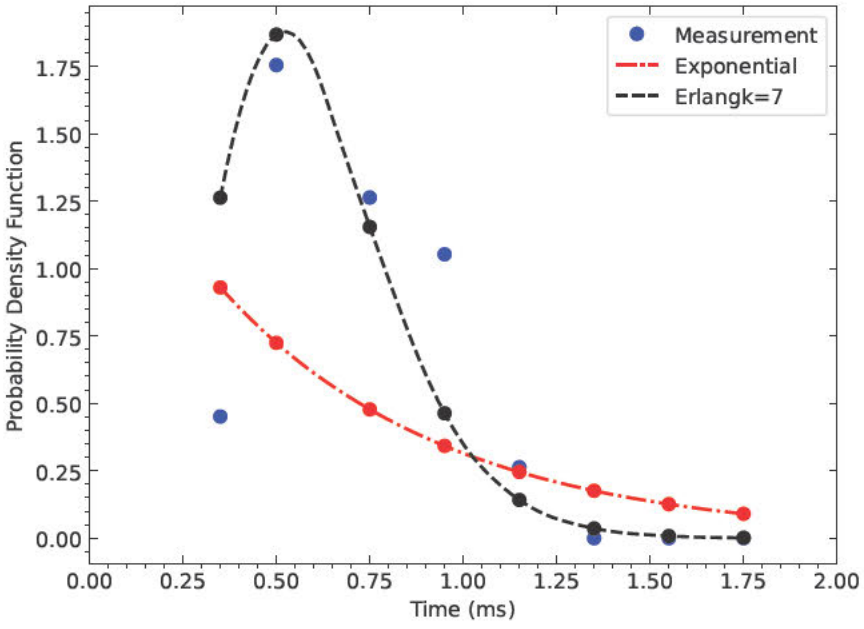

(c) Computer Laboratory

Figure 6.6: Burst-impulse Noise Events Service Time Distribution

$E_2/E_2/1$ and $E_5/E_7/1$ queue models are determined to be the most effective models for the SYL, PGO and the CL respectively. Therefore, the Erlang-k distribution is observed to adequately model the BI noise events service time and inter-arrival times.

Table 6.2: Error Analysis

Error Analysis Erlang _k

Single Impulse Events			
		Inter-arrival time	**Service time**
Second year lab			
RMSE	Erlang_k	x	0.7688
	Exponential	0.4248	1.0459
χ^2	Erlang_k	x	2.7272
	Exponential	1.074	5.7712
SL		15.5073	14.0671
Postgraduate office			
RMSE	Erlang_k	x	0.7185
	Exponential	0.3267	1.8717
χ^2	Erlang_k	x	1.2508
	Exponential	0.4833	10.1326
SL		15.5073	14.0671
Computer lab			
RMSE	Erlang_k	x	x
	Exponential	0.2347	0.708
χ^2	Erlang_k	x	x
	Exponential	0.6363	2.8478
SL		15.5073	14.0671
Burst Impulse Events			
		Inter-arrival time	**Service time**
Second year lab			
RMSE	Erlang_k	0.226	0.1293
	Exponential	0.2679	0.1538
χ^2	Erlang_k	0.4412	0.568
	Exponential	0.5237	0.7245
SL		15.5073	14.0671
Postgraduate office			
RMSE	Erlang_k	0.2517	0.2322
	Exponential	0.291	0.2681
χ^2	Erlang_k	0.5713	0.6398
	Exponential	0.604	1.1544
SL		15.5073	14.0671
Computer lab			
RMSE	Erlang_k	0.3625	0.4176
	Exponential	0.4431	0.6412
χ^2	Erlang_k	0.4301	1.4386
	Exponential	0.6875	4.8711
SL		15.5073	14.0671

6.4 Chapter Summary

In this chapter, the time series characteristics of the PLC impulsive noise events have been examined and the queueing theory approach has been employed to model their characteristics in this work. Depending on the variability of the data under consideration, appropriate parameters have been derived and the applicable queue models employed to determine the service and inter-arrival time distributions. For all the single impulse noise events under consideration, the exponential distribution is determined suitable in modelling the inter-arrival times and provides a suitable fit, indicating a high variance. The Erlang-k distribution is observed to provide better accuracy as compared to the exponential distribution in modelling the burst impulse noise events time series characteristics. It is also determined that the steady-state equilibrium of the impulse noise events inter-arrival and service time distribution exists.

Chapter 7

CONCLUSIONS AND FUTURE WORK

This chapter concludes the research and presents a summary of the thesis and future recommendations.

7.1 Concluding Remarks

In Chapter 1, an introduction to the PLC research area is provided, whereby the various applications of the PLC technology are discussed, including the existing and recent technologies. This is followed by a problem statement, which served as the motivation for conducting this research. The contributions to the PLC research area and the paper publications from the work carried out are outlined. Chapter 1 then concludes with the thesis structure.

Chapter 2 reviews PLC technology as a media for data transmission. To better understand the PLC network structure and regulations, an overview of the PLC network structure, PLC standards, and PLC technology classification is presented. In addition, the challenges affecting PLC technology are described, with a particular emphasis on PLC noise characteristics and modelling, which are the main focus of this work. Moreover, models popularly employed for PLC noise modelling are reviewed and gaps are identified, which form the objectives of the subsequent chapters.

The existing PLC noise models are developed through the top-down approach, where measurements are performed and parameters are then derived from the measurements. This is because obtaining comprehensive knowledge of PLC impulsive noise is a challenge due to the heterogeneous wiring practices, numerous joints and socket outlets connected to different loads in the low-voltage PLC networks. The core of this work is also based on measurements carried out in various indoor environments. Details of the measurement set-up, the locations considered for PLC noise measurement, and the loading conditions are described in Chapter 3. A thorough description of measurements carried out in the various locations is provided. This chapter then concludes with the measurement results, which subsequently form the basis for the development of noise models to describe the PLC impulsive noise characteristics as well as model validation.

The GM model has been widely employed in modelling PLC impulsive noise amplitude distribution since its heavy tail characteristics are comparable to those exhibited by the

PLC impulsive noise. However, the statistical distributions employed to determine the weights of the GM components, with the Bernoulli and Poisson distributions being the most common, have been found to be insufficient in modelling power line communication noise. Chapter 4 contributes to the modelling of the amplitude distribution of the PLC impulsive noise where Bayesian statistics are employed, such that the mixture weights are obtained from the data through unsupervised learning. The maximum likelihood estimation method is employed to determine the parameters of the proposed model via the EM algorithm. The GM model is determined to provide a suitable fit to the measured data, though it is prone to singularity cases and over-fitting of the data. Regression analysis is proposed in this case to solve the singularity problem.

The accuracy of the GM model proposed in Chapter 4 has been found to increase as the model complexity increases, in addition to the high tendency to overfit data. Chapter 5 thus seeks to improve on the GM model in Chapter 4, where the VB learning approach is proposed in modelling the amplitude distribution of the PLC impulsive noise. The VB learning approach also employs the GM to predict the PLC amplitude distribution. However, it is unaffected by singularity cases and data over-fitting, resulting in an adequate generalisation of the measurement data. The VB approach also provides a procedure for identifying the most suitable number of GM components for a specific data set. The derivations and implementation of the VB learning model are discussed in Chapter 5. The performance of the GM model in Chapter 4 is found to provide a fair fit to the measured data as compared to the VB model although the difference in performance is insignificant.

The models proposed in Chapters 4 and 5 model the PLC noise as i.i.d. random variables. Accordingly, the temporal correlation of the PLC noise is not considered. Chapter 6 presents the modelling of the inter-arrival and service time distribution of the PLC noise by adopting the queueing theory approach. The PLC inter-arrival and service time distributions have been determined to be adequately modelled as a superposition of several exponential distributions. However, the determination of the suitable number of exponential distributions is achieved using curve-fitting techniques. This problem is resolved in Chapter 6, where the appropriate number of exponential distributions is obtained from the mean and variance of the data by employing the Erlang-k distribution, which is also determined to provide a fair fit for the inter-arrival and service time distribution of the burst impulses.

7.2 Future Work

In the maximum likelihood approach, though flexible enough to find the parameters of the GM model, the optimum parameters at particular cases can be difficult to obtain in particular cases, especially if the EM algorithm does not converge. Therefore, other parameter estimation methods can be explored so as to fully benefit from the GM model in describing the amplitude distribution of the PLC impulsive noise.

Although the maximum likelihood approach is flexible enough to determine the GM

model's parameters, obtaining the optimum parameters in specific cases can be difficult, especially if the EM algorithm fails to converge. As a result, different parameter estimate approaches can be investigated to fully benefit from the GM model in describing the amplitude distribution of PLC impulsive noise.

The models proposed in Chapters 4 and 5 do not factor in the temporal correlation of the PLC noise, whereas the queueing theory model in Chapter 6 does not describe the PLC noise amplitude characteristic. The development of a model that integrates both the queueing theory and the GM models is a key area of interest.

**

Appendix A

Derivation of Update Equations

The optimal solution for the k_{th} component means and precisions can be derived from (5.41) as:

$$\begin{aligned}\log q(\mu_k, \phi_k) =& \mathbb{E}_{\mu,\phi}\left(\frac{1}{2}\left(\log\phi_k - \log 2\pi - \phi(x_n - \mu_k)^2\right)\sum_{n=1}^{N} z_{nk}\right) + \\ & \mathbb{E}_{\mu,\phi}\left(\frac{1}{2}\left(\log\phi_k + \log s_0 - \log 2\pi - \phi_k s_0(\mu_k - t_0)^2\right)\right) + \\ & \mathbb{E}_{\mu,\phi}\left((\alpha_0 - 1)\log\phi_k - \alpha_0\log\beta_0 - \log\Gamma(\alpha_0) - \frac{\phi_k}{\beta_0}\right) \\ & + constant\end{aligned} \tag{A.1}$$

Adding all terms not related to μ and ϕ to a constant, (A.1) becomes:

$$\begin{aligned}\log q(\mu_k, \phi_k) =& \mathbb{E}_{\mu,\phi}\left(\left(\frac{1}{2}\sum_{n=1}^{N} z_{nk} + \frac{1}{2} + (\alpha_0 - 1)\right)\log\phi_k\right) \\ & - \mathbb{E}_{\mu,\phi}\left(\frac{\phi_k}{2}\sum_{n=1}^{N} z_{nk}\left(x_n - x_k^+ + x_k^+ - \mu_k\right)^2\right) \\ & - \mathbb{E}_{\mu,\phi}\left(\frac{\phi_k}{\beta_0} - \frac{\phi_k s_0}{2}(\mu_k - t_0)^2\right) + constant\end{aligned} \tag{A.2}$$

where x_k^+ is defined in (5.19). Solving (A.2):

$$\begin{aligned}\log q(\mu_k, \phi_k) =& \left(\frac{1}{2}\sum_{n=1}^{N}\gamma_{nk}^+ + \frac{1}{2} + (\alpha_0 - 1)\right)\log\phi_k - \\ & \frac{\phi_k}{\beta_0} - \frac{\phi_k}{2}\left(\sum_{n=1}^{N}\gamma_{nk}^+ {x_k^+}^2 + t_0^2 s_0 + \sum_{n=1}^{N}\gamma_{nk}^+(x_n - x_k^+)^2\right) \\ & - \frac{\phi_k}{2}\left(\left(\sum_{n=1}^{N}\gamma_{nk}^+ + s_0\right){\mu_k}^2 - 2\left(\sum_{n=1}^{N}\gamma_{nk}^+ x_k^+ + t_0 s_0\right)\mu_k\right)\end{aligned} \tag{A.3}$$

Completing the square for the last term in (A.3), yields:

$$\begin{aligned}\log q(\mu_k,\phi_k) = &\left(\frac{1}{2}\sum_{n=1}^{N}\gamma_{nk}^{+}+\frac{1}{2}+(\alpha_0-1)\right)\log\phi_k-\frac{\phi_k}{\beta_0}\\ &-\frac{\phi_k}{2}\left(\sum_{n=1}^{N}\gamma_{nk}^{+}(x_n-x_k^{+})^2\right)-\frac{\phi_k}{2}\left(\sum_{n=1}^{N}\gamma_{nk}^{+}+s_0\right)\\ &\left(\mu_k-\frac{\sum_{n=1}^{N}\gamma_{nk}^{+}x_k^{+}+t_0s_0}{\sum_{n=1}^{N}\gamma_{nk}^{+}+s_0}\right)^2-\\ &\frac{\phi_k}{2}\left(\left(\sum_{n=1}^{N}\gamma_{nk}^{+}{x_k^{+}}^2+t_0^2s_0\right)+\frac{\left(\sum_{n=1}^{N}\gamma_{nk}^{+}x_k^{+}+t_0s_0\right)^2}{\sum_{n=1}^{N}\gamma_{nk}^{+}+s_0}\right)\end{aligned}\tag{A.4}$$

Simplifying (A.4):

$$\begin{aligned}\log q(\mu_k,\phi_k) = &\left(\frac{N_k}{2}+\frac{1}{2}+(\alpha_0-1)\right)\log\phi_k-\\ &\frac{\phi_k}{2}(N_k+s_0)\left(\mu_k-\frac{N_kx_k^{+}+t_0s_0}{N_k+s_0}\right)^2-\\ &\phi_k\left(\frac{1}{\beta_0}+\frac{1}{2}\left(N_ks_k^{+}+\frac{N_ks_0}{N_k+s_0}(x_k^{+}-t_0)^2\right)\right)\end{aligned}\tag{A.5}$$

where N_k is given by (5.20) and the update parameters can then be obtained from (A.4).

References

[1] O. Karakuş, E. E. Kuruoğlu, and M. A. Altınkaya, "Modelling impulsive noise in indoor powerline communication systems," *Signal, image and video processing*, vol. 14, no. 8, pp. 1655–1661, 2020.

[2] C. Cano, A. Pittolo, D. Malone, L. Lampe, A. M. Tonello, and A. G. Dabak, "State of the art in power line communications: From the applications to the medium," *IEEE Journal on Selected Areas in Communications*, vol. 34, no. 7, pp. 1935–1952, 2016.

[3] M. V. Ribeiro, M. d. L. Filomeno, Â. Camponogara, T. R. Oliveira, T. F. Moreira, S. Galli, and H. V. Poor, "Seamless connectivity: The power of integrating power line and wireless communications," *IEEE Communications Surveys & Tutorials*, 2023.

[4] F. Minamiyama, H. Koga, K. Kobayashi, and M. Katayama, "Power supply overlaid communication and common clock delivery for cooperative motion control," in *2011 IEEE International Symposium on Power Line Communications and Its Applications*, pp. 370–375, 2011.

[5] S. Barmada, M. Raugi, and M. Tucci, "Power line communication integrated in a wireless power transfer system: A feasibility study," in *18th IEEE International Symposium on Power Line Communications and Its Applications*, pp. 116–120, 2014.

[6] L. Zhang, X. Liu, and D. Xu, "A novel security monitoring system of coal mine based on power line communication dynamic routing technology," in *2014 IEEE Industry Application Society Annual Meeting*, pp. 1–6, 2014.

[7] V. Dégardin, E. Simon, M. Morelle, M. Liénard, P. Degauque, I. Junqua, and S. Bertuol, "On the possibility of using plc in aircraft," in *ISPLC2010*, pp. 337–340, 2010.

[8] S. Barmada, M. Raugi, M. Tucci, and T. Zheng, "Power line communication in a full electric vehicle: Measurements, modelling and analysis," in *ISPLC2010*, pp. 331–336, 2010.

[9] M. Antoniali, A. M. Tonello, M. Lenardon, and A. Qualizza, "Measurements and analysis of plc channels in a cruise ship," in *2011 IEEE International Symposium on Power Line Communications and Its Applications*, pp. 102–107, 2011.

[10] S. Barmada, A. Gaggelli, A. Musolino, R. Rizzo, M. Raugi, and M. Tucci, "Design of a plc system onboard trains: Selection and analysis of the plc channel," in *2008 IEEE International Symposium on Power Line Communications and Its Applications*, pp. 13–17, 2008.

[11] G. López, J. Matanza, D. De La Vega, M. Castro, A. Arrinda, J. I. Moreno, and A. Sendin, "The role of power line communications in the smart grid revisited: Applications, challenges, and research initiatives," *IEEE Access*, vol. 7, pp. 117346–117368, 2019.

[12] R. Martínez-Rodríguez-Osorio, M. Calvo-Ramón, Á. Miguel, and L. C. Navarrete, "Smart control system for leds traffic-lights based on plc," 2006.

[13] A. Gnazzo, A. Bergaglio, M. Palma, F. Pittoni, M. Giunta, and F. Ballesio, "Powerline technology over coaxial cables for in-home multimedia applications: Performances and emc issues," in *2011 IEEE International Symposium on Power Line Communications and Its Applications*, pp. 130–134, IEEE, 2011.

[14] C.-K. Lin, H.-W. Chu, S.-C. Yeh, M.-T. Lu, J. Yao, and H. Chen, "Robust video streaming over power lines," in *2006 IEEE International Symposium on Power Line Communications and Its Applications*, pp. 196–201, IEEE, 2006.

[15] Y. He, N. Jenkins, J. Wu, and M. Eltayeb, "Ict infrastructure for smart distribution networks," in *ISPLC2010*, pp. 319–324, IEEE, 2010.

[16] J. Liu, B. Zhao, J. Wang, Y. Zhu, and J. Hu, "Application of power line communication in smart power consumption," in *ISPLC2010*, pp. 303–307, IEEE, 2010.

[17] L. Lampe, A. M. Tonello, and D. Shaver, "Power line communications for automation networks and smart grid [guest editorial]," *IEEE Communications Magazine*, vol. 49, no. 12, pp. 26–27, 2011.

[18] M. Zimmermann and K. Dostert, "A multipath model for the powerline channel," *IEEE Transactions on communications*, vol. 50, no. 4, pp. 553–559, 2002.

[19] L. T. Berger, A. Schwager, and J. J. Escudero-Garzás, "Power line communications for smart grid applications," *Journal of Electrical and Computer Engineering*, vol. 2013, pp. 3–3, 2013.

[20] H. Philipps, "Modelling of powerline communication channels," *IEEE ISPLC*, vol. 99, pp. 14–21, 1999.

[21] J. Anatory, M. Kissaka, and N. H. Mvungi, "Channel model for broadband power-line communication," *IEEE transactions on power delivery*, vol. 22, no. 1, pp. 135–141, 2006.

[22] F. Zwane and T. J. O. Afullo, "An alternative approach in power line communication channel modelling," *Progress In Electromagnetics Research C*, vol. 47, pp. 85–93, 2014.

[23] M. P. Sibanda, P. A. J. van Rensburg, and H. C. Ferreira, "A compact economical plc band-pass coupler with impedance matching," in *2013 IEEE 17th International*

Symposium on Power Line Communications and Its Applications, pp. 339–344, IEEE, 2013.

[24] M. Zimmermann and K. Dostert, "Analysis and modeling of impulsive noise in broad-band powerline communications," *IEEE Transactions on Electromagnetic Compatibility*, vol. 44, no. 1, pp. 249–258, 2002.

[25] H. Meng, Y. L. Guan, and S. Chen, "Modeling and analysis of noise effects on broadband power-line communications," *IEEE Transactions on Power delivery*, vol. 20, no. 2, pp. 630–637, 2005.

[26] R. M. Vines, H. J. Trissell, L. J. Gale, and J. B. O'neal, "Noise on residential power distribution circuits," *IEEE Transactions on Electromagnetic Compatibility*, no. 4, pp. 161–168, 1984.

[27] M. Zimmermann and K. Dostert, "An analysis of the broadband noise scenario in powerline networks," 2006.

[28] V. Degardin, M. Lienard, A. Zeddam, F. Gauthier, and P. Degauquel, "Classification and characterization of impulsive noise on indoor powerline used for data communications," *IEEE Transactions on Consumer Electronics*, vol. 48, no. 4, pp. 913–918, 2002.

[29] S. P. Herath, N. H. Tran, and T. Le-Ngoc, "On optimal input distribution and capacity limit of bernoulli-gaussian impulsive noise channels," in *2012 IEEE International Conference on Communications (ICC)*, pp. 3429–3433, IEEE, 2012.

[30] G. Ndo, F. Labeau, and M. Kassouf, "A markov-middleton model for bursty impulsive noise: Modeling and receiver design," *IEEE Transactions on Power Delivery*, vol. 28, no. 4, pp. 2317–2325, 2013.

[31] T. Shongwe, A. J. H. Vinck, and H. C. Ferreira, "A study on impulse noise and its models," *SAIEE Africa Research Journal*, vol. 106, no. 3, pp. 119–131, 2015.

[32] F. Rouissi, A. H. Vinck, H. Gassara, and A. Ghazel, "Statistical characterization and modelling of impulse noise on indoor narrowband plc environment," in *2017 IEEE International Symposium on Power Line Communications and its Applications (ISPLC)*, pp. 1–6, IEEE, 2017.

[33] E. N. Gilbert, "Capacity of a burst-noise channel," *Bell system technical journal*, vol. 39, no. 5, pp. 1253–1265, 1960.

[34] S. Awino, T. Afullo, M. Mosalaosi, and P. Akuon, "Measurements and statistical modelling for time behaviour of power line communication impulsive noise," *International Journal on Communications Antenna and Propagation*, vol. 9, no. 4, pp. 236–246, 2019.

[35] F. Chelangat and T. J. O. Afullo, "Modelling of the powerline communication bursty impulsive noise," in *2023 Photonics & Electromagnetics Research Symposium (PIERS)*, pp. 1450–1455, 2023.

[36] H. Chaouche, F. Gauthier, A. Zeddam, M. Tlich, and M. Machmoum, "Time domain modeling of powerline impulsive noise at its source," *Journal of Electromagnetic Analysis and Applications*, vol. 2011, 2011.

[37] F. Chelangat and T. J. O. Afullo, "Analysis of the steady-state distribution of plc impulsive noise characteristics," in *2023 Southern Africa Telecommunication Networks and Applications Conference (SATNAC)*, pp. 163–167, 2023.

[38] H. Meng, S. Chen, Y. Guan, C. Law, P. So, E. Gunawan, and T. Lie, "Modeling of transfer characteristics for the broadband power line communication channel," *IEEE Transactions on Power delivery*, vol. 19, no. 3, pp. 1057–1064, 2004.

[39] J. A. Corchado, J. A. Cortés, F. J. Canete, and L. Díez, "An mtl-based channel model for indoor broadband mimo power line communications," *IEEE Journal on Selected Areas in Communications*, vol. 34, no. 7, pp. 2045–2055, 2016.

[40] K. Dostert, *Powerline Communications*. Prentice Hall communications engineering and emerging technologies series, Prentice Hall PTR, 2001.

[41] M. Mosalaosi, *Characterization and modelling of the channel and noise for broadband indoor powerline communication (plc.) networks.* PhD thesis, 2016.

[42] F. Chelangat, *Power line communication impedance profiling and matching for broadband applications.* PhD thesis, 2018.

[43] J. F. Adami, P. Silveira, M. Martinez, R. C. Perez, and A. C. Dallbello, "New approach to improve high-voltage transmission line reliability," *IEEE Transactions on Power Delivery*, vol. 24, no. 3, pp. 1515–1520, 2009.

[44] A. Cataliotti, A. Daidone, and G. Tinè, "Power line communication in medium voltage systems: Characterization of mv cables," *IEEE Transactions on Power Delivery*, vol. 23, no. 4, pp. 1896–1902, 2008.

[45] S. Galli, A. Scaglione, and Z. Wang, "For the grid and through the grid: The role of power line communications in the smart grid," *Proceedings of the IEEE*, vol. 99, no. 6, pp. 998–1027, 2011.

[46] S. T. Mak and T. G. Moore, "Twacs™, a new viable two-way automatic communication system for distribution networks. part ii: inbound communication," *IEEE transactions on power apparatus and systems*, no. 8, pp. 2141–2147, 1984.

[47] S. T. Mak and D. L. Reed, "Twacs, a new viable two-way automatic communication system for distribution networks. part i: Outbound communication," *IEEE Transactions on Power Apparatus and systems*, no. 8, pp. 2941–2949, 1982.

[48] L. Lampe, A. M. Tonello, and T. G. Swart, *Power Line Communications: Principles, Standards and Applications from multimedia to smart grid.* John Wiley & Sons, 2016.

[49] A. A. Atayero, A. Alatishe, and Y. A. Ivanov, "Power line communication technologies: modeling and simulation of prime physical layer," in *Proceedings of the World Congress on Engineering and Computer Science*, vol. 2, pp. 24–26, 2012.

[50] A. M. Tonello and A. Pittolo, "Considerations on narrowband and broadband power line communication for smart grids," in *2015 IEEE International Conference on Smart Grid Communications (SmartGridComm)*, pp. 13–18, IEEE, 2015.

[51] P. Strong, "Regulatory & consumer acceptance of powerline products," in *Proceedings of the 5th International Symposium on Power-Line Communications and its Applications (ISPLC)*, pp. 4–6, 2001.

[52] A. R. Ndjiongue, A. Snyders, H. C. Ferreira, and S. Rimer, "Review of power line communications standards in africa," in *e-Infrastructure and e-Services for Developing Countries: 5th International Conference, AFRICOMM 2013, Blantyre, Malawi, November 25-27, 2013, Revised Selected Papers 5*, pp. 12–21, Springer, 2014.

[53] A. Haidine, A. Tabone, and J. Müller, "Deployment of power line communication by european utilities in advanced metering infrastructure," in *2013 IEEE 17th International Symposium on Power Line Communications and Its Applications*, pp. 126–130, IEEE, 2013.

[54] I.-T. 9904, "Narrowband orthogonal frequency division multiplexing power line communication transceivers for prime networks," 2012.

[55] A. Sendin, M. A. Sanchez-Fornie, I. Berganza, J. Simon, and I. Urrutia, *Telecommunication networks for the smart grid.* Artech House, 2016.

[56] S. Galli and O. Logvinov, "Recent developments in the standardization of power line communications within the ieee," *IEEE Communications Magazine*, vol. 46, no. 7, pp. 64–71, 2008.

[57] E. Marthe, F. Rachidi, M. Ianoz, and P. Zweiacker, "Indoor radiated emission associated with power line communication systems," in *2001 IEEE EMC International Symposium. Symposium Record. International Symposium on Electromagnetic Compatibility (Cat. No. 01CH37161)*, vol. 1, pp. 517–520, IEEE, 2001.

[58] R. Vick, "Radiated emission caused by in-house plc-systems," in *IEEE Int. Symp. on Power Line Commun. and Its Applications (ISPLC)*, 2001.

[59] N. Pavlidou, A. H. Vinck, J. Yazdani, and B. Honary, "Power line communications: state of the art and future trends," *IEEE Communications magazine*, vol. 41, no. 4, pp. 34–40, 2003.

[60] F. Chelangat, T. Afullo, and M. Mosalaosi, "Impedance modelling, profiling and characterisation of the powerline communication channel," in *2018 Progress in Electromagnetics Research Symposium (PIERS-Toyama)*, pp. 2165–2171, IEEE, 2018.

[61] O. G. Hooijen, "On the relation between network-topology and power line signal attenuation," in *International Symposium on Power Line Communications*, pp. 45–56, 1998.

[62] M. H. Chan and R. W. Donaldson, "Attenuation of communication signals on residential and commercial intrabuilding power-distribution circuits," *IEEE Transactions on Electromagnetic compatibility*, vol. 28, no. 4, pp. 220–230, 1986.

[63] M. P. Sibanda, P. A. J. van Rensburg, and H. C. Ferreira, "Passive, transformerless coupling circuitry for narrow-band power-line communications," in *2009 IEEE International Symposium on Power Line Communications and Its Applications*, pp. 125–130, IEEE, 2009.

[64] W.-h. Choi and C.-y. Park, "A simple line coupler with adaptive impedance matching for power line communication," in *2007 IEEE International Symposium on Power Line Communications and Its Applications*, pp. 187–191, IEEE, 2007.

[65] P. A. J. van Rensburg, M. P. Sibanda, and H. C. Ferreira, "Integrated impedance-matching coupler for smart building and other power-line communications applications," *IEEE Transactions on Power Delivery*, vol. 30, no. 2, pp. 949–956, 2014.

[66] L. Qi, S. Jingzhao, and F. Zhenghe, "Adaptive impedance matching in power line communication," in *ICMMT 4th International Conference on, Proceedings Microwave and Millimeter Wave Technology, 2004.*, pp. 887–890, IEEE, 2004.

[67] F. Chelangat, T. J. O. Afullo, and M. Mosalaosi, "Impedance bidirectional adaptive coupler for broadband plc," in *2018 Southern Africa Telecommunication Networks and Applications Conference (SATNAC)*, pp. 364–369,, 2018.

[68] J. Auvray and M. Fourrier, *Problems in Electronics (including Lumped Constants, Transmission Lines, and High Frequencies)*, vol. 61. Pergamon, 1973.

[69] M. Mosalaosi and T. J. O. Afullo, "A deterministic channel model for multi-access broadband powerline communication," in *AFRICON 2015*, pp. 1–5, IEEE, 2015.

[70] M. Tanaka, "High frequency noise power spectrum, impedance and transmission loss of power line in japan on intrabuilding power line communications," *IEEE Transactions on Consumer Electronics*, vol. 34, no. 2, pp. 321–326, 1988.

[71] T. Bai, H. Zhang, J. Wang, C. Xu, M. Elkashlan, A. Nallanathan, and L. Hanzo, "Fifty years of noise modeling and mitigation in power-line communications," *IEEE Communications Surveys & Tutorials*, vol. 23, no. 1, pp. 41–69, 2020.

[72] S. O. Awino, T. J. Afullo, M. Mosalaosi, and P. O. Akuon, "Empirical identification of narrowband interference in broadband plc networks at the receiver," in *2018 Progress in Electromagnetics Research Symposium (PIERS-Toyama)*, pp. 2160–2164, IEEE, 2018.

[73] R. Alaya and R. Attia, "Narrowband powerline communication measurement and analysis in the low voltage distribution network," in *2019 International Conference on Software, Telecommunications and Computer Networks (SoftCOM)*, pp. 1–6, IEEE, 2019.

[74] J. Yin, X. Zhu, and Y. Huang, "3d markov chain based narrowband interference model for in-home broadband power line communication," in *2016 IEEE Global Communications Conference (GLOBECOM)*, pp. 1–6, IEEE, 2016.

[75] M. Asiyo and T. Afullo, "Prediction of long-range dependence in cyclostationary noise in low-voltage plc networks," in *2016 Progress in Electromagnetic Research Symposium (PIERS)*, pp. 4954–4958, IEEE, 2016.

[76] O. Ohno, M. Katayama, T. Yamazato, and A. Ogawa, "A simple model of cyclostationary power-line noise for communication systems," in *International Symposium on Power Line Communications and Its Applications (ISPLC)*, pp. 115–122, 1998.

[77] T. Pande, I. H. Kim, and A. Batra, "A method for narrowband interference mitigation in ofdm by minimizing spectral leakage," in *2015 IEEE International Symposium on Power Line Communications and Its Applications (ISPLC)*, pp. 19–23, IEEE, 2015.

[78] H. A. Suraweera and J. Armstrong, "Noise bucket effect for impulse noise in ofdm," *Electronics Letters*, vol. 40, no. 18, pp. 1156–1157, 2004.

[79] B. Han, Y. Lu, K. Wan, and H. D. Schotten, "Merging the bernoulli–gaussian and symmetric α-stable models for impulsive noises in narrowband power line channels," *Physical Communication*, vol. 33, pp. 135–141, 2019.

[80] L. Di Bert, P. Caldera, D. Schwingshackl, and A. M. Tonello, "On noise modeling for power line communications," in *2011 IEEE International Symposium on Power Line Communications and Its Applications*, pp. 283–288, IEEE, 2011.

[81] B. Han, V. Stoica, C. Kaiser, N. Otterbach, and K. Dostert, "Noise characterization and emulation for low-voltage power line channels across narrowband and broadband," *Digital Signal Processing*, vol. 69, pp. 259–274, 2017.

[82] D. Middleton, "Non-gaussian noise models in signal processing for telecommunications: New methods an results for class a and class b noise models," *IEEE Transactions on Information Theory*, vol. 45, no. 4, pp. 1129–1149, 1999.

[83] D. Middleton, "Procedures for determining the parameters of the first-order canonical models of class a and class b electromagnetic interference [10]," *IEEE Transactions on electromagnetic compatibility*, no. 3, pp. 190–208, 1979.

[84] D. Middleton, "Statistical-physical models of electromagnetic interference," *IEEE transactions on Electromagnetic Compatibility*, no. 3, pp. 106–127, 1977.

[85] G. Laguna-Sanchez and M. Lopez-Guerrero, "On the use of alpha-stable distributions in noise modeling for plc," *IEEE Transactions on Power Delivery*, vol. 30, no. 4, pp. 1863–1870, 2015.

[86] S. M. Çürük, "Impulsive noise models used in power line communications," *Balkan Journal of Electrical and Computer Engineering*, vol. 7, no. 2, pp. 115–122, 2019.

[87] G. Samorodnitsky, "M. s. taqqu," *Stable Non-Gaussian Random Processes, Stochastic Models*, 1994.

[88] T. Shongwe, A. H. Vinck, and H. C. Ferreira, "A study on impulse noise and its models," *SAIEE Africa Research Journal*, vol. 106, no. 3, pp. 119–131, 2015.

[89] D. Fertonani and G. Colavolpe, "On reliable communications over channels impaired by bursty impulse noise," *IEEE Transactions on Communications*, vol. 57, no. 7, pp. 2024–2030, 2009.

[90] P. Amirshahi, S. M. Navidpour, and M. Kavehrad, "Performance analysis of uncoded and coded ofdm broadband transmission over low voltage power-line channels with impulsive noise," *IEEE Transactions on power delivery*, vol. 21, no. 4, pp. 1927–1934, 2006.

[91] J. Mitra and L. Lampe, "Convolutionally coded transmission over markov-gaussian channels: Analysis and decoding metrics," *IEEE Transactions on Communications*, vol. 58, no. 7, pp. 1939–1949, 2010.

[92] E. O. Elliott, "Estimates of error rates for codes on burst-noise channels," *The Bell System Technical Journal*, vol. 42, no. 5, pp. 1977–1997, 1963.

[93] D. Liu, E. Flint, B. Gaucher, and Y. Kwark, "Wide band ac power line characterization," *IEEE Transactions on Consumer Electronics*, vol. 45, no. 4, pp. 1087–1097, 1999.

[94] A. Voglgsang, T. Langguth, G. Korner, H. Steckenbiller, and R. Knorr, "Measurement characterization and simulation of noise on powerline channels," in *Proc. Int. Symp. Power-Lines Commun*, pp. 139–146, 2000.

[95] A. Emleh, A. De Beer, H. Ferreira, and A. H. Vinck, "The influence of fluorescent lamps with electronic ballast on the low voltage plc network," in *2014 IEEE 8th International Power Engineering and Optimization Conference (PEOCO2014)*, pp. 276–280, IEEE, 2014.

[96] J. Nguimbis, S. Cheng, Y. Zhang, and L. Xiong, "Coupling unit topology for optimal signaling through the low-voltage powerline communication network," *IEEE Transactions on Power Delivery*, vol. 19, no. 3, pp. 1065–1071, 2004.

[97] T. Samakande, T. Shongwe, A. S. de Beer, and H. C. Ferreira, "The effect of coupling circuits on impulsive noise in power line communication," in *2018 IEEE International Symposium on Power Line Communications and its Applications (ISPLC)*, pp. 1–5, IEEE, 2018.

[98] M. Antoniali, F. Versolatto, and A. M. Tonello, "An experimental characterization of the plc noise at the source," *IEEE Transactions on Power Delivery*, vol. 31, no. 3, pp. 1068–1075, 2015.

[99] J. Rosenblatt and M. H. Friedman, "Direct and alternating current machinery," *(No Title)*, 1963.

[100] S. Awino, T. Afullo, M. Mosalaosi, and P. Akuon, "Time series analysis of impulsive noise in power line communication (plc) networks," *SAIEE Africa Research Journal*, vol. 109, no. 4, pp. 237–249, 2018.

[101] M. Mosalaosi and T. Afullo, "Prediction of asynchronous impulsive noise volatility for indoor powerline communication systems using garch models," in *2016 Progress In Electromagnetic Research Symposium (PIERS)*, pp. 4876–4880, IEEE, 2016.

[102] M. Nassar, K. Gulati, Y. Mortazavi, and B. L. Evans, "Statistical modeling of asynchronous impulsive noise in powerline communication networks," in *2011 IEEE Global Telecommunications Conference-GLOBECOM 2011*, pp. 1–6, IEEE, 2011.

[103] S. Saoudi, T. Derham, T. Ait-Idir, and P. Coupe, "A fast soft bit error rate estimation method," *EURASIP journal on wireless communications and networking*, vol. 2010, pp. 1–13, 2010.

[104] J. Dong, *Estimation of bit error rate of any digital communication system.* PhD thesis, Télécom Bretagne, Université de Bretagne Occidentale, 2013.

[105] J. Ma, X. Jiang, J. Jiang, and Y. Gao, "Feature-guided gaussian mixture model for image matching," *Pattern Recognition*, vol. 92, pp. 231–245, 2019.

[106] I. D. Gebru, X. Alameda-Pineda, F. Forbes, and R. Horaud, "Em algorithms for weighted-data clustering with application to audio-visual scene analysis," *IEEE transactions on pattern analysis and machine intelligence*, vol. 38, no. 12, pp. 2402–2415, 2016.

[107] E. Shireman, D. Steinley, and M. J. Brusco, "Examining the effect of initialization strategies on the performance of gaussian mixture modeling," *Behavior research methods*, vol. 49, pp. 282–293, 2017.

[108] Y. Li and Y. Chen, "Research on initialization on em algorithm based on gaussian mixture model," *Journal of Applied Mathematics and Physics*, vol. 6, no. 1, pp. 11–17, 2018.

[109] B. Panić, J. Klemenc, and M. Nagode, "Improved initialization of the em algorithm for mixture model parameter estimation," *Mathematics*, vol. 8, no. 3, p. 373, 2020.

[110] M. P. Deisenroth, A. A. Faisal, and C. S. Ong, *Mathematics for machine learning*. Cambridge University Press, 2020.

[111] C. Bishop, "Pattern recognition and machine learning," *Springer google schola*, vol. 2, pp. 531–537, 2006.

[112] B. Ghojogh, A. Ghojogh, M. Crowley, and F. Karray, "Fitting a mixture distribution to data: tutorial," *arXiv preprint arXiv:1901.06708*, 2019.

[113] S. Awino, T. Afullo, M. Mosalaosi, and P. Akuon, "Gmm estimation and ber of bursty impulsive noise in low-voltage plc networks," in *2019 PhotonIcs & Electromagnetics Research Symposium-Spring (PIERS-Spring)*, pp. 1828–1834, IEEE, 2019.

[114] F. Chelangat and T. Afullo, "Low-voltage plc noise modelling," *International Journal on Communications Antenna and Propagation (IRECAP)*, vol. 12, no. 4, 2022. doi:10.15866/irecap.v12i4.22089.

[115] A. M. Nyete and T. Afullo, "A novel technique for the modeling of power line noise for plc low voltage applications," *vol*, vol. 6, pp. 1243–1253, 2017.

[116] H. Attias, "A variational bayesian framework for graphical models," *Advances in neural information processing systems*, vol. 12, 1999.

[117] A. Corduneanu and C. M. Bishop, "Variational bayesian model selection for mixture distributions," in *Artificial intelligence and Statistics*, vol. 2001, pp. 27–34, Morgan Kaufmann Waltham, MA, 2001.

[118] N. Nasios and A. Bors, "Variational learning for gaussian mixture models," *IEEE Transactions on Systems, Man, and Cybernetics, Part B (Cybernetics)*, vol. 36, no. 4, pp. 849–862, 2006.

[119] W. Penny and S. Roberts, "Variational bayes for 1-dimensional mixture models," *Techn. Rep. PARG–00–2, Dept. of Engineering Science, University of Oxford*, 2000.

[120] Y. Ying, "A note on variational bayesian inference," 2009.

[121] F. Chelangat and T. Afullo, "Variational bayesian learning for the modelling of indoor broadband powerline communication impulsive noise.," *Progress In Electromagnetics Research B*, vol. 100, 2023.

[122] F. Valente and C. Wellekens, "Variational bayesian speaker clustering," in *ODYSSEY04-The Speaker and Language Recognition Workshop*, 2004.

[123] K. Vastola, "Threshold detection in narrow-band non-gaussian noise," *IEEE Transactions on Communications*, vol. 32, no. 2, pp. 134–139, 1984.

[124] G. Ndo, F. Labeau, and M. Kassouf, "A markov-middleton model for bursty impulsive noise: Modeling and receiver design," *IEEE Transactions on Power Delivery*, vol. 28, no. 4, pp. 2317–2325, 2013.

[125] F. Rouissi, V. Degardin, A. Ghazel, M. Lienard, and F. Gauthier, "Impulsive noise modelling using markov chains in indoor-environment-comparison with stochastic model," in *2005 12th IEEE International Conference on Electronics, Circuits and Systems*, pp. 1–4, IEEE, 2005.

[126] F. Rouissi, H. Gassara, A. Ghazel, and S. Najjar, "Comparative study of impulse noise models in the narrow band indoor plc environment," in *10th Workshop on Power line Communications*, 2016.

[127] U. Narayan Bhat, *An introduction to queueing theory: modeling and analysis in applications*. Springer, New York, 2007.

[128] F. S. Hillier and G. J. Lieberman, *Introduction to operations research*. McGraw hill Companies, Inc., 2001.